April 2018

The Role of Phosphohistidine Phosphatase 1 in Ethanol-induced Liver Injury

Daniel Richard Martin
University of South Florida, martin32@mail.usf.edu

The Role of Phosphohistidine Phosphatase 1 in Ethanol-induced Liver Injury

by

Daniel Martin

A dissertation submitted in partial fulfillment
of the requirements for the degree of
Doctor of Philosophy
Department of Cell Biology, Microbiology, and Molecular Biology
College of Arts and Sciences
University of South Florida

Co-Major Professor: Stanley M. Stevens, Jr, Ph.D.
Co-Major Professor: Brant Burkhardt, Ph.D.
Meera Nanjundan, Ph.D.
David Merkler, Ph.D.

Date of Approval:
March 25, 2018

Keywords: proteomics, phosphohistidine, Label Free Quantification, Alcoholic Liver Disease

Dedication

I would like to dedicate this doctoral dissertation to my parents and brothers. I sincerely appreciate the love and support provided by my family. Sheryl and Leonard Martin, I attribute a majority of my success up to this point to the lessons and skills you have taught me. I would also like to dedicate this to my older brothers, MK1 Robert Martin (USCG) and Major Joshua Martin (USAF). I am profoundly proud of and inspired by your accomplishments and greatly appreciate your service to this country.

Acknowledgements

I would like to thank my mentors Dr. Stanley Stevens and Dr. Brant Burkhardt for your guidance and advice especially over this last year. Also, thank you Dr. Stevens for taking a chance by hiring me as an undergraduate and spring-boarding my career into science. I would also like to thank my other committee members, Dr. Meera Nanjundan and Dr. David Merkler, for your feedback and support during the completion of this project. Thank you to my closest friends, Jacob Gil and Victoria Prescott, who have been there for me through my undergraduate and graduate school careers. A special thank you my colleagues, Dr. Dale Chaput and Jennifer Guergues for literally working next to me for the past four years. Finally, thank you to my fiancé, Jessica Ireland, for your love and support through my final year of graduate school.

Table of Contents

List of Tables

List of Figures

Abstract

Chronic liver diseases, which includes alcoholic liver disease (ALD), are consistently among the top 15 leading causes of death in the United States. ALD is characterized by progression from a normal liver to fatty liver disease (hepatic steatosis), which can lead to cirrhosis, alcoholic hepatitis, and liver failure. We have identified a novel role of phosphohistidine signaling, mediated through phosphohistidine phosphatase 1 (PHPT1), in the onset of hepatic steatosis. We have identified PHPT1 as a target of selective oxidation following acute ethanol exposure as well as being downregulated following chronic ethanol exposure. We mapped the oxidative modification site and developed a mass-spectrometry based phosphohistidine phosphatase assay to determine the impact of PHPT1 oxidative modification during acute ethanol exposure. To further understand the role of PHPT1 and phosphohistidine signaling during chronic ethanol exposure, we have developed PHPT1 overexpression and knockout mouse models. These mouse models were characterized using mass spectrometry-based proteomics. They were then utilized in a 10-day chronic ethanol plus binge model to determine the impact of PHPT1 expression on the onset of ethanol-induced hepatic steatosis. In addition, advanced mass spectrometry-based phenotypic characterization was performed on the treated liver tissues to determine the key regulators and canonical pathways influencing phosphohistidine signaling during chronic ethanol exposure. We have evidence to suggest that PHPT1 overexpression plays a protective role in the onset of hepatic steatosis, the PHPT1 heterozygous model is more susceptible to liver damage, and the complete knockout model is embryonically lethal. Additionally, we have identified novel pathways and regulators involved in phosphohistidine signaling during the development of ethanol-induced hepatic steatosis.

Chapter 1 – Introduction

Alcoholic liver disease

Alcoholic liver disease (ALD) categorizes a plethora of specific conditions, including fatty liver, steatohepatitis, and cirrhosis. In addition, patients are more susceptible to non-alcoholic related diseases such as non-alcoholic fatty liver disease, and chronic viral hepatitis when developing ALD. A combination of these diseases, including obesity, significantly increases a patient's risk for developing cancer or liver failure. Alcohol can be contributed to 44% of all liver disease related deaths in 2003 [1], while liver cirrhosis was the 12th leading cause of death in the United states in 2010 [2]. This is largely due to the prevalence and socioeconomic burden of alcoholism. The consumption of ethanol can be traced back for centuries when fermentation was necessary for disinfection [3]. Alcohol is a psychoactive drug which means it alone can lead to dependence. It has been classified by the World Health Organization to be among the top five leading risk factors for disease/disability and death in 2011 [4, 5]. In 2013, alcohol was number 4 of the 10 leading level 3-risk factors in developed countries for both sexes in terms of attributable deaths, years of life lost, years lived with disability, and disability-adjusted life-years [6]. Alcohol use, in general, accounted for 2.8 million deaths in 2013 which was an increase in total and percent deaths from previous years [6]. The wide prevalence of alcohol use, as well as its great burden of disease and death around the world is the sole contributor to the development of alcoholic liver disease.

Alcohol consumption is generally classified by binge, chronic, or moderate consumption. The National Institute on Alcohol Abuse and Alcoholism (NIAAA) classifies binge drinking as bringing one's blood alcohol concentration (BAC) greater than or equal to 0.08 g/dl. This is also, classified by the Substance Abuse and Mental Health Services Administration (SAMHSA) as

having more than 4-5 drinks in one day or occasion. Chronic drinking is considered by the SAMHSA as having more than 4-5 drinks in one occasion 5 or more times over a 30-day period. Moderate or low risk consumption is considered anything less than binge drinking in a single day or 7/14 drinks per week for women/men, respectively. Although actual consumption may vary amongst individuals, these consumption classifications are widely used to classify different models of consumption and their effects on disease progression. Chronic and binge drinkers are considered most at risk for disease development. Alcohol has been linked to disease development in almost every organ system in the human body. This includes gastrointestinal complications in the stomach, pancreas, and colon, as well as heart disease and muscle degeneration [7]. The brain and the liver however, are the two most commonly discussed organs associated with heavy alcohol consumption. The brain is probably the most effected organ given that changes in judgement can occur with a BAC as low as 0.02 g/dl, followed by impairment of motor functions and reaction time occurring between 0.06-0.10 g/dl, with cognitive ability and involuntary muscle impairment setting in around a 0.15-0.20. A BAC higher than this is associated with immediate permanent brain damage and can also result in death. The other main organ directly affected by alcohol consumption is the liver. As the main filtration system for removing alcohol from the blood stream, the liver undergoes a great amount of ethanol-induced stress in both chronic and binge drinkers. ALD is generally a progression from mild and asymptomatic, to severe and life threatening (Figure 1).

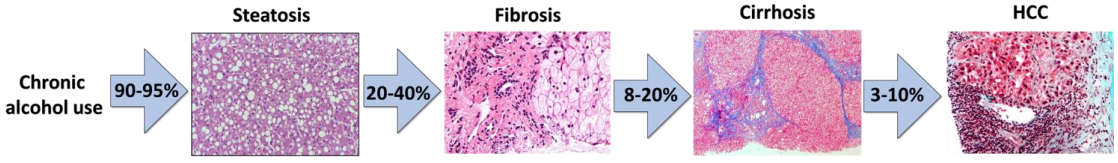

Figure 1. Alcoholic liver disease progression. With continual chronic ethanol exposure, chances of developing steatosis and more severe forms of ALD increase. Risk factors such as sex, obesity, and genetic predispositions can further increase the chances of developing the severe forms of ALD. The most severe being hepatocellular carcinoma (HCC) which causes liver failure and can lead to metastatic tumor development in other areas of the body. Adapted from *Gao et al. 2011*

When it comes to disease progression, moderate consumption rarely leads to any disease onset. However, it is estimated that 90% of individuals who are considered chronic drinkers will develop steatosis [8]. This is classified by the enlargement of the liver and histologically by the presence of lipid droplets in the hepatocytes. This injury can also be accompanied by inflammation, which usually suggests a more severe condition developing. If drinking persists 35% of those individuals will progress to steatohepatitis and up to 20% will develop liver cirrhosis without first experiencing steatohepatitis. Steatohepatitis shows more exacerbated symptoms to that of steatosis, with the increase in size and quantity of lipid droplets, development of inflammation, hepatocyte necrosis, as well as Mallory bodies [9]. Up to 70% of those who do not abstain from alcohol following development of steatohepatitis will progress to cirrhosis. Even of those that do abstain after the development of steatohepatitis only roughly 27% will recover fully to a normal liver, whereas 18% will develop cirrhosis regardless [10]. Cirrhosis is characterized by the deposition of extracellular matrix proteins via the onset of widespread fibrosis and inflammation throughout the liver. This condition is also accompanied by hepatocellular necrosis and predominantly macronodular development [9].

Disease prognosis depends on the stage of progression with fewer viable options as the severity increases. If caught in the early stages of steatosis and fatty liver development, the conditions are completely reversible with abstinence. However, the likelihood of full recovery decreases with steatohepatitis and once cirrhosis begins to develop complete recovery from abstinence alone is rare. Generally, treatment with corticosteroids or pentoxifylline is necessary once the disease has progressed to steatohepatitis [11, 12]. These treatments are also limited in their effectiveness. In many cases the only option for full recovery is a liver transplant. To receive a transplant, the patient must be able to prove at least 6 months of abstinence to be placed on the waiting list. The patient could then potentially wait years for a liver from a compatible donor to become available. In addition, liver transplant surgery has its own risks, with potential physiological rejection of a donor liver. These conditions make it very difficult for

patients with late stage ALD to fully recover, often requiring them to undergo regular blood transfusions to overcome symptoms associated with decreased liver function. Furthermore, with development of cirrhosis comes an increase in likelihood for liver cancer and malignancies that can cause complications elsewhere. Ideally, prevention and early identification of this disease is best. Prevention can obviously be accomplished through absolute abstinence or even moderate drinking. In addition, a diet with high antioxidants has also been shown to play a protective role in disease onset [11]. Unfortunately, early detection is difficult because often, fatty liver disease is asymptomatic and can only be confirmed with a histologically stained biopsy [13]. This makes identifying circulating biomarkers and molecular determinants of disease critical for treatment. Disease onset is further complicated by the multiple mechanisms involved in disease pathogenesis.

Ethanol pathogenesis involves a plethora of pathways and cellular response activated following consumption (Figure 2). In addition, the expression level and effectiveness of these pathways change as consumption increases. This coincides with the higher correlation in risk factors seen in chronic drinkers, as compared to moderate. Initially, ethanol is primarily processed and metabolized in the liver. Only about 10% of ethanol consumed is lost directly

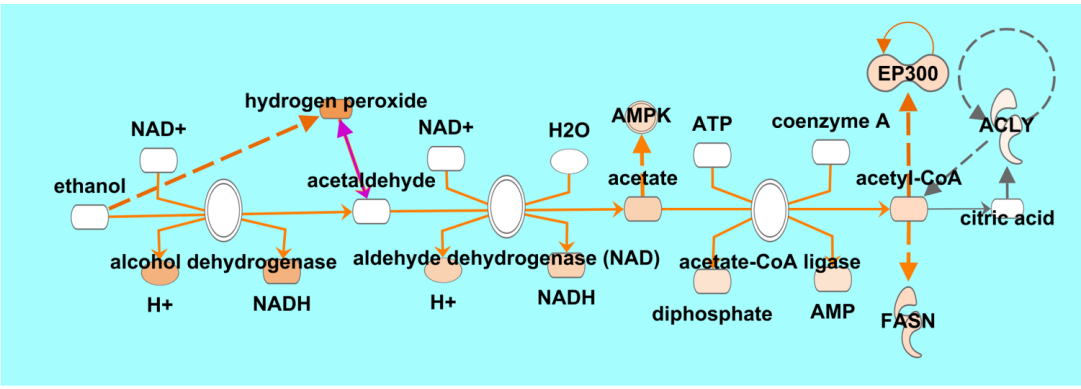

Figure 2. Basic ethanol metabolism. Ethanol is primarily metabolized by alcohol dehydrogenase or CYP2E1 (not shown) to produce acetaldehyde. Acetaldehyde can directly lead to ROS production as well be further metabolized into acetate and acetyl-CoA. As ethanol intake increases, the concentration of oxidized nicotinamide adenine dinucleotide (NADH) increases, disrupting the citric acid cycle. This pressures the acetyl-CoA pool into use for lipid production (FASN) and protein acetylation (EP300).

through sweat, lung, and kidneys [14]. Hepatocytes are the resident cells of the liver that primarily metabolize ethanol due to their expression all three of the enzymes essential for ethanol metabolism. Catalase is one of these enzymes, however, it is strictly expressed within peroxisomes [15], so ethanol metabolism is primarily mediated by alcohol dehydrogenase in the cytosol and cytochrome P450 2e1 (CYP2E1) within the endoplasmic reticulum (ER) [15-17]. Both enzymes yield acetaldehyde from the reaction, as well as generate the reduced form of nicotinamide adenine dinucleotide (NAD^+/NADH), and nicotinamide adenine dinucleotide phosphate ($NADP^+$/NADPH), respectively. The presence of acetaldehyde can lead directly to stress on the cell in the form of reactive oxygen species (ROS). Acetaldehyde and ethanol are directly involved in the creation of ROS such as hydrogen peroxide (H_2O_2) and superoxide anion (O_2^-) [18]. Fortunately, acetaldehyde is converted into acetate by aldehyde dehydrogenase which has high expression in hepatocytes and results in the creation of an additional NADH. Initially, CYP2E1 only accounts for 10% of ethanol metabolism, but is substrate induced and increases expression in chronic ethanol users [16, 17]. In addition, high frequency of ethanol metabolism leads to an accumulation of NADH. This not only inhibits aldehyde dehydrogenase, which results in more ROS via acetaldehyde accumulation, but also interferes with the citric acid cycle (the main route for acetate metabolism), causing an overall increase in acetyl-CoA present in the cell [13]. Both increased ROS production and acetyl-CoA accumulation will cause significant downstream influences on hepatocyte function.

The presence of hydrogen peroxide and superoxide anion (known ROS) can create even more hazardous free radicals and ferric oxide ions [19]. These highly reactive species lead directly to protein oxidation, and cause stress on organelles, like the ER and the mitochondria. The primary source of protection against ROS are free radical scavenging proteins such as glutathione, epoxide hydrolase 1 (EPHX1) [20-23], and heme oxygenase-1 (HO1) in the ER [24]. When ethanol exposure continues, however, the protective role of these proteins becomes diminished, as they are oxidized leaving the cell susceptible to oxidation-mediated damage.

ROS is directly created in the ER through CYP2E1 metabolization of ethanol, resulting in acetaldehyde formation. Protein oxidation in the ER can lead directly to accumulation of unfolded proteins. The cell reacts by activating NF-κβ and JNK, leading to an inflammatory response [25, 26]. In addition, unfolded proteins can stimulate the phosphorylation of Interferon regulatory factor 3 (IRF3), which will stimulate mitochondrial stress via caspase activation [27].

These insults, will further activate the steatogenic pathway through sterol regulatory element-binding protein (SREBP) activation, specifically SREBP1c [28, 29]. This pathway is primarily regulated by adenosine monophosphate-activated protein kinase (AMPK) signaling, which is inhibited directly by ethanol and acetaldehyde and indirectly via TNF (Tumor necrosis factor) signaling [30]. TNF is released from adipose tissue following ethanol-mediated inflammation [31]. Inhibition of AMPK activates SREBP1c and inhibits protective regulators, such as peroxisome proliferator-activating receptor α (PPARα) and the RXR-α pathway [13, 32-34]. This alteration in lipid homeostasis results in an increase in lipogenesis, via SREBP1c activation of fatty acid synthase (FASN), and a decrease in lipid oxidation, which is necessary for export. This outcome is additionally accompanied by an increase in acetyl-CoA present due to inhibition of the Krebs cycle. This is mediated through the inhibition of isocitrate dehydrogenase due to the NAD^+/NADH imbalance in the cell. The resulting accumulation of citrate is then exported back into the cell in the form of acetyl-CoA by ATP-citrate lyase (ACL), which is regulated by a phosphohistidine modification [35]. This influx in the acetyl-CoA pool is not only utilized for fatty acid synthesis, but it is also needed for protein acetylation. Histone acetyl transferases (HATs), such as EP300, are stimulated by an increase in the acetyl-CoA pool. This results in an increase in histone acetylation, which is known to activate protein transcription. Concurrent pressure on the cell to increase lipogenesis, decrease fatty-acid oxidation, and increase transcription leads directly to the onset of fibrosis. Consistent activation of these pathways results in the disease progression from fatty liver/steatosis to more severe steatohepatitis and cirrhosis.

Phosphohistidine phosphatase 1

Phosphatases and kinases have been widely studied in mammalian and other cellular models. These enzymes are responsible for the addition or removal of phosphate molecules to protein targets. This modification has been shown to be a major player in a plethora of cellular pathways, including cell metabolism, signal transduction, and transcription initiation. The most familiar forms of phosphorylation occur on threonine, tyrosine, and serine residues. Their roles in numerous cascades and protein function alterations have been widely studied and examined. The significance of phosphohistidine, however, has been relatively uninvestigated. The gap in knowledge around this modification can be mostly attributed to its unstable nature and challenges in isolation, rather than its possible limited importance in cellular function when compared to other well-investigated residues. The importance of phosphohistidine is already highlighted in the few, yet critical targets that have been identified to date. Phosphohistidine was first identified as an enzymatic intermediate for phosphoryl group transfer between enzymes [36]. It has further been identified as a lasting modification which regulates targets such as ATP-citrate lyase (ACL) [35], G-protein (β subunit) [37], Histone H4 [38] and KCa3.1 [39]. The development and loss of this modification on these targets can be attributed to phosphohistidine kinases and phosphatases. However, to this date, only a few of them have been identified in mammalian cells. Examples of these include nucleoside diphosphate kinase (NDPK), which has phosphohistidine kinase activity [40], as well as phosphohistidine phosphatase 1 (PHPT1) [41] and others [42].

PHPT1 is a 14kDa protein identified in porcine liver in 2002 with phosphatase activity for phosphohistidine residues [41]. It has also been shown to poses dephosphorylation activity for phosphoramidate [43] and phospholysine *in vitro* [44]. PHPT1 regulation of phosphohistidine levels include activation/deactivation of known phosphohistidine targets. PHPT1 expression has been linked to ACL function in multiple studies. Human-PHPT1 overexpression in murine neuroblastoma cells was shown to decrease ACL activity and lead to a decrease in cell viability

[45]. However, the same group showed two years later that siRNA-mediated knockdown of PHPT1 decrease ACL expression in pancreatic β-cell islets, and PHPT1 expression had no impact on cell viability [46]. Although, these studies seem conflicting, they do show PHPT1 expression to be an important regulator in ACL function. In addition, PHPT1 was also shown as an important regulator in the activation of G-protein during nutrient-induced insulin secretion [46].They showed that siRNA knockdown of PHPT1 reduced glucose-induced insulin secretion, but had no effect on KCL-induced secretion. This finding suggests PHPT1 was involved in G-protein-signaling steps to mediate insulin secretion. It is known that G-protein has a key phosphorylation site at His266 that is a target of NDPK and PHPT1 [47]. Although the significance of this modification is not fully understood, it is believed to be necessary for G-protein β/γ coupling to activate the holoenzyme [37]. PHPT1 plays an inhibitory role in the KCa 3.1 potassium ion channel where histidine phosphorylation is necessary for the channels activation [39]. Histone H4 regulation is unknown but it has been identified as a target for PHPT1 *in vitro* in many studies [38, 43, 48].

It is clear that PHPT1 and phosphohistidine are not involved in just a singular pathway in mammals. PHPT1 is part of the Janus family of proteins and is the only phosphohistidine phosphatase part of this family identified to date. This characterization is according to the family domain classification available on the universal protein resource (uniport.org). The Janus family proteins are best characterized by their involvement in sex differentiation in *Drosophila melanogaster* [49]. PHPT1 and NDPK have been identified as players in disease progression as well such as hepatocellular carcinoma (HCC), meningiomas, and lung cancer [50-53]. However, the role of PHPT1 in each disease does not coincide across all conditions and cell types. PHPT1 knockdown in lung cancer cells resulted in an inhibition of migration and invasion mediated through actin cytoskeletal rearrangement modulation [51]. PHPT1 expression was shown to be elevated in HCC tissues as well as in meningiomas [52, 53]. In HCC, siRNA mediated knockdown of PHPT1 resulted in an increase in apoptosis and inhibited cell

proliferation as the G1-S phase transition [52]. In addition, according to The Cancer Genome Atlas, PHPT1 has been shown to be amplified in multiple cancers, most notably in neuroendocrine prostate cancer (Trento/Cornell/ Broad, 2016) and pancreatic cancer (UTSW cancer center). PHPT1 seems to be influencing many different pathways in the cell which gives insight into the significance of the phosphohistidine modification itself.

Phosphohistidine signaling

The phosphohistidine modification was initially published in 1962 and first described in bovine mitochondria [36]. Since this time, there has been relatively little investigation in the significance of this modification in mammals as compared to tyrosine, threonine, or serine phosphorylation. This finding is in spite of the fact that it has been estimated that phosphohistidine accounts for 6% of protein phosphorylation in eukaryotic cells [54], which is two-fold more abundant than phosphotyrosine [55]. The main reason for the disparity in study of this modification is its hydrolytic lability which is much higher than the better studied forms of phosphorylation. This makes the modification very unstable in neutral conditions and even more so in acidic environments, with a half-life of less than 30 seconds in 1M HCL [56]. In addition, the modification can occur in two different conformations, at the 1N or at the 3N, of the imidazole ring on histidine (Figure 3). The first discovery was on the 1N of the ring where it

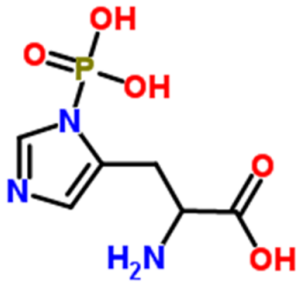

Figure 3. Structure of phosphohistidine. The histidine amino acid shown has an attached phosphate group at the N1 location on the imidazole ring. This phosphate group can also be attached at the N3 location on the imidazole ring.

played an intermediate role carrying a phosphoryl group between a substrate and the phosphate donor on kinases and phosphatases [36]. This conformation has functioned in this manner in many cases [56, 57]. The 3N location however has been identified as the location of

the lasting modification that influences enzymatic activity on known targets such as ACL [35], G-proteinβ [37], and KCa3.1 [39], in addition to two component histidine kinase autophosphorylation that occurs in *Escherichia coli in vivo*, and on Suc-AHPF-pNA and H4 [38] *in* vitro. The function of phosphohistidine has been best characterized in bacterial and plant cells [58], and their two component histidine kinase systems are well known for their regulation of cell signaling and transcription[59]. Most of these studies, however, have investigated phosphohistidine in a targeted manor. Targeted investigation is necessary because standard cell lysis procedures, as well as mass spectrometry sample preparations, call for acidic solutions and can result in complete loss of the modification before measurements are taken [60]. Although these pathways are not present in mammalian cells, studies have shown phosphohistidine levels to be significantly altered in diseases, including cancer, and to be involved with a diverse list of pathways [61]. Recently, the development of pan-phosphohistidine antibodies and phosphohistidine sensitive protocols have allowed the significance modification to be further investigated.

Structure

To date there have been three main studies on the structure of PHPT1 and the residues involved in substrate binding [57, 62, 63]. All studies have shown the primary and crystalline structure of PHPT1 being highly conserved between mammals (Figure 4). The secondary structure is composed of six β-stands, which are flanked by two α-helices and short unstructured regions at the C- and N-terminals, 4 and 5 amino acids long, respectively [54]. Mutagenesis and NMR studies identified H53A in human PHPT1 to be catalytically inactive [56]. Other mutations that resulted in a significant decrease in k_{cat} were M95D, A96D, K21A, and S94A [56]. It was concluded that the substrate binding site was located at α1 and β4 on one side and α2 and β5 on the other [55]. The residues involved directly in this region were Glu51, Tyr52, His53, Try92, and Met95 [55]. Ser94 was determined to assist with phosphate

stabilization via the -OH side chain [55]. His53 was determined to be the bound amino acid during phosphoryl group transfer between substrate and donor [54-56]. In addition, the His53 was shown to stabilize the binding site via H53A mutagenesis causing destabilization of this area [62]. All studies showed H102A mutagenesis to influence substrate binding as well, even though it is located far away from the binding region [54-56]. This influence was determined to be a result of its location in a highly hydrophobic core region of the protein. H103A-mediated destabilization of the core region, had global protein conformational consequences resulting in a decrease in catalytic efficiency [55].

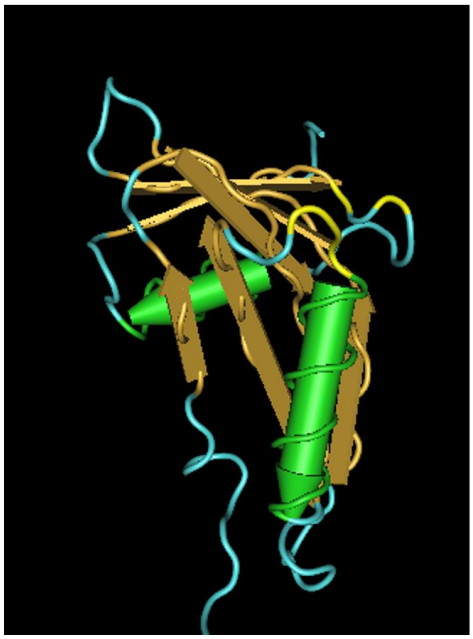

Figure 4. Structure of PHPT1. PHPT1 structure is composed of two α-helices (green) and six β-strands (gold). The binding region of the protein is highlighted in yellow and unstructured regions are highlighted in blue.

Unfortunately, these studies were limited to PHPT1 function toward peptide or molecular substrates, and not full protein interactions. Additionally, there have been no studies investigating the binding mechanism of PHPT1 toward the N-ε-phosphorylation of lysine which it was recently determined to target [44]. The influence of post-translational modifications on PHPT1 activity is relatively uninvestigated. To date, only two modifications have been characterized on PHPT1. One of these is an N-terminal protein acetylation [64] that occurs on PHPT1 following N-terminal methionine cleavage. The other modification, which was characterized in this dissertation, is Met95 oxidation which occurs via oxidative stress [65].

Initial hypothesis of alcoholic liver disease pathogenesis

As discussed previously (Chap. 1 Alcoholic liver disease), there are multiple pathogenic pathways involved in the onset of the ALD. The main pathways include oxidative stress that causes an accumulation of ROS and can directly cause necrosis and apoptotic cell death. In addition, the influx of acetyl-CoA, as well as signals from adipose tissue, lead to an increase in lipid synthesis and a decrease in fatty acid oxidation. This change results in lipid accumulation and the ethanol-induced hepatic steatosis phenotype. Both ROS and lipid accumulation contribute to an increase in inflammation and protein transcription. This phenotype contributes to the development of more severe conditions, such as cirrhosis or hepatocellular carcinoma via cell differentiation. Many players in these pathways are known but progression and mechanism of development still needs to be further investigated. Our investigation aims to identify novel players in the onset of alcohol-induced hepatic steatosis and determine the mechanism in which they are involved in disease progression.

A known key player in ethanol metabolism, ACL, is responsible for the conversion of citrate into acetyl-CoA and oxaloacetate, and the reverse reaction. This reaction is necessary following accumulation of citrate caused by citric acid cycle inhibition, which can come from chronic ethanol ingestion that creates a high ratio of NADH:NAD^+. In the later instance, the synthesized oxaloacetate can be converted into malate by cytosolic malate dehydrogenase, which utilizes the high concentration of NADH available to create NAD^+. Malate can then return back to the citric acid cycle within the mitochondria and be oxidized again to oxaloacetate to maintain the function of the electron transport chain. This conversion prevents further accumulation of NADH, but results in additional accumulation of acetyl-CoA. Acetyl-CoA accumulation leads directly to fatty acid synthesis as well as histone acetylation. This result in combination with ROS-induced inhibition of fatty-acid oxidation results in the lipid accumulation responsible for the ethanol-induced hepatic steatosis phenotype. ACL is known to be transcriptionally induced by insulin and glucose. These molecules simultaneously activate the

PI3K/Akt pathway which is known to phosphorylate and activate ACL. In addition, PHPT1 overexpression and siRNA-mediated knockdown models have been shown to directly impact ACL activity. ACL is a known target of phosphohistidine modification and PHPT1 dephosphorylation.

Our initial hypothesis was that the regulation of ACL by PHPT1 was being influenced following acute or chronic ethanol exposure. We hypothesized that ethanol-induced factors such as ROS were altering PHPT1 activity via modification or expression levels which decreased regulation of ACL. Furthermore, we wanted to investigate the role of PHPT1 in the onset of alcohol-induced hepatic steatosis. In addition to ACL, we believed there are many other factors PHPT1 and phosphohistidine modification influenced that were involved in the onset of ALD. Despite this, the role of PHPT1 and the significance of phosphohistidine signaling following ethanol-induced hepatic steatosis has not been investigated. Although, as previously mentioned, PHPT1 has been identified to be involved in other diseases, such as neuroendocrine prostate cancer, and lung cancer [51, 66].

Other roles of PHPT1

Beyond the previously mentioned known targets, there have been many additional suggestions into the role of PHPT1. As previously mentioned from a domain standpoint, PHPT1 fits in the Janus family of proteins. This family is best characterized in *Drosophila melanogaster* as being involved in sex differentiation and development. It is likely that PHPT1 plays a role in cell differentiation in mammals as well. This theory is further supported by PHPT1 being linked to cancer development in multiple studies. In lung cancer, it is believed to be involved in cell migration through actin cytoskeleton rearrangement. Furthermore, the expression of PHPT1 in lymph nodes and lung cancers correlated with the severity of the cancer from human samples [51, 66]. PHPT1 is believed to be influencing tumor progression through NF Kappa B signaling pathway by inducing MMP9 [67]. These studies suggest that PHPT1 plays a major role overall

in cancer progression and cellular homeostasis although there are no currently known targets to suggest this.

In addition, relatively little is known about PHPT1 regulation. Studies have shown broad expression regulators, such as HNF4α, to influence PHPT1 expression [68]. HNF4α is a key regulator of many proteins involved in lipid homeostasis [69]. These include the PXR and RXR pathways, which interact with the acetyl-CoA pool and contribute to fatty acid metabolism [70, 71]. PHPT1 may be involved in this regulation through its interaction with ACL or other unknown targets involved in lipid metabolism. In addition, expression levels have also been shown to correlate with phosphohistidine kinases, such as nucleoside diphosphate kinase-B (NDKB) [72]. NDKB is also known to be a transcriptional regulator of MYC, a well-known oncogene [73]. Phosphohistidine kinases are best characterized in two component histidine kinase systems in prokaryotic cells. These systems are also vital in signal transduction, resulting in transcriptional activation [59]. Furthermore, both histone H4 and H1 have shown to be targets of PHPT1 *in vitro* [43, 44]. PHPT1 has been shown to dephosphorylate H4 and have phospholysine activity to dephosphorylate H1 *in vitro*. PHPT1-mediated histone dephosphorylation has potential to widely influence protein expression. It is well known that transcription can be mediated through a plethora of histone modifications. However, the impact of these modifications and full characterization of PHPT1 regulation has not been elucidated.

Proteomics & alcoholic liver disease

As previously mentioned, ALD can develop in many ways, and monitoring its progression in a patient and a model is difficult. To properly investigate the onset of this disease, as well as elucidate pathways involved that have yet to be discovered, it is necessary to use an approach that will both, provide information about known disease states, and unbiased information for discovering novel players. A key indicator of cellular functions and disease state is protein expression levels. Protein expression data provides a snapshot of the genes that have been activated, as well as PTMs that may be influencing activation. These data

differ from genetic information, such as DNA or mRNA, that only show the potential expression profile. In the case of ALD, the expression levels of key proteins such as epoxide hydrolase (EPHX1) and cytochrome P450's (CYP2E1) are critical indicators for onset of hepatosteatosis [24]. Other proteins such as the PPAR family (α, β, and γ), the LXR or RXR proteins, or inflammatory proteins like cytokines or JAK/STATS, provide critical information about the severity of the disease and the mechanism of onset. Therefore, to thoroughly study this disease, we must be able to identify these proteins and their abundances in an accurate and reproducible manner. However, to elucidate new mechanisms involved in disease progression, our approach must also remain unbiased toward known targets. To obtain measurable and reproducible unbiased data regarding the global proteome expression levels, we will utilize mass spectrometry-based proteomics techniques. Specifically, shotgun proteomics using data-dependent acquisition, followed by label free quantification of purified tryptic peptides from samples lysates, to determine significant protein expression changes between treatments.

Mass spectrometry and proteomics.

Initial proteomic studies involved 2D separation gels, which would discriminate proteins based on their molecular weight on one axis and the isoelectric point on another axis. This technique allowed sufficient separation of proteins in a lysate to determine expression difference of a single protein or protein group between treatments. It would then be required to determine the identity of each protein recognized as differentially expressed. This process could be done by extracting the protein or protein group, purifying, and performing an NMR or mass spectrometry analysis of each. This method was tedious and highly objective in determining which protein groups differed between treatments. Given the recent advances in mass spectrometry, and the ability to pair with separation methods, such as liquid or gas chromatography, mass spectrometry-based proteomics has now become a highly accurate, high-throughput method.

Advances in instrumentation have enabled the use of mass spectrometry to investigate molecules faster and of varied sizes and complexities. Both time-of-flight (TOF) and Orbitrap instruments have provided significant advances in resolving power, resolution, and mass accuracy of multiple charged ions, such as peptides and proteins. These advances in detection methods are paired with the creation of hybrid instruments which allow more accurate quantification with less interference from neutral molecules or undesired ions. Hybrid instruments incorporate a multi-stage system that maximizes ion detection efficiency using ion optics to focus and normalize ion beams and velocity, followed by multi-pole (quadrupoles and octupoles) stages, which create mass and ion filters and further stabilized ion beams, prior to entering main or secondary detection components. The addition of a linear ion trap can allow simultaneous MS/MS filtration and detection, while the primary detector such as an Orbitrap is performing full-scan detections. MS/MS has also been improved for proteomic purposes. There now exists a plethora of MS/MS dissociation techniques that can break specific bonds of the investigators choice. Additionally, MS/MS is no longer limited to MS^2, and multiple instruments can perform MS^n where n is limited typically by the abundance of the molecule being investigated. The advancements in instrument ionization methods also enhanced mass spectrometry-based proteomics. Specifically, the development of electrospray ionization (ESI), paired with liquid chromatography, and matrix assisted laser desorption/ionization (MALDI), make it possible for relatively easy ionization of complex protein samples for mass spectrometry analysis. Continuing advances in instrumentation and ionization methods are making mass spectrometry-based proteomics a highly accessible field.

Another key aspect that has allowed mass-spectrometry to become the go-to method for proteomic analysis is the pairing with liquid chromatography [74]. Liquid chromatographs (LC) use pumps and filtered columns to create separation of a sample on the molecular level, creating a stable and reproducible gradient of molecular influx in-line with the mass spectrometer. This technique is performed using sold phase and liquid phase separation. In the

case with proteomic studies, the liquid phases are an aqueous buffer (hydrophilic) and an organic buffer (hydrophobic). The solid phase is usually carbon chains of specified length and density which bind to the proteins/ peptides present in a complex sample. Peptides that are highly polar and most soluble in the aqueous phase will not bind to the solid phase (column) and be the first to flow through in a reverse phase column set-up. Coinciding with MS detection, the LC will increase the ratio of organic: aqueous liquid phase, creating a gradient. This gradient will allow increasingly polar peptides to solubilize and release from the column for mass spectrometry identification. In-line LC allows for stable peptide influx, preventing the instrument from being overwhelmed with numerous peptides simultaneously, and provides a reproducible polarity-based gradient for reference. Liquid chromatography, paired with an ESI source, has made it possible to analyze a complex protein mixture efficiently and accurately. Advancements in liquid chromatography, including high-pressure and ultra-high pressure (HPLC and UHPLC) systems, have allowed for even more efficient separation of peptides and higher degrees of reproducibility in liquid chromatography-paired mass spectrometry (LC-MS).

Numerous advancements in mass spectrometry have made it the ideal instrument for proteomics studies. In our studies, we will be utilizing LC-MS for label free quantification of cell lysates, individual proteins, and animal tissue lysates. This method will allow us to identify and quantify proteins present in these tissues in a reproducible and accurate manner. The primary instrument utilized will be a hybrid quadrupole-Orbitrap instrument (Q-Exactive Plus, Thermo), using a top 10 data-dependent acquisition method. Further information on the exact specifications of this instrumentation will be included in the respective methods sections.

Label free quantitation

The process of protein quantification begins with the sample preparation immediately following protein purification. Following lysis and protein purification, protein concentrations are determined from each sample and standardized across all samples being analyzed. For our studies standard protein quantities (between 100-200 µg) are then added to filter-aided sample

preparation (FASP) columns to undergo buffer exchange and trypsin digestion, as described previously [75]. The purpose of the buffer exchange is to remove the detergents, which were used for lysis, that cause interference with LC/MS analyses. This exchange is accomplished using 8M urea as a wash buffer to keep the proteins solubilized. Then, all proteins are reduced to break disulfide bonds and immediately alkylated to prevent unwanted reactivity of free thiol groups. These modifications assure that all proteins are denatured and help insure the complete digestion by trypsin. Following modifications, another buffer exchange takes place to allow for trypsin function in ammonium bicarbonate. Trypsin digestion occurs at 37° C overnight, creating peptides that are either lysine or arginine-terminated. This digestion also allows the peptides to now flow through the filter. Peptides then must undergo a desalt procedure. Salt analytes interfere with ionization efficiency and can create adducts that change peptide masses and interfere with quantification. The desalt procedure is concluded with elution by acetonitrile, which is then placed under a vacuum until dryness. Samples are resuspended in 0.1% formic acid in water at a concentration of 1-5 µg/µl. There are a variety of other sample processing methods available including, in-solution and in-gel digestions, but most methods apply the same chemical manipulations of reducing, alkylating, and digesting proteins to produce purified peptides in a slightly acidic solution.

Samples then undergo LC-MS analyses consecutively, using the same procedure, column, and ESI tip for each sample to ensure reproducibility. Instrumental standards are run before and after samples for quality assurance. Samples are run with either technical or biological replicates as well. LC-MS analysis provides qualitative information of individual peptide masses, as well as quantitative information of peak intensities relative to the noise level. In addition, MS/MS data provides peptide backbone information that can be used to identify specific amino acids and modification on each peptide. This information is then searched against the known proteome database to match the identified peptide peaks in the MS data with known proteins.

In our studies database peptide identification is performed using the MaxQuant (maxquant.org) search algorithm to determine peptide identifications and quantity. Peptide IDs are determined using a 0.01% false discovery rate to guarantee accurate protein recognition. This algorithm quantifies the protein abundances by converting the relative peptide intensities originating from the same protein into label free quantification intensities. This calculation is done following peptide identification across all samples and replicates. The algorithm then assumes most protein abundances should remain constant across all samples, regardless of treatment type. In addition, the algorithm considers the number of peptides (unique and repeated) identified that relate to each protein, as well the total intensity of all the peptides from the same protein. Using these factors, MaxQuant creates a label free quantification (LFQ) intensity which is then used for quantification, in lieu of the absolute intensity of each peptide provided by the LC-MS raw data. LFQ peptide count cut-offs are set to 1 to minimize lost intensities with a majority of the calculated LFQ intensities being within a few percent of the absolute intensity values. The LFQ values are then used to compare control and treatment samples and to determine significant differentially expressed proteins. Label free quantitation has been shown to be a reliable method for comparing protein expression from multiple samples to each other [76]. To further strengthen the confidence in the LFQ method, the use of multiple ($n \geq 3$) technical or biological replicates is necessary.

Proteomic studies using animal models

The primary animal model used in these studies has been *Mus musculus*. The mouse model provides more biological relevance than mouse or human cells alone. The homogeneity between mice and human organ functions and systems, combined with their short lifespan and quick reproductive cycle, make them an ideal candidate. Mouse models of alcoholism have also already been well developed and characterized [77, 78]. The primary mouse strain we used was the C57BL6/J mouse which has been widely used in the 10-day chronic ethanol plus binge

model. This model has been shown to induce severe hepatosteatosis apparent by the development of lipid droplets and inflammation [77].

Further validation of this model and the disease state is accomplished through mass spectrometry-based proteomics. Proteome-wide LFQ quantification of differentially expressed proteins between the treatment and controls groups will identify proteins significantly changed during disease onset. This method has been validated against known proteome changes such as increase in expression of CYP2E1 and EPHX1 [24], as well as other indicators of hepatosteatosis [77]. Using proteomics in combination with an organism physiologically similar to humans allows us a more accurate depiction of the disease state and cellular components being influenced.

The other advantage of using a mouse model for proteomic disease analysis is that proteome database for *Mus musculus* is available and well-annotated. This database is used to identify the proteins discovered from mass spectrometry-detected peptides. A well-annotated database is important to have in that it will provide more complete information about the proteins identified rather than an abundance of uncharacterized proteins. The primary database used for the mouse model searches is extracted from UniProt (uniprot.org) and updated regularly to incorporate all recent annotations. These annotations are of additional importance following identification and quantification, as they are used for mechanistic analyses as well. The similarity of human and mouse cellular functions and pathways allows the protein expression information to be employed for determining upstream and downstream regulators influenced by the identified differentially expressed proteins. This analysis is a key step in elucidating novel enzymes and mechanisms involved in the disease being investigated.

Significance of protein modification in alcoholic liver disease

Post-translational modifications can influence all aspects of protein function. There is a plethora of modifications that can occur on an individual protein causing biochemical changes in the proteins conformation. These modifications can directly impact protein function or

expression, or indirectly impact a protein affecting its downstream targets or upstream regulators. Ethanol can induce a wide variety of modifications through a direct manor with the creation of ROS or an indirect manner through signaling mechanisms brought on by its presence. Ethanol can lead to the creation of ROS such as acetaldehyde, hydrogen peroxide, and free radicals. These are known to oxidize susceptible amino acid residues, such as methionine, which often leads to loss of function [79]. This inhibition is observed in calmodulin and interferon kappa B alpha, as well as other proteins [80-82]. Other modifications such as phosphorylation, acetylation, and methylation are induced by ethanol as well. These modifications are induced by the change in metabolism and cell signaling brought on by ethanol, and they will further influence cellular function and protein expression.

Oxidative modification is the most prevalent PTM directly induced by ethanol [83]. Oxidation is notorious for causing loss of function and disturbing vital cellular functions [79]. The presence of ROS is contested directly by anti-oxidants and hydroxylation enzymes such as glutathione and epoxide hydroxylase [22, 84]. The role of these molecules is to hydrolyze the oxidants preventing them from directly impacting vital proteins. In binge and acute models of ethanol exposure, the presence of these molecules is initially decreased as they are overwhelmed by the abundance of ROS present. However, in chronic models, the cell responds to continual ethanol exposure by overexpressing oxidant scavengers such as EPHX1 [24]. Once depleted, however, antioxidants initially present in the cell take time for replenishment, leaving the cells more susceptible to ethanol-induced oxidative damage.

Other modifications are impacted as well following chronic ethanol exposure. A consistent increase in ethanol metabolism will change the ratio of molecules involved in glycolysis and the citric acid cycle. Ethanol must be metabolized by alcohol dehydrogenase and then further by aldehyde dehydrogenase to prevent the presence of acetaldehyde [15]. This reaction results in an increase of NADH molecules which can inhibit the activity of the citric acid cycle. This stall will cause an increase in citrate in the mitochondria, which gets converted back

into acetyl-CoA in the cytoplasm via ACL. An increase in the acetyl-CoA pool directly correlates to acetylation of proteins, including histones, which will directly result in expression changes [85]. Furthermore, abundance of acetyl-CoA can also dysregulate glycolysis and activate alternative pathways for cellular metabolism. This effect leads to greater protein modifications occurring, such as methylation, phosphorylation, and the previously mentioned oxidation and acetylation [85]. Even minor changes in PTM's of regulatory proteins like histones or MAP-kinases will result in massive expression alterations [86]. Continuous ethanol exposure in a chronic model will lead to irreversible expression changes via PTM's and result in the development of severe ALD [13].

Summary of approaches and project aims

The adverse effects of alcoholism on the human liver are well known. Chronic ethanol consumption is strongly correlated to a unique pathology of liver diseases known as ALD. The mechanisms and players involved in the onset and progression of this disease are still poorly understood. Many of the proteins believed to be key regulators have been identified through mRNA characterization or biased approaches targeted at individual proteins. Our study aimed to identify and characterize a novel player in the onset of ALD through the global proteomic analysis of an ethanol-induced hepatic steatosis models. An acute model study using HepG2, hepatocyte-like cells, was performed and characterized using the SILAC approach to determine expression and modification changes. This study identified a phosphohistidine phosphatase (PHPT1) as being selectively oxidized but showed no change in expression levels following the acute exposure. Further characterization of this modification and its influence on PHPT1 was performed using mass-spectrometry based modification site mapping and a novel phosphohistidine phosphatase assay.

In addition, a 10-day chronic plus binge mouse model was used to determine more biologically relevant effects of long-term chronic ethanol exposure on the development of liver injury. Following a global proteome characterization between ethanol and control diet-fed mice

using high-resolution mass spectrometry, we identified PHPT1 as being significantly downregulated by ethanol exposure. This discovery created the basis for the second and third aim in determining the significance of PHPT1 expression prior to and following ethanol-induced hepatic steatosis. To investigate this, we developed both a liver-specific overexpression model and bred an organism-wide knockout model. Overexpression was accomplished using an adenoviral-based vector delivery of PHPT1 paired with a liver-specific albumin promotor administered intravenously through the tail. This yielded a significant increase in PHPT1 expression specifically in the liver, which lasted for multiple weeks. In addition, we requested creation of a non-conditional PHPT1 knockout mouse through cre-mediated *lacZ* substation by UC Davis. The heterozygous genotype yielded an average of 50% mRNA and protein expression, compared to wild-type, in all tissues tested but displayed no obvious phenotypic changes. All heterozygous crosses, however, did not yield a complete PHPT1 knockout offspring. This result suggests that PHPT1 is critical for early development. Both models where then characterized using mass spectrometry-based phenotypic characterization to determine the mechanisms impacted by PHPT1 expression alteration.

Finally, both models were used in the 10-day chronic plus binge ethanol exposure model to determine the influence of PHPT1 on the development of ethanol-induced hepatic steatosis. Groups were pair-fed with a control (sucrose supplemented) or ethanol diet. Disease progression was determined using liver sectioning histology and circulating aspartate aminotransferase (AST), alanine aminotransferase (ALT), and triglyceride (TAG) levels. PHPT1 expression levels were determined using western blot and LFQ values from global proteomic analyses. Finally, mass spectrometry-based phenotypic characterization was performed on liver tissue from each mouse. This method was used to identify mechanisms and pathways influenced by PHPT1 during chronic ethanol exposure. Conclusions of these studies provide greater insight into the role PHPT1 and phosphohistidine signaling plays in the onset of ethanol-induced hepatic steatosis and potential contribution to the pathogenesis of ALD.

Chapter 2: Structural and activity characterization of human PHPT1 after oxidative modification

Summary

The structure and primary function of PHPT1 has been recently elucidated (Chapter 1 section) [57, 62]. However, the biological influence of PHPT1 phosphatase activity on cellular functions and vice-versa are not fully understood. The number of confirmed targets of PHPT1 remain minute in comparison to the estimated 6% of the protein phosphorylation being attributed by histidine phosphorylation [87]. Furthermore, the influence of post-translational modifications (PTMS) such as phosphorylation or oxidation on PHPT1 have not been investigated. Currently, only one PTM has been identified on PHPT1 and that modification, being constitutive N-terminal acetylation [64], is the most common modification in eukaryotic proteins [88]. The role of PHPT1 and how PTMs influence its activity and structure is necessary to further characterize the significance of this protein. Specifically, we wanted to determine how ethanol-induced PTMs influenced PHPT1 phosphatase activity givens its regulation of ATP-citrate lyase, a key protein in ethanol metabolism. This study was conducted by first creating an acute ethanol exposure model with HepG2 cells, exposing them to high amounts of ethanol for 8-12 hours. This exposure led us to identify PHPT1 as a target of increased oxidation following ethanol exposure. This acute exposure was recreated *in vitro* using the known reactive oxygen species (ROS) hydrogen peroxide. Following treatment, we used mass spectrometry-based modification site mapping to determine the exact location and quantify the percent of oxidized PHPT1. For activity characterization, we used oxidized and non-oxidized PHPT1 in a mass spectrometry-based phosphohistidine phosphatase assay and explicit solvent molecular dynamics using computer simulations of the known PHPT1 structure with and without the

oxidative modification. Our investigation found that PHPT1 can be selectively oxidized on Met95 located in the substrate binding region; however, the oxidation does not limit PHPT1 phosphohistidine phosphatase activity *in vitro*. This result suggested PHPT1 plays a more complex role in ROS-mediated cellular response.

Introduction

Ethanol-induced reactive oxygen species

A large influx of reactive oxygen species (ROS) are present in hepatocyte cells following acute and chronic ethanol exposure models. These ROS are generated both directly and indirectly by ethanol metabolism. Ethanol leads directly to the generation of hydrogen peroxide and acetaldehyde consequentially of ethanol's metabolism. Acetaldehyde is directly created by alcohol dehydrogenase and hydrogen peroxide, which can result from the natural decomposition of ethanol in an intercellular environment [18]. Furthermore, both molecules can lead to the creation of free radicals such as a superoxide radical and reactive nitrogen species like peroxynitrite. This influx of radicals exacerbates the amount of ROS present in the cell. In an acute model, oxidation is most likely to occur more readily due to the cell not having the opportunity to increase expression levels of protective antioxidant, or hydroxylase enzymes, and decrease the production of acetaldehyde via alcohol dehydrogenase [89]. In chronic exposure models, ethanol metabolism is primarily performed by CYP2E1 as a consequence of alcohol dehydrogenase inhibition due to an increase in NADH and acetaldehyde [90]. Additionally, overexpression of protective hydroxylase enzymes occurs to reverse the effects of ROS [91].

HepG2 cells

HepG2 cells were derived from a a fifteen-year-old caucasian American male with well differentiated hepatocellular carcinoma. The cells resemble immortalized human hepatocytes and can be used to simulate liver experiments. HepG2 cells have been used previously to investigate the liver metabolism of toxic reagents including ethanol [92]. However, given the absence of expression of CYP2E1 and ADH1, these cell are not the ideal model for studying

oxidative stress. Similar to hepatocytes, HepG2 cells express high amounts of albumin and transferrin.

Oxidation modification

Oxidation modifications have been observed in a wide variety of proteins. This oxidative modification can occur on methionine, tyrosine, tryptophan, or cysteine residues and can occur as single, di- or tri-oxidation in some situations. An increase in the presence of ROS can lead to an increase in global protein oxidation. These oxidants can lead directly to protein oxidation by interacting with a susceptible residue or can increase oxidation indirectly by saturating glutathione, and increasing CYP2E1 production in cells exposed to ROS over long periods of time [89]. CYP2E1 activation leads to an increase in expression and results in the creation of more $NADP^+$. Reduction of $NADP^+$ to NADPH leads directly to more ROS present in the cell. Protein oxidation, especially on methionine residues, leads to inhibition of enzymatic function in the well documented case of calmodulin and interferon kappa B alpha [81, 82, 93]. The exception to this is with glutathione-S-transferase, which can be oxidized on multiple methionine residues without any influence in activity [84]. PHPT1 has two methionine residues as potential targets of oxidation (Met64 and Met95) and multiple other residues susceptible to oxidation (cysteine, tryptophan, and tyrosine) as well. One methionine residue occupies the middle of the substrate binding region of PHPT1 (Met95) and has been shown to be directly involved in substrate binding region stability [62]. Due to the susceptibility of this residue to oxidation, its importance in substrate binding, and the nature of the oxidative modification, we hypothesize that if PHPT1 oxidation is selectively occurring at this residue, and PHPT1 phosphatase activity will decrease as a result of oxidative modification.

Phosphohistidine phosphatase assay

Phosphohistidine is known to be an unstable modification *in vitro*. Therefore, the development of a reliable phosphohistidine phosphatase assay is not trivial. Currently, the only phosphohistidine phosphatase assays that have been used rely on phosphohistidine analogs

that are more stable during the experiment. The benefit in stability, however, is accompanied with a decrease in specificity. This compromise makes the assay less reliable when comparing to *in vivo* results. Another phosphohistidine phosphatase assay developed relies on a malchite green reporter molecule that is activated by the removed phosphatase group [48]. This method requires the reaction to take place completely. This requirement makes it an indirect measurement and does not allow reaction monitoring in real-time. We will aim to develop a mass spectrometry-based assay utilizing a small histidine-phosphorylated peptide, which can be identified and verified using MS/MS. In addition, the reaction can be monitored in real-time and take place during direct infusion so any changes in phosphorylation can be seen immediately following enzymatic activity. This novel assay will look directly at the phosphorylated and non-phosphorylated peptides and can be used to quantify the amount of each present in the sample at each time point.

Modification site mapping

Post translational modifications are a wide variety of chemical additions than can occur on many different amino acids. They can influence activity, signaling, and even protein longevity. Mass spectrometry is a valuable tool used to identify these modifications. Using full scan analysis of trypsin-digested peptides, modified peptides can be identified by a mass shift equivalent to the added modification. This measurement will allow identification of the modified peptides and what modification is present. To determine the location of this modification a second scan is employed following fragmentation. This MS/MS scan takes place after a specific (modified) peptide has been selected for isolation. Following isolation, the peptide undergoes fragmentation such as collision induced dissociation (CID), which will break the peptide bonds. This fragmentation method results in neutral losses of individual amino acid from the parent peptide. The resulted peptide fragment masses will be seen in the MS/MS scan showing C-terminal retaining Y ions and N-terminal retaining B-ions. The amino acid which contains the modification will display a mass shift equal to that of the modification at the respective B or Y ion

location. This method will allow us to determine the exact location of the modification. Finally, this peptide can be quantified using the area-under-the-curve created by the intensity of the peptide signal over the time the signal was present. This quantification method will allow us to compare relative abundance of modified peptides to non-modified peptides.

Materials and methods

Stable isotope labelling in cell culture

Stable isotope labelling in cell culture (SILAC) was performed as previously described [94] on HepG2 cells in a preliminary study by a previous member of the lab. In brief, heavy L-arginine (R) (^{13}C6, ^{15}N4) and L-lysine (L) (^{13}C6, ^{15}N2) isotopes (Sigma Aldrich) were supplemented into R&L depleted Dulbecco's modified eagle medium. HepG2 cells were cultured in either the heavy labelled medium or normal medium (light labels) to integrate the labels into the proteome. Following multiple passages heavy labelled cells were treated with 200 mM ethanol for 4-hours. Control samples were treated with PBS. All cells were collected following the 4-hour treatment. Cells were lysed with 2% SDS and following protein isolation and quantification samples were mixed at a 1:1 heavy: light protein concentration ratio. Samples were prepared using the filter-aided sample preparation method followed by desalting on a C_{18} column and placed under vacuum until dry.

Western blot analysis

Western blot analysis was performed as previously described by Bell-Temin et al. [94]. In brief, proteins were separated by SDS-PAGE and transferred to nitrocellulose. S Ponceau stain was used to confirm complete transfer. Blocking was performed with 5% dry milk in PBS containing 0.1% Tween 20. The blot was incubated in the primary antibody overnight at 4° C with rabbit polyclonal anti-PHPT1 (SC-130229, Santa Cruz). PHPT1 primary antibody binding was detected by incubation with goat anti-rabbit secondary (1:10000, Cell Signaling Technology) and activation by picomolar sensitive chemiluminescent reagents (Pierce). Images were developed on film and quantified using densitometry with Image J. Intensity's were

normalized against GAPDH with a rabbit polyclonal anti-GAPDH antibody (1:5000, Cell Signaling Technology) following stripping and reprobing.

Results and discussion

The initial study with HepG2 cells showed a two-fold increase in PHPT1 oxidation following acute ethanol exposure compared to the control samples that were untreated. The western blot analysis revealed that this occurred independent of expression change as PHPT1

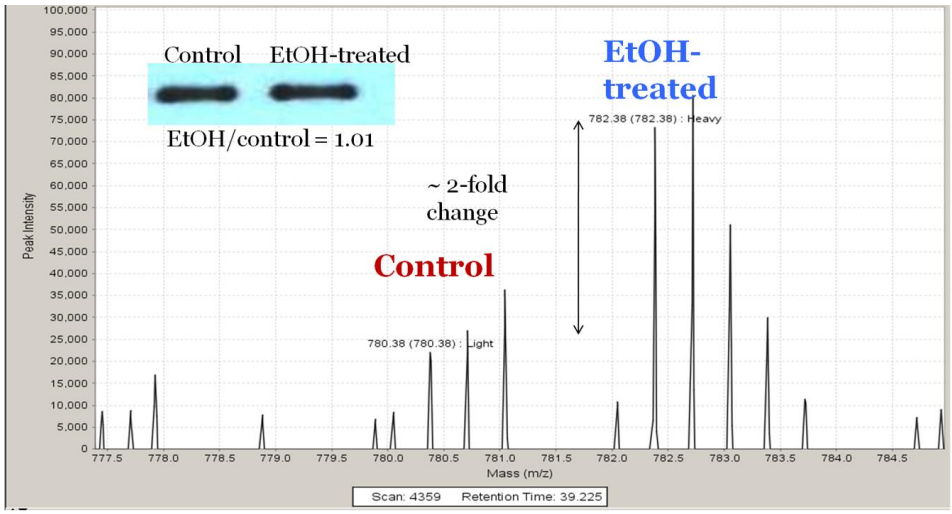

Figure 5. **Acute ethanol exposure study.** *SILAC* based *p*roteomic data shows PHPT1 oxidation increases 2-fold after 200 mM ethanol treatment for 4 hours, but protein expressional levels remain the same (Western blot image, top left) in human hepatocyte-like cells (HepG2 cells).

abundance was the same after 4-hour ethanol exposure (Figure 5). To verify the ethanol-mediated targeted oxidation of PHPT1, we performed modification site mapping using human recombinant PHPT1 (hPHPT1) to determine if targeted oxidation of PHPT1 was taking place following ROS exposure. Furthermore, we determined the influence of this modification on the phosphatase activity of PHPT1 using a novel mass spectrometry-based phosphohistidine phosphatase assay, a colorimetric phosphatase assay, and explicit solvent molecular dynamic simulations. The remaining results are contained in previously published work [65] and are contained in Appendices A and B. This article has been reproduced with the consent of the publisher (Appendix C).

Chapter 3: Development and characterization of phosphohistidine phosphatase 1 knockout and overexpression models in *Mus musculus*.

Summary

Phosphohistidine modification and signaling in mammalian models has not been well characterized despite its importance in other cell types in mechanisms such as two component histidine kinase signaling in bacterial models [59]. The presence of a known phosphohistidine-specific phosphatase in mammals, PHPT1, further suggests phosphohistidine plays a crucial role in cellular functions. In this study, we use two methods to create a PHPT1 overexpression and knockout model for further understanding phosphohistidine signaling. The overexpression method employs an adenoviral-based construct for liver-specific overexpression, and the knockout was achieved using cre recombinant-based gene recombination. Furthermore, these models were both characterized using high resolution mass spectrometry-based proteomics to further validate the models and provide insight into the influence of phosphohistidine signaling manipulation. These models allowed us to identify PHPT1 as embryonically lethal and determine novel key regulators influenced by its expression. Implementation of these models in future studies will lead to further insight into the role of phosphohistidine signaling and PHPT1 regulation in mammalian cells.

Introduction

Phosphohistidine phosphatase (PHPT1) was discovered in porcine liver in 2002[41]. PHPT1 shows phosphatase activity toward phosphohistidine residues *in vivo* and can catalyze the dephosphorylation of phosphoramidate [43] and phospholysine [44] *in vitro*. PHPT1 has only a few known targets include KCa3.1 calcium ion channel [39], ATP-citrate lyase [35], and G-

protein (β subunit) [37]. Given the robustness of phosphohistidine modifications predicted to occur in mammalian cells it is likely that there are many other targets of PHPT1 yet to be elucidated [87]. Additionally, the effect of PHPT1 expression on cellular function *in vivo* has yet to be fully understood. Studies investigating the effects of PHPT1 knockdown have been performed in a few different cell types. In pancreatic β cells and neuronal cells, PHPT1 has been shown to influence important pathways, such as insulin secretion and cell proliferation, respectively [45, 46]. PHPT1 overexpression has also been performed on cancer cell lines, showing PHPT1 plays a role in cell migration and possibly epithelial-mesenchymal transition (EMT) [51, 66]. These studies show that PHPT1 expression has influence on critical cellular pathways throughout the mammalian system. PHPT1 expression is shown to be most elevated in heart, spleen, liver, muscle, and brain tissues [41, 95]. PHPT1 is also part of the Janus family of proteins according to the family domain classification available on the Universal Protein Resource (uniport.org), which are best characterized in *Drosophila melanogaster* and involved in sex differentiation during development [49]. It is the only known phosphohistidine phosphatase to be a part of this family of proteins.

PHPT1 targets phosphorylated histidine residues for removal of the phosphate group from the amino acid [41]. Phosphohistidine is also not well characterized. The modification is best known for its acid labile nature [56], which makes it more difficult to study than the well characterized phospho- serine, threonine, and tyrosine residues [96]. Phosphohistidine can take place at the N-1 or N-3 on the imidazole side chain [36]. The N-1 modification is generally less stable and most often occurs as an intermediate on phosphatase or kinase enzymes during phosphate group transfer between ATP and the substrate [97]. Histidine residue on these enzymes are often the catalytic amino acid, which is the case for H53 in PHTP1 [62] as well. The N-3 modification is associated with long-term phosphorylation and requires a kinase and phosphatase for addition and removal [87]. Targets of this kind of phosphohistidine modification

include those of PHPT1 as well as histone H4 (which is shown to be a target of PHPT1 *in vitro* but not *in vivo*) [38, 43].

Despite the lack of knowledge currently on phosphohistidine signaling in mammals, it is still estimated that 6% of protein phosphorylation occurring are phosphohistidine modifications [87]. This modification has been shown in well characterized species and mammals to cause activation/inhibition and influence signaling of molecules. Therefore, PHPT1, a phosphohistidine specific phosphatase, is likely a key player in many pathways via phosphohistidine regulation. Canonical pathways regulated by phosphohistidine can be elucidated using PHPT1 expression manipulation followed by proteomic analysis. Using an *in vivo* mouse model will provide a model with high translational potential due to similarity with the human proteome. Furthermore, characterization of the PHPT1 expression in a large vital organ such as the liver will provide ease in targeting, large quantity of tissue available per animal, and insight into consequences of influencing liver regulatory pathways, which are key for the entire organ system function.

Expression manipulation has been achieved in two ways. Overexpression of PHPT1 was assessed using a tail-vein injection method of adenoviral vectors encoding for PHPT1 and enhanced green fluorescent protein (eGFP) control viruses with an albumin promoter (for liver specificity). This method has been previously described in Wilson *et al* [98]. Adenoviral vectors were obtained and constructed by Vector Biolabs (Pennsylvania). To create the knockout model, male and female C57BL/6J PHPT1tm1.1(KOMP)Vlcg heterozygous(het) mice were created by the KOMP repository at University of California (UC) Davis through cre-mediated deletion with a LacZ gene substitution. These mice were obtained at 4-6 weeks old and were cross bred with C57BL/6J wild-type mice to confirm fertility and for colony establishment. Characterization was performed using discovery-based proteomics, allowing us to take a snapshot of proteomic changes induced by PHPT1 expression alteration. With this study, we hope to further understand the role PHPT1 plays in cellular regulation in vivo.

Materials and methods

Adenovirus animal models

Male C57BL/6J mice were obtained from the Jackson Laboratory and fed a standard rodent chow and water ad libitum, whilst maintained on a 12h light and dark cycle. Adenoviral vectors encoding for PHPT1 and eGFP control viruses with an albumin promoter (for liver specificity) were obtained and constructed by Vector Biolabs (Pennsylvania). Mice were injected with 1X109 plaque-forming units (pfu) of adenovirus via tail vein at 10-12 weeks of age. Mice were sacrificed 5 days later for gene expression analysis. All animal studies were performed in compliance with IACUC approved protocols by the University of South Florida.

Cre recombinant animal models

Male and female C57BL/6J PHPT1tm1.1(KOMP)Vlcg heterozygous mice were created by the KOMP repository at University of California (UC) Davis through cre-mediated deletion with a LacZ gene substitution. These mice were obtained at 4-6 weeks old and were cross bred with C57BL/6J wild-type mice to confirm fertility and for colony establishment. Tail snips were obtained for genotype verification. Mice were sacrificed at 15 weeks old and multiple tissues were obtained and immediately snap frozen in liquid nitrogen for preservation to be used for phenotyping and characterization.

Genotyping

Tail snips were obtained from mice less than 21 days old for DNA extraction. DNA purification was performed using the GeneJET genomic DNA purification Kit (K0722, Thermo Scientific) according to the manufacturer's instructions. PCR primers for both the PHPT1 and LacZ+ gene were provided by UC Davis, and PCR's were performed using a PTC-200 thermo cycler (MJ Research) at UC Davis specified parameters. DNA separation was carried out on a 1% agarose gel in Tris Borate EDTA (TBE) buffer (Thermo Scientific) with 0.1% ethidium bromide. Visualization was completed using the LICoR AI600 instrument with UV light exposure of less than 0.5 sec.

Phenotyping

PHPT1 expression levels were determined using western blot analyses of various tissue types. Tissues were homogenized in a 125 mM Tris buffer with protease and phosphatase inhibitors on ice. Protein extraction was performed in a 4% SDS buffer at 95° C followed by sonication and centrifugation for protein purification. Protein quantification was performed using the Pierce 660 nm protein assay solution (Thermo Scientific) supplemented with an ionic detergent compatibility reagent (Thermo Scientific) on a 96 well plate. Three technical replicates were used for each sample and two for each BSA standard. Western blot analysis was carried out using TGX any KD gels (Bio-Rad) followed by a semi-dry transfer to either nitrocellulose or PVDF membranes. Nitrocellulose membranes were Ponceau stained immediately following transfer for confirmation of equivalent loaded total protein. PHPT1 was probed for using a 1:500 dilution in 5% BSA of the N-23 anti-PHPT1 antibody (SC-130229, Santa Cruz). A 1:5000 dilution in milk of the HRP conjugated goat anti-rabbit secondary (Cell Signaling Technology) was used. Development was carried out using SuperSignal chemiluminescent reagent (Thermo Scientific) and signal intensity was measured on the AI600 (LICoR) instrument. Loading control was carried out using either a 1:2000 dilution of anti-GAPDH (Cell Signaling Technology), or 1:1000 dilution of anti-β-actin (Cell signaling technology), depending on the tissue type, and a 1:5000 dilution in milk of an HRP conjugated rabbit anti-mouse secondary (Cell Signaling Technology).

Further quantification analysis was performed using an eGFP ELISA kit (Abcam, ab171581). The procedures were followed according to the manufacturer, in brief, standards were created in technical duplicates and samples in technical triplicates and PBS was used for the blank. Wells contained 100 µl of either samples or standard as well as 10 µl of the balance solution and 50 µl of the conjugate solution. Plate was mixed for 1 hour at 37° C. Following washing, 50 µl of substrate A and B were added to each well and incubated for another 15 min at 37°C. The reaction was halted with 50 µl of Stop solution and read on a microplate reader

(Versa Max, Molecular Devices) at 495 nm. Results were calculated using SoftMax Pro software (version 5.4.1) based on a 4-parameter logistic standard curve fit.

Mass spectrometry-based phenotypic characterization

Following protein extraction from liver tissues, 150 µg of protein from tissue lysates were prepared for mass spectrometry analysis using the filter aided sample preparation (FASP) method previously described [75]. In brief, samples were placed on a 30kDa filter spin column (Millipore) and washed with 8 M urea to remove any detergents. Buffer exchange was followed by N-terminal alkylation and reduction using Idoacetamide and DTT respectively. Samples were then trypsin/Lyc-C digested (Promega) overnight at 37° C and eluted with 50mM Ammonium bicarbonate and 0.5 M sodium chloride. Samples were then desalted using a Sep-Pak C_{18} desalt columns (Waters). Following centrifugation under vacuum until dryness, samples were resuspended in 0.1% formic acid for mass spectrometric analysis.

Generated peptides were separated using a reversed phase PepMap100 C_{18}, 3 µM, 100 Å, 75 µM I.D. X 50 cm nanoviper column (Thermo), with a PepMap100 C_{18}, 3 µM, 100 Å, 75 µM I.D. X 2 cm cap trap (Thermo), on an Ultimate 3000 (Thermo Fischer) HPLC system over a two-hour gradient (5-40% acetonitrile in 0.1% formic acid). Mass spectrometric analysis was performed by a hybrid quadrupole-Orbitrap instrument (Q-Exactive Plus, Thermo), using a top 10 data-dependent acquisition method with a dynamic exclusion time of 20 seconds. Full scan and MS/MS resolution was 70,000 and 17,500 respectively. High-resolution MS data were then searched against the Uniprot mouse proteome database using the MaxQuant (1.6.0.16, maxquant.org) search algorithm. Variable mods included phosphorylated serine, threonine, and tyrosine, and methionine oxidation. First search peptide tolerance was 20 ppm and the main search peptide tolerance was 4.5 ppm. Identifications were accepted at a protein and peptide false discovery rate of less than 1% and overall localization probabilities of ≥95% for modified peptides.

Normalized protein abundances were organized as label free (LFQ) intensities in the protein groups file generated by MaxQuant. Further LFQ statistical filtering was performed using Perseus (version 1.6.0.7, http://www.perseus-framework.org/) software to determine significantly differentially expressed proteins between treatment groups. Significant protein expression fold changes between groups were uploaded to Ingenuity Pathway Analysis (IPA) (Qiagen) for a bioinformatic analysis revealing predicted upstream and downstream regulators as well as activated/inhibited pathways. IPA results were used for phenotypic characterization of PHPT1 overexpression and knockout models and key regulators identified were validated by western immunoblotting. Liver samples were compared between male PHPT1 and eGFP overexpression, with male het and wild-type mice of similar ages.

Statistical analysis

Data are presented as means with error bars representative of ± standard error. Statistical significance was determined by an unpaired, two-tailed, Welch modified T-test. Microsoft Excel (Office 365, 2012) and Perseus (version 1.6.0.7, http://www.perseus-framework.org/) were used to perform statistical analyses of PHPT1 and eGFP overexpression as well as PHPT1 het and wild-type data. Proteomic dataset filtering utilized a Z-score for each protein determined statistically significantly by Welch's t-test for additional filtering of LFQ data. This method has been used previously to produce highly efficient discriminative analysis of LFQ data [76].This Z-score for each protein reflects the difference between the fold change of that protein and the mean fold change of all proteins, relative to the standard deviation of the population [99]. Proteins with a Welch modified t-test value of <0.05 and a $|Z\text{-score}|>1$ were deemed significant and uploaded for Ingenuity pathway analysis.

Results and discussion

Validation of adenoviral PHPT1 expression in mouse models

To study the effects of PHPT1 overexpression in vivo in male C57BL/6J mice adenoviral based injections were used. Adenovirus has been shown to specifically target the liver [98]. In

addition, an albumin promoter was added to the viral vector to increase liver specificity. This methodology is advantageous in that it allowed us to specifically target a single organ in adult mice to prevent any adverse effects of PHPT1 expression on development. Mice injected with either the PHPT1 or eGFP viral constructs showed liver specific overexpression and no change in expression in the spleen or other organs. Western blot of PHPT1 expression showed a

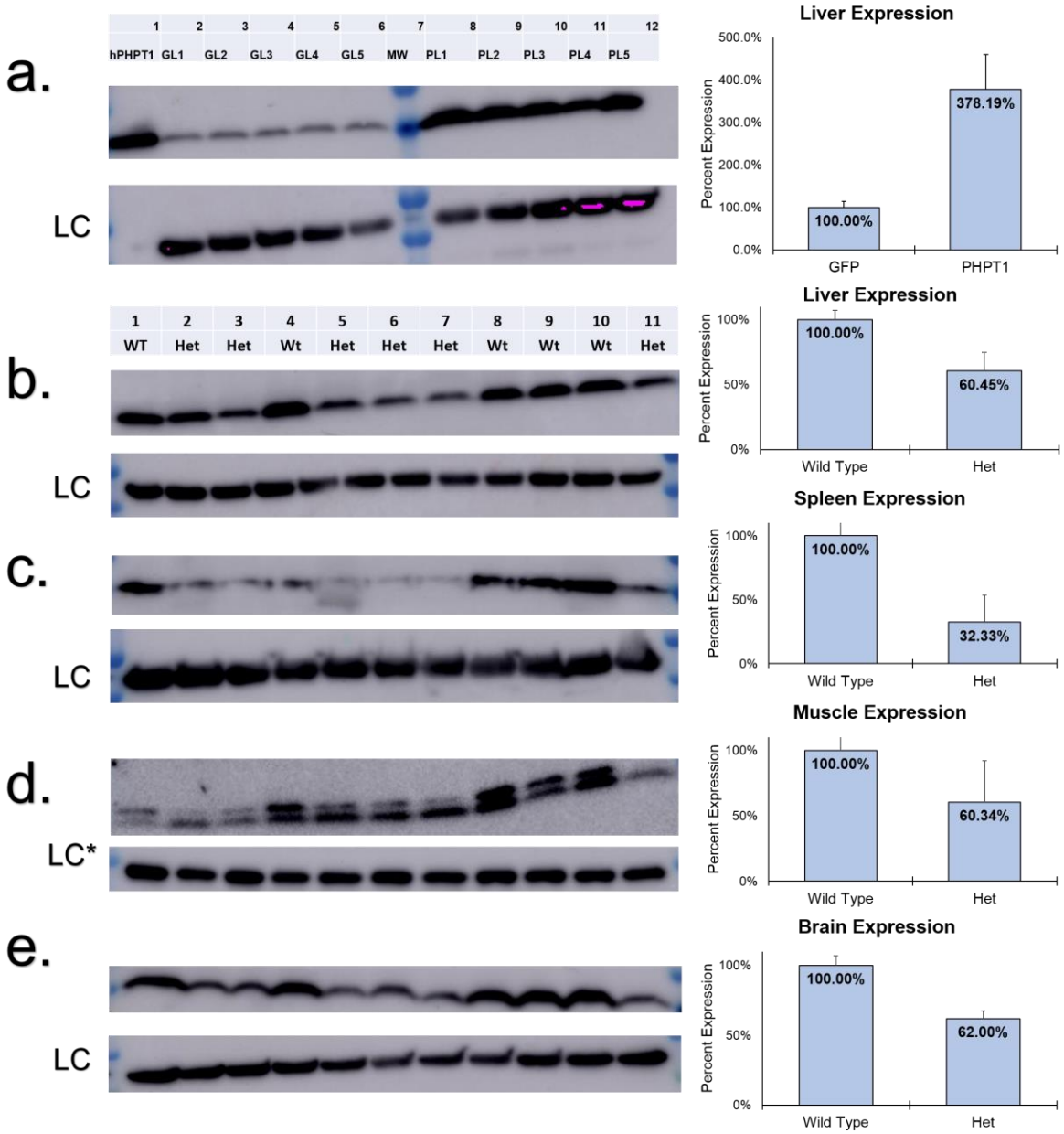

Figure 6. PHPT1 expression validation. PHPT1 expression was measured by western blot in Ad-PHPT1 (PL) mice, Ad-eGFP mice (GL), wild-type mice, and PHTP1 heterozygous mice and normalized to either a β-actin (LC) or GAPDH (LC*) loading controls. a.) PHPT1 showed a significant 3-fold increase in expression following Ad-PHPT1 injection as compared to the Ad-eGFP. b-e.) PHPT1 expression showed, on average, a significant decrease of approximately 50% in the heterozygous mouse tissues b.) liver, c.) spleen, d.) muscle, and e.) brain when compared to the wild-type.

significant increase in PHPT1 expression compared to the eGFP mice, 5 days post injection (Figure 6a). To further validate this overexpression model and liver specificity eGFP translational expression was confirmed using an ELISA kit to measure absolute protein expression. EGFP expressing liver samples showed approximately 2 ng/ml of GFP as compared to less than 0.1 ng/ml in the PHPT1 liver samples and both spleen samples.

In the knockout model, phenotypic validation of PHPT1 expression was performed on tissues known to highly express PHPT1 in wild-type mice (liver, spleen, muscle, and brain). PHPT1 protein expression in the het mice was seen to significantly decrease on average by approximately 50% in liver, spleen, muscle, and brain tissues as compared to the wild-type (Figure 6b). This result is concurrent with the genotype data in which the het mice contain only one of the two alleles for PHPT1 expression. These data suggest that PHPT1 transcription and translation are reduced organism wide by 50%.

Breeding colony development and validation

Male and female C57BL/6J mice were genetically modified at the KOMP repository with a PHPT1tm1.1(KOMP)Vlcg method. This method created heterozygous mouse with a non-conditional knock-out *lacZ* gene. Genotypes of these mice were initially confirmed using tail-snip

	Het-Het cross breeding statistics				
Ratio of 1:2:1 Wt:Het:KO	K pairs	Het	WT	KO	Total
	Actual	96	32	0	128
	Expected	64	32	32	128
	Deviation	-32	0	32	
	Deviation^2	1024	0	1024	
	d2/e	16	0	32	48

Table 1. **Breeding statistics from het-het crosses.** Het males were bred with het females in a cross that should result in a 1:2:1 ratio of wild-type: heterozygous: knockout according to Mendelian genetics. Following genotyping and a chi squared analysis of offspring genotyping from over 20 crosses it was determined with a >99% probability that this is not following Mendelian inheritance genetics.

DNA amplification of PHPT1 and the *lacZ* recombinant gene through a PCR analysis. The wild-type mice displayed expression of only the PHPT1 gene, whereas the heterozygous knockout (het) showed expression of both the PHPT1 gene and the *lacZ* reporter gene. These mice were bred, and offspring were similarly genotyped to determine the viability of a full PHPT1 knockout. Following multiple het-het crosses (n>20) genotyping revealed no post embryonic complete PHPT1 knockout mice. This result suggests a full knockout of PHPT1 is dying *in-utero*. A chi-square test of the total offspring born from these crosses (N=128) allows us to say with >99% probability (2 degrees of freedom), that the het-het crosses do not follow the expected Mendelian genetics (Table 1). Possible mechanisms for this lethality were not investigated, however, many of the pathways that PHPT1 is known to be associated with could be involved in this mechanism.

Age expression validation of PHPT1

After expression validation of PHPT1 models was complete we determined if the expression of PHPT1 was dependent on the age of the mouse considering our different model validations came from varying age ranges. Liver from 11-18 weeks old mice were extracted from both sexes and compared to each other and the 8-10-week-old mice used for the ethanol exposure models (Chapter 4). Expression validation was performed using a western blot against PHPT1 and a β-actin loading control. There was no significant difference between PHPT1 expression regardless of age group or sex. Through these results, we were able to conclude that age and gender does not influence PHPT1 expression levels.

PHPT1 animal model characterization

Following the creation and validation of our PHPT1 overexpression and knockout models, we wanted to further characterize the influence of PHPT1 expression and phosphohistidine signaling on liver function. Global proteome levels where measured using

high-resolution mass spectrometry from liver extracts from eGFP, PHPT1 overexpression, wild-type, and Het mice. Mass spectrometry intensities were used to further validate PHPT1 expression between samples. Data showed a 13-fold increase in PHPT1 expression compared to the eGFP mice and a 2-fold increase from the het to the wild-type mice (Figure 6a & b). These data coincided with our western blot analysis data used for initial validation.

Using high-resolution mass spectrometry proteome expression data, we next investigated key regulators, pathways, and possible downstream targets influenced by PHPT1 expression changes. These results were elucidated using the core analysis feature in Ingenuity Pathway analysis, which predicts these factors based on experimentally provided expression fold-changes. IPA utilizes a z-score algorithm, in which a z-score of greater than 2 or less than -2 represents activation or inhibition, respectively. The p-value of overlap represents the overlap in targets influenced by the regulator or pathway and those identified experimentally as significantly changed. A low p-value of overlap represents a key regulator that shares many targets influenced by our experimental treatment, in this case PHPT1 expression.

	-Log10 Pvalue of Overlap	
Upstream regulators	**PHPT1 Het**	**PHPT1 OE**
MYC	2.017	1.885
HSD17B1	2.220	2.189
17β-estradiol	1.701	2.745
Canonical pathways		
Cytotoxic T Lymphocyte-mediated Apoptosis of Target Cells	3.234	0.000
Nur77 Signaling in T Lymphocytes	2.690	0.000
Type I Diabetes Mellitus Signaling	2.160	0.000
S-methyl-5'-thioadenosine Degradation II	0.000	2.113
α-tocopherol Degradation	0.000	1.937
Glycogen Degradation II	0.000	1.616

Table 2. Overlap of PHPT1 expression targets with upstream regulators and canonical pathways. Ingenuity Pathway Analyses (Quiagen) calculates a pValue of overlap between identified significantly influenced proteins and the know targets of upstream regulators or canonical pathways. Shown is the –log10 pvalue of overlap for the top3 regulators and top3 canonical pathways in each comparison (heterozygous induced (PHPT1 Het) and PHPT1 overexpression induced (PHPT1 OE)). A significance of 1.30=0.05 and 2=.01 pvalue.

Bioinformatic analysis of protein expression fold changes revealed both PHPT1 overexpression and knockout models shared significant overlap of downstream targets with key regulators HSD17B7, 17β-estradiol, and MYC (Table2). HSD17B7 is involved in steroid and

cholesterol regulation via 17β-estradiol synthesis and 3-ketosteriod reductase function [100]. MYC and 17β-estradiol are regulators of cell survival [101] and proliferation [102], respectively, and both well-known players in cancer development [103, 104]. Although, both PHPT1 overexpression and knockout induced expression changes have significant overlap with these regulators, it appears they are influencing these processes through unrelated mechanisms.

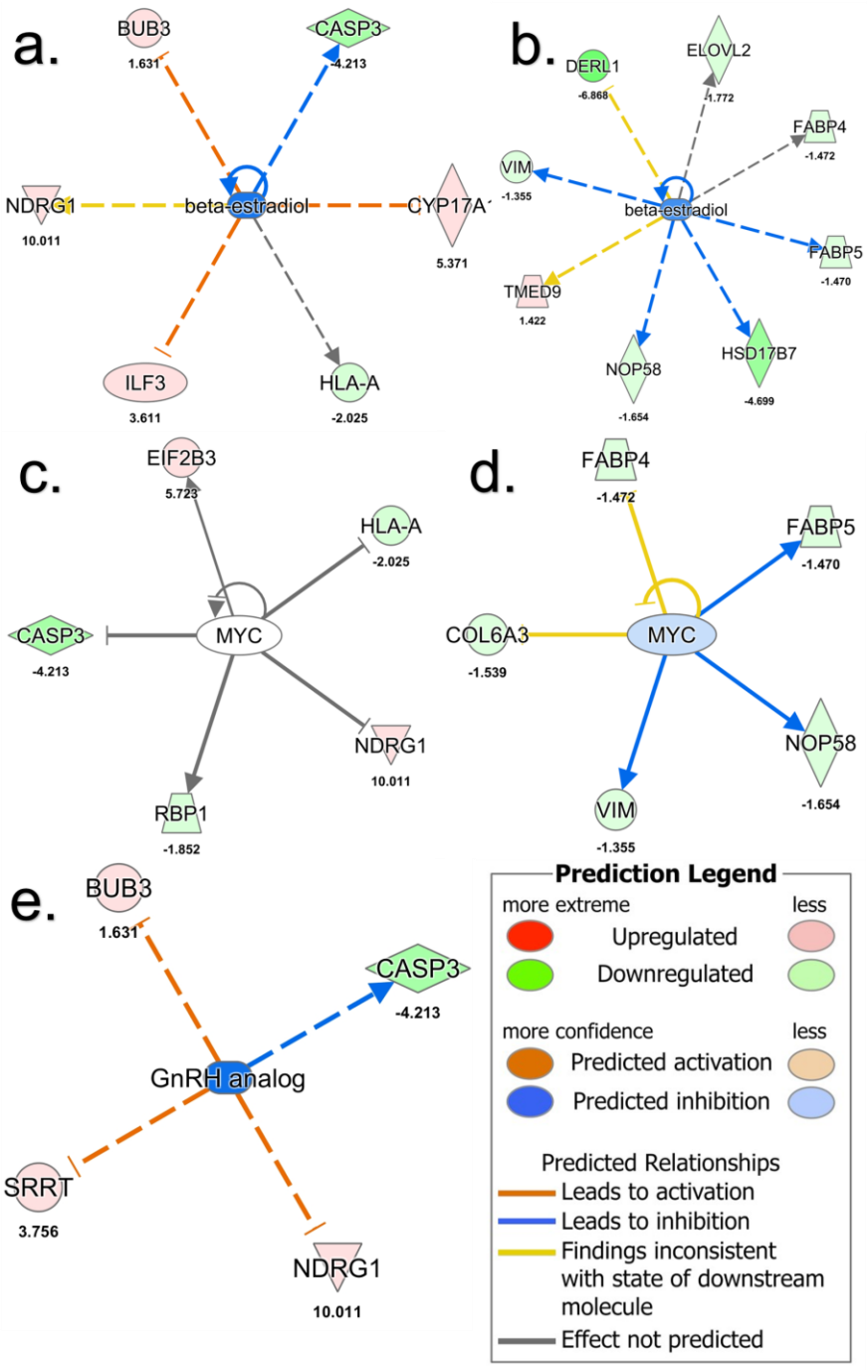

Figure 7. Predicted upstream regulator networks. The networks displayed show the proteins identified to be significantly influence by PHPT1 expression and their respective fold changes as the outer nodes and their predicted influence on the upstream regulator as the inner node. The pathways are split by PHPT1 expression with the left (a, c, and e) and right (b and d) being PHPT1 knockout and overexpression respectively. a-d.) have significant p-Values of overlap but figure e.) has a significant z-score (-2).

Furthermore, the proteins influenced by each PHPT1 expression state differ greatly. The proteins identified as significantly influenced and overlapped with these regulators were unique to each PHPT1 condition (outer nodes Figure 7a-d). PHPT1 knockout identified the GnRH analog as the unique regulator to be predicted as significantly influenced by expression changes (Figure 7e). PHPT1 overexpression did not identify any regulators as significantly influenced (-2<z-score>2).

Furthermore, the overlap with the top 3 canonical pathways of each condition do not coincide (Table 2), and there were no pathways identified with significant overlap in both conditions. However, the pathways identified in each condition give much insight into possible mechanisms being influenced by PHPT1 expression. PHPT1 overexpression changes show overlap with three pathways of degradation. The glycogen and S-methyl-5'-thioadenosine degradation pathways are often a result in an increase of cell proliferation and transcriptional activation [105, 106]. In addition, the degradation of α-tocopherol is in response to an increase in antioxidant production [107] and leads to an increase in β-oxidation via the production of α-carboxyethylhydroxychroman [108]. Alternatively, the heterozygous PHPT1 model has significant overlap with two pathways that lead to lymphocyte-mediated apoptosis (Table 2). Specifically, in the Nur77 signaling pathway, apoptosis is activated via Nur77 interaction with RXRα [109]. In addition, overlap is observed with diabetes type 1 signaling. This kind of signaling originates from incomplete hormone response between the liver and the kidney[110]. All three of these pathways were identified due to the measured decrease expression of CASP3 and MHC I. MHCI is one of many known upstream indicators of all three pathways, and CASP3 is a common downstream indicator of pathway activation. CASP3 inhibition is also an indicator of cell survival as its activation is necessary for apoptosis[111]. These pathways of overlap reflect a PHPT1 overexpression phenotype which is thriving and prepared for an oxidative stress response, and a heterozygous phenotype that seems to be reacting to an external stress

already. The only difference between the two cell types is the initial expression levels of PHPT1 and the resulting potential change in phosphohistidine modifications.

Conclusions

The significance of phosphohistidine signaling in mammals is yet to be fully understood. Despite its likelihood of being highly utilized in key pathways and functions, it remains one of least understood phosphorylation modifications, especially compared to phospho- serine, tyrosine, and threonine. Implications of further understanding the role of phosphohistidine signaling go beyond just understanding cellular mechanisms. Phosphohistidine has been shown to play roles in various diseases, including many forms of cancers [52, 53, 66, 67, 112] and pancreatic diseases such as type II diabetes [46]. In this investigation, we created and characterized much-needed animal models for investigating the role of PHPT1-mediated phosphohistidine signaling.

Adenoviral-based constructs have previously been shown as effective tools for inducing liver-specific overexpression of a protein of interest. In our study, we effectively used this to create a liver-specific PHPT1 overexpression model. This model shows a significant increase in PHPT1 overexpression that can be maintained for several weeks (see Chapter 4: Expression Validation). In addition, the creation of the PHPT1 overexpression model requires very little time and provides an easily reproducible method for inducing PHPT1 overexpression. Our characterization of this model provides insight into the impact decreased phosphohistidine levels have on liver homeostasis. In addition, these data provide a reliable control to compare to treated PHPT1 overexpression models. The ease and specificity of this method gives it the potential to be utilized for organ-specific siRNA mediated knockdown, in addition to overexpression. We intend to apply this method for liver-specific PHPT1 knockdown in future studies.

However, we did create and characterize a knockout model employing the Cre-mediated recombinant heterozygous mice provided by the KOMP repository at UC Davis. We validated the genomic expression and translational expression of PHPT1 in this model across multiple tissues. We demonstrated that this model is a valid animal-wide PHPT1 heterozygous knockout. Further characterization of liver tissue from this model was done to create a direct comparison with our overexpression model. This characterization provides two benefits: we now have a base model for experimental comparison and we gained insight into the influence of increasing phosphohistidine signaling on an organism-wide level.

We also determined for the first time that PHPT1 is an embryonic lethal knockout in C57BL/6J mice through offspring genotyping and Mendelian genetic comparisons. This discovery adds to the potential importance PHPT1 has in cell regulation and highlights it is a necessary protein during embryonic development. PHPT1 is part of the Janus family of proteins which are well characterized in *Drosophila melanogaster* as proteins involved in sex differentiation and development. So, it is likely PHPT1 may have similar roles in mammalian development that have yet to be determined. Furthermore, PHPT1 overexpression has been shown to be involved in EMT in cancer cells [67]. This study further suggests that PHPT1 and phosphohistidine are involved in regulating cell differentiation. A complete PHPT1 knockout could be disturbing the fragile differentiation of cells during development, leading to embryonic lethality. Further investigation of the mechanisms involved in PHPT1-induced embryonic lethality are needed.

Most importantly, characterization of these two models reveals PHPT1 expression has a wide range of influence on cellular functions. It appears that overexpression and knockout of PHPT1 impacts cellular function through distinct mechanisms that do not coincide. PHPT1 knockout experiments in cell cultures have been shown previously to influence ACL expression [45], and cell movement [51]. Furthermore, PHPT1 overexpression studies, have been

correlated to cell viability [45], cell proliferation [66], and insulin regulation [46] via ACL function. Our study shows a great amount of overlap in expression targets with these mechanisms. However, we reveal varying signaling pathways induced by PHPT1 overexpression versus the heterozygous mouse model. Further investigation into how PHPT1 expression is interacting with the downstream targets is necessary to better understand the significance of phosphohistidine signaling in the mammalian liver.

Chapter 4 – The influence of PHPT1 expression on ethanol-induced hepatic steatosis during chronic ethanol exposure

Summary

Following characterization of both the PHPT1 overexpression and knockout models, further investigation of the influence of PHPT1 expression on ethanol-induced hepatic steatosis was investigated. Initial studies of the 10-day chronic plus binge ethanol mouse model confirmed the model validity. Overexpression of two key ethanol response proteins CYP2E1 and EPHX1 were identified (Figure 8a). In addition to model validation, this initial study determined PHPT1 expression to be significantly decreased following chronic ethanol exposure

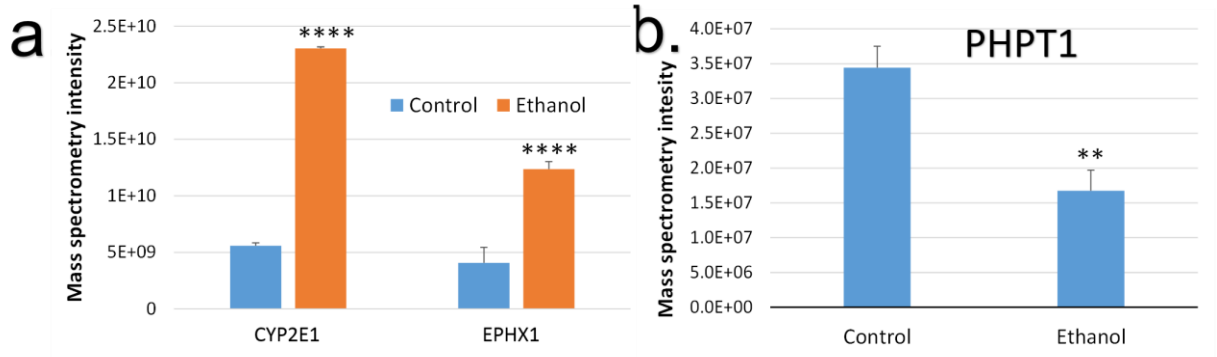

Figure 8. Expression changes induced by chronic ethanol exposure . The above graphs show changes in expression between the control and ethanol pair-fed mice. a.) CYP2E1 and Ephx1 are known markers of chronic ethanol exposure and are upregulated as expected in this model (****pValue<0.0001). b.) PHPT1 was shown to be downregulated following chronic ethanol exposure (** pvalue<.01).

(Figure 8b). Further model validation was reflected by the formation of lipid droplets and hepatocyte ballooning seen in the ethanol-treated mouse livers but not in the pair-fed control mice (Figure 9). This discovery led us to further investigate the influence of PHPT1 expression on the onset of alcoholic liver disease and elucidate possible upstream regulators and canonical pathways involved in phosphohistidine signaling.

Both the PHPT1 overexpression and PHPT1 knockout models were administered the 10-day chronic plus binge ethanol exposure model and livers were collected for phenotype characterization. Samples from each treatment group were analyzed for disease progression markers such as AST, ALT, triglyceride levels, and blood alcohol concentration. Samples were also taken for H&E staining to assess the development of steatosis. PHPT1 expression validation was also performed post treatment. Finally, mass-spectrometry based phenotypic

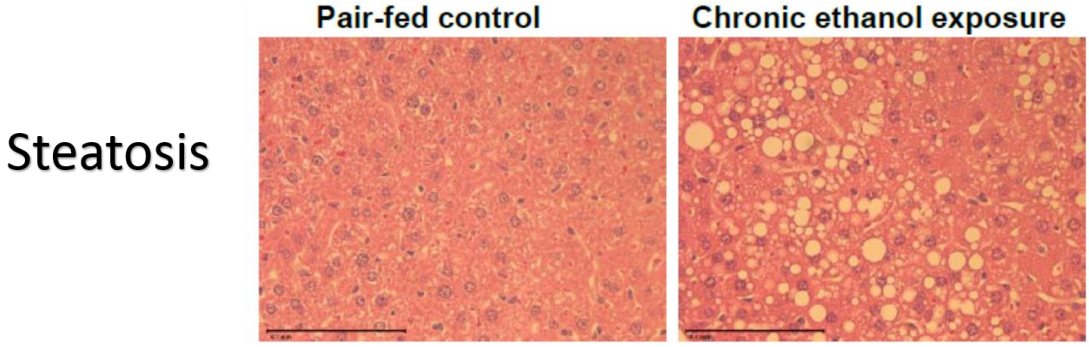

Figure 9. Ethanol-induced steatosis. The H & E stained tissue show the development of fatty liver disease in tissue from animals exposed to the 10-day chronic ethanol model. This induced hepatocyte ballooning and lipid droplet formation in only the tissue from the animal exposed to ethanol treatment.

characterization was done using label free quantitation of liver lysates to determine significantly differentially expressed proteins following ethanol response and between PHPT1 expression cohorts. This information was used to determine upstream regulators and canonical pathways involved in phosphohistidine signaling during chronic ethanol exposure.

Experiments revealed that PHPT1 overexpression mice had a decrease in circulating triglycerides and a lower development of steatosis, which was assessed via independent pathology scoring, than the ethanol treated GFP overexpression control group. However, our PHTP1 heterozygous mice showed additional susceptibility to developing high triglyceride levels and the onset of steatosis. This result was reflected by similar phenotypes observed between the heterozygous control groups which were provided a higher-fat controldiet with no ethanol, and our wild-type ethanol groups. Both groups demonstrated significantly high triglyceride levels and large amounts of hepatocyte ballooning and lipid droplet accumulation. In addition, the heterozygous control group showed increased inflammation and necrosis around the vascular

islets in the liver. This result was also observed in the heterozygous ethanol treated samples, but not in the wild-type control samples. This information suggests PHPT1 expression correlates with the onset of liver steatosis, and possibly plays a role in the development of ALD and non-alcoholic fatty-liver disease (NAFLD).

To further understand the mechanism by which PHPT1 is influencing the development of fatty liver disease, we performed advanced mass-spectrometry based phenotypic characterization. Proteomics allowed us to take a snapshot of the global proteome following the control and ethanol treatments and to quantify changes in protein expression between (patho)physiological states. Furthermore, it also allowed validation of PHPT1 expression and disease progression. Our analysis found that PHPT1 expression was consistently decreased, in the range of 20-60%, following ethanol exposure regardless of its initial expression levels. Furthermore, bioinformatic analysis predicted PHPT1 expression to influence susceptibility of ethanol-induced hepatic steatosis. This susceptability is predicted to be mediated through PPARα/ RXRα pathway regulation as well as regulation of cytochrome P450s via ABCB6 signaling and other transcriptional regulators. These pathways are known players in ethanol metabolism and ROS response [13]; however, they have not previously been shown to be involved in phosphohistidine signaling. Although further validation of these targets is necessary to fully understand the mechanism of PHPT1 and phosphohistidine signaling in these pathways, it is clearly apparent that PHPT1 expression is playing a novel role in liver injury susceptibility.

Introduction

Ethanol-induced hepatic steatosis

The progression and severity of ALD has been widely discussed previously (Introduction: Alcoholic liver disease). As mentioned previously, the progression of this disease begins with the onset of fatty liver or more specifically ethanol-induced hepatic steatosis. The development of this phenotype is characterized primarily by the histological changes that take place in hepatocytes. These changes are induced by overactivation of ethanol metabolism

pathways and result in dramatic changes in lipid homeostasis and cell signaling [11]. Hepatocytes perform the primary role of the liver to remove toxins from the blood stream. Given this, hepatocytes are well suited with a plethora of metabolites and anti-oxidant proteins to compete against moderate ethanol exposure [113]. However, chronic ethanol exposure will interfere with normal ethanol metabolism. This interference occurs in multiple ways, including ROS oxidation, changing in the acetyl-CoA pool, and disruption of fatty acid oxidation [11]. The metabolism alterations directly create visual changes in hepatocyte histology. Development of hepatocyte ballooning and Mallory bodies occurs as a result of the increase in fatty acid production and decrease in fatty acid β-oxidation [13]. In addition, hepatocyte stress leads to recruitment of the resident liver immune cells, Kupffer cells, which release inflammation causing cytokines and interferons [19]. This change results in further liver damage. Often this damage is initially present exclusively surrounding the portal veins where blood first interacts with the liver. However, as these cells become deactivated due to over exposure, this phenotype spreads to the rest of the liver. This damage combined with efforts to replace and repair damaged cells leads to liver swelling, which is often the earliest identified symptom of ALD [13]. However, at this point, fibrosis is occurring, and the development of early stage hepatitis is occurring. At this stage, the potential for minimally invasive full recovery is significantly lower than during initial hepatosteatosis [2]. Unfortunately, without a biopsy, hepatosteatosis is generally asymptomatic. Further understanding in how this disease develops and finding novel mechanisms influenced by chronic ethanol exposure will aid in early identification and prevention.

Mouse models of ethanol feeding

The mouse model has been an exemplary one used to study the onset, progression, and impact of ALD for many years. During this time, many models of exposure have been developed for understanding different facets of disease progression [78]. These exposure models vary by focus of study in the progression of ALD. Models which are developed to look simply at animal

behavior or habituation often give the mouse a choice between ethanol consumption and not [114]. Models looking for short-term exposure or studying the immediate impact of ethanol on the organism will often employ a gavage ranging from 10-1 g ethanol/kg bodyweight depending on the desired severity of the binge. This range gives blood ethanol concentrations (BEC) from 0.5 g/dl to 0.05 g/dl, respectively. Another binge model that has been recently developed uses ethanolinfused gelatin to encourage quick but less forceful consumption [115]. Furthermore, there are many models which investigate the impact of long term or chronic ethanol exposure. These models range from a multichoice consumption [116], to a purely ethanol supplemented diet [77], and even a normal chow but using ethanol vapor to provide consistent ethanol exposure [117]. These models usually aim at inducing reproducible severity of alcoholic liver disease while at the same time having a relevant control that is exposed to the same environmental factors but not ethanol. This accomplishment can be challenging considering the caloric burden and stress ethanol consumption has on an organism.

The model we choose to use is the 10-day chronic plus binge ethanol model, which consists of a liquid 5% ethanol diet for 10 days and is concluded with a 5 g ethanol/kg body weight gavage [77]. The control groups from this model also receive a liquid diet which contains the same calorie contents and are given a gavage supplemented with maltose dextrin equal in calories/volume to that of the ethanol diet. This model is well characterized in creating moderate to severe liver steatosis (Figure 8). This phenotype is validated by H&E stained liver sections developing motifs such as hepatocyte ballooning, lipid droplet, and Mallory body formation (Figure 9) [77]. In addition, liver injury is characterized further by showing an increase in the amounts of circulating ALT, AST, and triglyceride levels as compared to the pair-fed controls. In human models, the ratio of AST/ALT levels have been shown to indicate severity of ethanol-induced liver injury [118]. However, in the mouse model, significant upregulation of either of these metabolites are considered a marker of ALD [77]. We have also verified that known

ethanol-induced expression changes are taking place on proteins such as CYP2E1 and EPHX1 (Figure 8a), which are both known to be upregulated following chronic ethanol exposure [24]. It was also found the PHPT1 expression levels are down regulated following the exposure model as well (Figure 8b). This led us to investigate further how expression of PHPT1 is influencing the onset of this liver injury.

Materials and Methods

10-Day chronic plus binge ethanol diet

PHPT1 expression altered, eGFP induced, and wild-type C57BL/6 mice were split into cohorts for ethanol or control diet treatments. Male and female mice were used for the heterozygous and wild-type cohorts and only male mice were used for the PHPT1 and eGFP overexpression models. Each cohort initially consisted of 3-10 mice per treatment type. This model was based on the publication of Bertola *et al* [77] using the Lieber DeCarli liquid diet formula. In brief, ethanol-treated mice received a liquid diet that was 5% vol/vol ethanol as their only source of nourishment. Control mice received a liquid diet as well that did not contain ethanol but was equivalent in calories per serving. Consumption of this diet was monitored for both groups over 10-days to ensure consistent intake occured between pair-fed groups. Following the 10^{th} day of consumption, ethanol treated mice received a 5 g/kg ethanol/body weight gavage with a 31.5% vol/vol ethanol solution. Control mice receive a gavage consisting of 9g/kg maltose dextrin/body weight with a 45% wt/vol solution. Mice were then sacrificed 9hours later and their blood alcohol concentration, AST, ALT, and triglyceride levels were tested to determine disease severity.

Fluorescence microscopy

Florescence microscopy was carried out on formaldehyde-fixed tissue sample slides prepared by the Moffitt Tissue core. Samples that were not stained were provided and used to

determine eGFP expression via fluorescent excitation. Slides were first treated with a DAPI nuclear counterstain solution (Pierce) to stain the nuclear envelope. This was most effective on single cells near the edge of the formaldehyde-fixation area. Slides were viewed using an UtlraVIEW ERS spinning disk confocal microscope (Perkin Elmer) with a solid-state laser emission at 405nm and image capturing was performed using the Velocity software set to the same parameters for all samples. This instrumentation was provided generously by the CMMB core facilities.

Western blotting

Lysates were derived from control and ethanol diet-treated mouse livers and were analyzed by western blot to verify PHPT1 expression levels. Western blot analysis was carried out using TGX any KD gels (Bio-Rad) followed by a semi-dry transfer to either nitrocellulose or PVDF membranes. Nitrocellulose membranes were ponceau stained immediately following transfer for confirmation of equivalent loaded total protein. PHPT1 was probed for using a 1:500 dilution in 5% BSA of the N-23 anti-PHPT1 antibody (SC-130229, Santa Cruz). A 1:5000 dilution in milk of the HRP conjugated goat anti-rabbit secondary (Cell signaling technology) was used. Development was carried out using SuperSignal chemiluminescent reagent (Thermo scientific) and signal intensity was measured on the AI600 (LICoR) instrument.

Histology

Immediately following sacrifice, liver tissue sections were taken for paraffin-embedding and hematoxylin and eosin staining. Tissue sections were taken from the center of a large lobe of liver tissue and from pair-fed animals in each treatment group. Paraffin-embedding, formaldehyde-fixation and H & E staining was performed at the Moffitt Cancer Center Tissue Core Histology services. Tissues were then analyzed to identify histological motifs of hepatic steatosis including the development of lipid droplets, Mallory bodies, hepatocyte ballooning, and

inflammation. Steatosis scoring was performed on tissues when available based on the presence of these factors. Samples were formaldehyde-fixed to slides and analyzed under 40X magnification using a DM2000 upright fluorescent microscope (Leica) with the SPOT camera and SPOT basic software (Spot imaging) and keeping settings consistent between samples.

Clinical chemistry

Animal serum was removed immediately where approximately 200 ul of whole blood was acquired from each animal and aliquoted for determining metabolite concentrations. Serum was tested for ALT, AST, and circulating triglyceride levels by either assay kits (Point Scientific Inc.) according to the manufacturer's instructions on a PowerWave XS (BioTek) microplate reader shortly after extraction, or it was sent to the Moffitt College of Medicine Vivarium, which used an IDEXX Vettest chemistry analyzer. Metabolite levels where compared between treatment types and sexes to determine relationship of disease state and fold change in metabolite levels.

Blood ethanol concentration

Blood ethanol concentration of each mouse was also quantified using blood serum samples. This method was performed using the BEC kit (Sigma-Aldrich). In brief, serum was spun from the blood samples and 5 µl was diluted at 1:10 for the quantification. BEC standards were analyzed in duplicate and both a negative and positive control was included in triplicate. Each sample was tested in triplicate after adding the activating enzyme and sample absorbance was read on a PowerWave XS (BioTek) microplate reader. Sample concentration varied from 0.005-0.5 g/dl. This concentration translates directly to BEC levels with anything less than 0.08 g/dl considered insignificant and greater than 0.08 g/dl consistent with the binge ethanol consumption model. BEC levels were tested for all mice in which enough serum was able to be extracted.

Label free quantitation of ethanol treated mouse liver samples

Mouse liver samples were obtained from each cohort immediately following the conclusion of ethanol treatment and sacrifice. Livers were preserved by cryo freezing and 35-40 µg biopsies were used for protein extraction. Following homogenization, lysis took place using a 4% SDS, 100 mM DTT, 100 mM Tris-HCl, pH 7.4 at 95° C for 5 minutes. Total protein was quantified using the Pierce 660 assay method supplemented with an ionic detergent compatibility reagent (IDCR) (Pierce). Equal amount of protein was taken from each sample (150 µg) for detergent removal using the FASP method [75]. In brief, samples were washed three times with 8 M Urea on a 30 kDa filtered column (Corning). Proteins were then alkylated using 100 mM iodoacetamide and another buffer exchange was performed to prepare for Trypsin digestion in 50 mM ammonium bicarbonate. Mass spec grade Trypsin/Lys-C was added at a 1:50 ratio to protein for digestion overnight at 37° C. Peptides were then extracted for desalt on Sep-Pak C_{18} columns on a Supelco Vacuum manifold. Finally, peptides were dried and resuspended in MS-grade 0.1% formic acid.

Samples were analyzed on a Q-Exactive plus (Thermo Fischer) in-line with an Ultimate 3000 HPLC (Thermo Fischer). Separation was performed on a 75µm X 50cm reversed phase analytical column, packed with Pepmap100, 3 µm, 100 Å C_{18}. This analytical column was followed by a 75 µm X 2 cm cap trap packed with Pepmap100, 3 µm, 100 Å C_{18}. Samples were run on a 120 min gradient from 2% to 50% B (0.1% formic acid in acetonitrile). Full MS survey scans were performed with a maximum resolving power of 70,000 and 17,500 for MS/MS resolution. Data dependent analysis was performed selecting the top 10 most abundant peptides for MS/MS CID fragmentation analyses with a dynamic exclusion time of 20 seconds. Sample from the same experiment were analyzed concurrently with blanks and quality controls included throughout the sequence.

High-resolution raw MS data files were searched against the *Mus musculus* Uniprot database using MaxQuant (1.6.0.16, maxquant.org) search algorithm. Label free quantification parameters were selected for data normalization in MaxQuant to ensure consistency between samples. Search parameters also included a first search peptide tolerance of 20 ppm and a main search peptide tolerance of 4.5 ppm with a false discovery rate of less than 1% and overall localization probabilities of ≥95% for modified peptides. The resulting normalized protein abundances were used for statistical analysis.

Statistical filtering began with removal of any protein that was not observed in at least two thirds of a single treatment group. All intensities were then log2 transformed for statistical analysis. Perseus software (1.6.0.7, http://www.perseus-framework.org/) was used to determine imputation values, for samples without intensity values, that did not influence the expression distribution of the data. A Welch's t-test was performed between treatment types with a significance threshold of a p-value <0.05. In addition, a Z-score was calculated to determine the significance of the Welch's t-test difference between samples and provide further statistical stringency [76]. Analysis between treatment groups was performed by utilizing a ratio of ratios between treatments and models. To fully elucidate the influence of PHPT1 expression on development of ethanol-induced hepatic steatosis, alike variables between groups had to be offset. This analysis was completed by determining the fold change differences between the control and ethanol groups of the wild-type models and PHPT1 expression-influenced models individually. These ratios were then compared to each other to determine factors that were only affected by the amplified or reduced expression of PHPT1, following ethanol exposure.

To determine possible mechanisms involved in phosphohistidine signaling that are affecting the development of ethanol-induced hepatic steatosis, we uploaded the significantly influenced fold-changes to IPA for a core analysis. This program uses our identified fold-change expression differences to predict regulators, canonical pathways, and disease states being

activated/inhibited, based on their known relationships. This kind of analysis is known as a core analysis and searches the database for all known protein interactions. Analytical data provides a p-value of overlap and z-score of activation for significance. The p-value of overlap represents the likely hood of overlap in targets identified from the data and a regulator or function known to interact with those targets in the IPA database. The z-score represents the likelihood of activation or inhibition of the predicted pathway based on its interactions with the uploaded data. To further understand the mechanisms involved in phosphohistidine signaling following ethanol treatment core analysis of the significantly differentially expressed proteins were performed. Then comparisons between PHPT1 expression models was performed by either taking a ratio of ratios or by comparing the core analyses of the two models directly to each other, using the comparison analysis feature, to differentiate regulators and pathways uniquely influenced from those activated independently of PHPT1 expression. This program provided bioinformatic insight for determining pathways being influenced by PHPT1 expression that have yet to be identified. Using IPA to determine potential targets is an especially invaluable tool in the case of phosphohistidine signaling. Unfortunately, more conventional ways of targeted identification are far more difficult in the case of phosphohistidine signaling due to its extremely labile nature.

Results and Discussion

Expression validation

For the Ad-PHPT1 and Ad-GFP mouse model's initial validation that liver-specific expression remained following the 10-day chronic ethanol exposure was performed. This validation was done using ELISA and microscopy data to assess eGFP expression and western blot data to quantify PHPT1 expression. Additionally, mass-spectrometry data was also used to verify increase expression of both proteins when performing the global proteomic investigation. EGFP expression was shown to remain constant between the control and ethanol-treated samples and showed no significant expression in the Ad-PHPT1 samples (Figure 10a).

Furthermore, fluorescence microscopy was used to visualize the eGFP expression in the Ad-GFP livers. This method was also performed on Ad-GFP spleen tissue and Ad-PHPT1 liver tissue as negative controls. Only the Ad-GFP liver tissue displayed green fluorescence indicative of eGFP expression (Figure 10b-d).

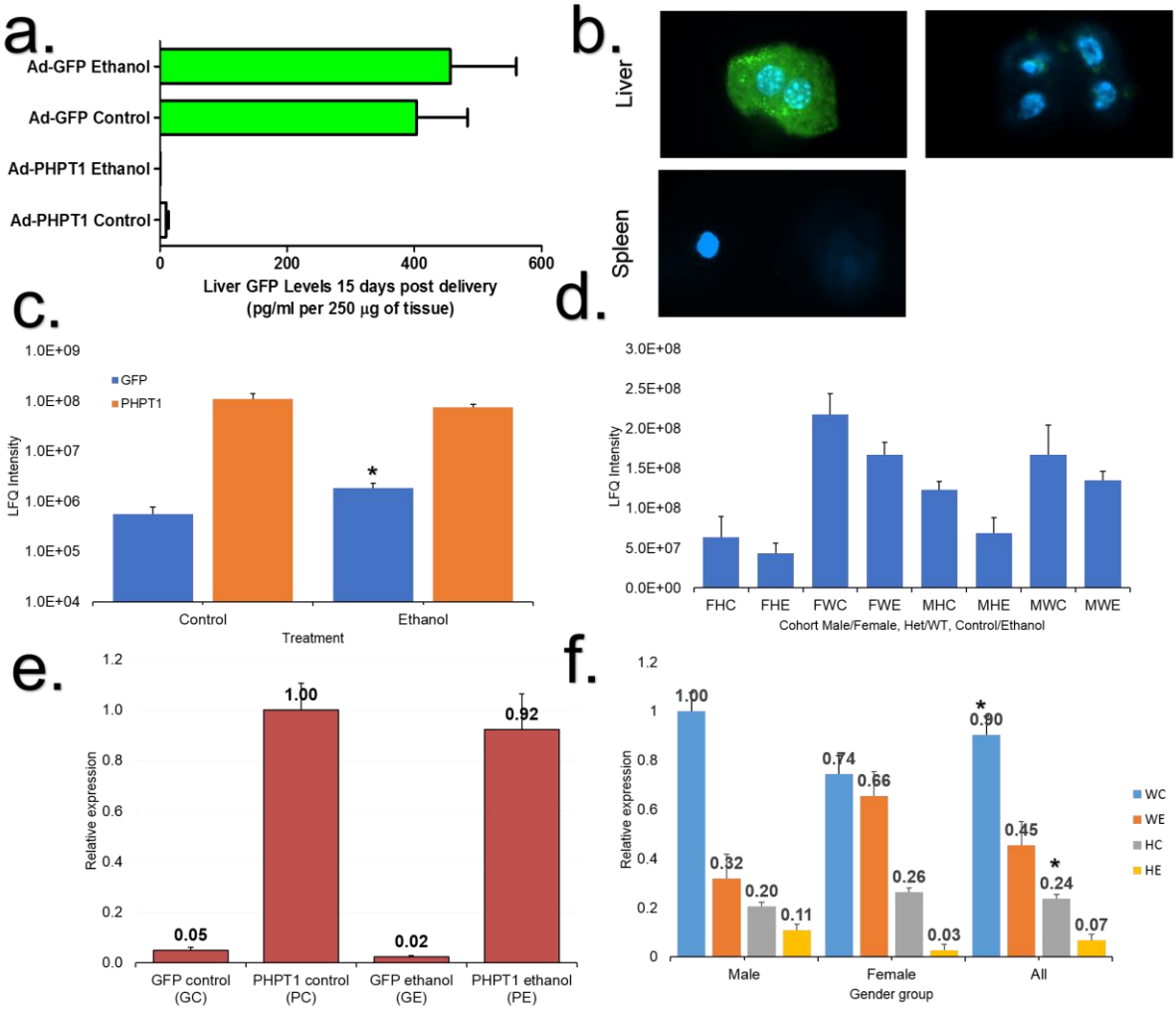

Figure 10. PHPT1 expression validation after treatment. Following chronic ethanol exposure animal tissues were analyzed to verify PHPT1 and eGFP expression. a.) Only ad-GFP samples had significant amounts of eGFP, based on ELISA, following control or ethanol treatment. b.) Fluorescent microscopy was performed on ad-GFP liver, spleen, and ad-PHPT1 liver samples to ensure targeted expression of the vector. EGFP fluorescence was only seen in the ad-GFP liver sample. Mass spectrometry analyses showed intensity levels for c.) Ad-PHPT1 and Ad-GFP after treatment, as well as d.) male and female heterozygous, and wild-type samples. PHPT1 specific western blot analyses of each group (e.)Ad-PHPT1 and Ad-GFP, and f.) heterozygous and wild-type) was performed for further validation (* pvalue<.05).

All mice fed ethanol-containing diet were validated for PHPT1 expression following treatment. PHPT1 overexpression samples were compared directly to the eGFP overexpression counterpart and heterozygous samples were compared directly to the wild-type mice. PHPT1

expression levels were initially shown to increase 3-fold between the Ad-PHPT1 overexpression and Ad-GFP models, and we began with a 2-fold decrease between the wild-type and heterozygous model (Chapter 3: Figure 6). Ad-PHPT1 and Ad-GFP samples were analyzed using western blot analysis after ethanol or control diet exposure (Figure 10e). This result revealed a consistent overexpression of PHPT1 as compared to the eGFP, following exposure of both the ethanol and control diets. This result was consistent with our mass spectrometry LFQ data (Figure 10c). PHPT1 expression levels were significantly greater than that of the eGFP throughout all experimental factors. We did not, however, observe significant decrease in PHPT1 expression between the ethanol and control mice in either the Ad-GFP or Ad-PHPT1 groups. In addition, the decrease of PHPT1 expression in the wild-type group following ethanol treatment still remained higher than the PHPT1 expression of the control heterozygous mice (Figure 10d and f). This result means that these mice began with PHPT1 levels below that of normal ethanol downregulation. In addition, there was a consistent decrease in PHPT1 expression between control and ethanol-fed mice in the western blot data (Figure 10f). A significant ethanol-induced decrease in PHPT1 expression was observed in both the wild-type and heterozygous groups (Figure 10f).

Disease state

Tissues from each treatment and expression group were analyzed for disease progression in using various techniques. Samples from each group were tested for ALT, AST, and circulating triglyceride levels in the blood using clinical chemistry. In addition, blood ethanol concentrations were determined for each mouse, provided a sufficient amount of blood was available, to verify effectiveness of the gavage. Pair-fed mice had liver tissue biopsies removed to be paraffin-embed and H&E stain to determine steatosis scores and immunohistochemical analyses. Mass spectrometry data were also used to verify increased expression of the known alcohol-induced liver injury markers, CYP2E1 and EPHX1.

BECs from the mice were between 0.005-0.040 g/dl for the control mice and 0.14-0.20

g/dl for the ethanol-treated mice. This result shows a significant increase in BEC levels following treatment, as expected. Furthermore, AST and ALT levels were expected to be elevated in the ethanol-treated mice as compared to the control-fed mice. This result was observed for both ALT and AST in the Ad-GFP mice and the female wild-type mice as seen in Figure 11a & b. However, no significant changes were observed between treatments for any other samples. The measurements for the Ad-GFP and Ad-PHPT1 samples were taken using different methods and instruments than the heterozygous and the wild-type samples. This inconsistency in methods

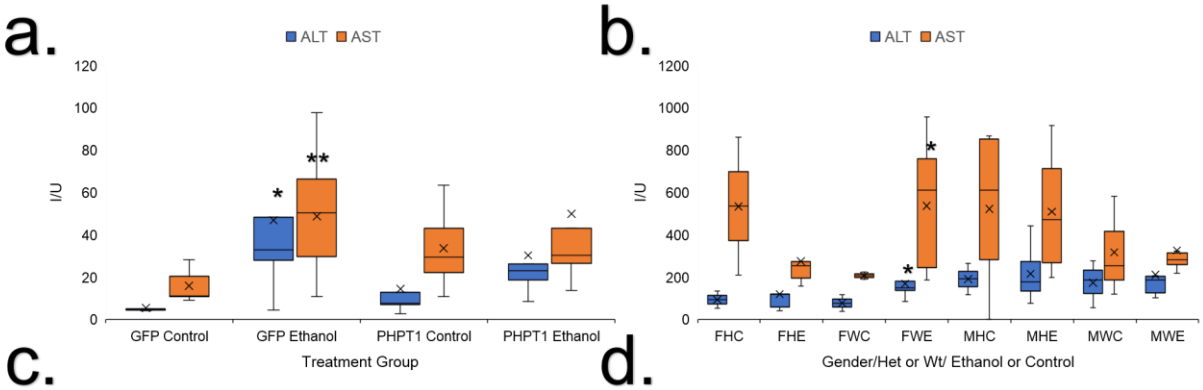

Experimental group	Mean steatosis score[a]	Serum TG (mg/dL)	Relative serum TG[b]
Ad-GFP Control	0.7 (mild)	119.0 ± 13.2	51%
Ad-GFP Ethanol-treated	2.0 (moderate)	234.3 ± 79.3	100% (1.96 ± 0.36)
Ad-PHPT1 Control	0.3 (normal)	119.8 ± 15.6	51%
Ad-PHPT1 Ethanol-treated	1.3 (mild)	151.2 ± 18.5	64% (1.25 ± 0.18)

Figure 11. Disease phenotype. The disease phenotypes were first assessed based on the results of the clinical chemistry tests performed on each cohort. ALT and AST levels are known to be upregulated in response to hepatic steatosis. Their levels were measured following sacrifice for the a.) overexpression model and the b.) heterozygous model(*pvalue<0.5, ** pvalue<0.01). c.) Both circulating triglyceride and steatosis scores were calculated for the overexpression model and d.)only triglyceride levels were able to be measured for the heterozygous models.

could potentially alter the average quantity of the measurements taken, considering the sensitivity of the two separate methods used varied. Triglyceride (TAG) levels were also investigated using various methods (described in Chapter 4: methods). Circulating TAG levels were expected to increase following chronic ethanol exposure and as a result of liver injury development. A significant increase in TAG following ethanol treatment was observed in all

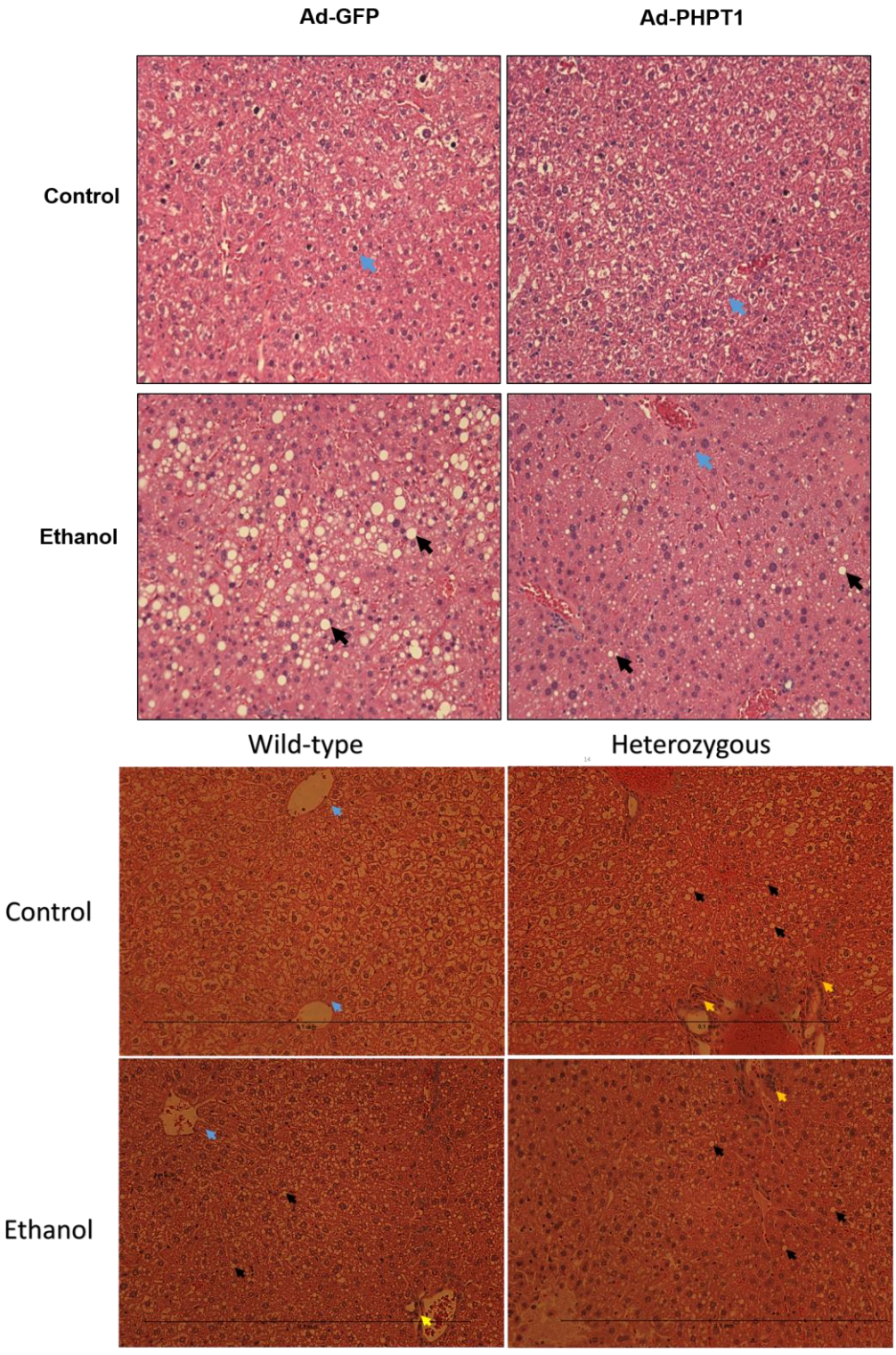

Figure 12. Hematoxylin and eosin stained tissue analysis. Liver tissue sections were paraffin-embedded, H & E stained, and formaldehyde-fixed to a slide immediately following sacrifice. Tissues were analyzed for signs of ethanol-induced hepatic steatosis. The primary hallmarks above show the progression from healthy hepatocytes (blue arrows) to lipid droplet development (black arrows) and inflammation (yellow arrows).

samples except for the female heterozygous serum (Figure 11c & d). In addition, TAG levels

were significantly lower in the Ad-PHPT1 ethanol treated sample that in the Ad-GFP sample. This suggests PHPT1 overexpression is decreasing the amount of TAG levels produce in response to ethanol. The opposite of this was observed in our female heterozygous model where measured TAG levels were pre-elevated in the control sample and remain that way through the ethanol treatment.

Additional disease phenotyping was performed immunohistochemically using H & E-stained paraffin-embed livers from pair-fed mice. Ad-GFP and Ad-PHPT1 livers were scored based on steatosis development using a scale of 0- normal, 1- mild, 2- moderate, and 3-severe. Three liver samples were scored from each treatment and the average score was determined and shown in Figure 11c. As expected, the Ad-GFP control sample showed a mild score and ethanol treatment induced a severe steatosis score for the treated samples. The control Ad-PHPT1 samples, however, were scored as normal while steatosis development following ethanol treatment was only mild. This scoring is reiterated in the histology of the Ad-PHPT1 and Ad-GFP samples as seen in Figure 11a & b. Both the Ad-PHPT1 and Ad-GFP samples show very few (if any) hepatocyte ballooning and lipid droplet formations, which are common hallmarks of steatosis (Figure 12a) [77]. Ethanol-treated Ad-GFP mice show extensive hepatocyte ballooning, and lipid droplets in approximately 60% of the hepatocytes, which is indicative of hepatosteatosis. In the ethanol-treated Ad-PHPT1 mice, however, very little to no hepatocyte ballooning is observed and lipid droplets appear in less than 30% of the hepatocytes (Figure 12). This histological pattern suggests PHPT1 overexpression is playing a protective role in the development of fatty liver. PHPT1 heterozygous and wild-type samples were not able to be officially scored for steatosis. However, in-house histological analysis of the H & E stained samples was performed to assess the severity of liver injury (Figure 12). The wild-type control and ethanol-treated mice show similar results to that of the Ad-GFP samples, which is expected. This result is reflected by a development of lipid droplets in approximately 40% of the hepatocytes in the ethanol-treated group and none in the control. However, in the heterozygous

mice, we observed lipid droplet formation and inflammation in both the ethanol-treated and control groups (Figure 12, black and yellow arrows). Lipid droplet formation is consistently 30-40% confluent in both the heterozygous and wild-type ethanol-treated groups. However, inflammation in the heterozygous control and ethanol samples appears more severe compared to the wild-type groups (Figure 12, yellow arrows). This difference was seen consistently throughout histological tissue assessments. Development of inflammation and steatosis during the control treatment suggests an increase susceptibility to hepatic steatosis induced by decreased expression of PHPT1.

Phenotypic characterization

To further understand the mechanisms involved in the role of phosphohistidine signaling and PHPT1 during chronic ethanol exposure, we used mass spectrometry-based proteomics to characterize the phenotypes induced by each treatment type in each model. This analysis was accomplished by determining significantly differentially expressed proteins between the control and ethanol treatment in each model. Then a full core analysis was performed in IPA to

Z-Score of Activation			
Canonical Pathway	**PHPT1 Het**	**Wild-Type**	**PHPT1 OE**
PPARα/RXRα Activation	-2.00	-0.82	1.63
Integrin Signaling	2.00	1.63	-1.00
CXCR4 Signaling	2.00	N/A	-1.00
Rac Signaling	2.00	N/A	0.00
NRF2-mediated Oxidative Stress Response	2.00	N/A	2.00
Upstream regulators			
ABCB6	-2.21	2.60	2.80
NR1I3	-1.16	2.68	3.25
ethanol	-1.11	3.53	3.20
MYC	2.36	-0.72	-1.69

Table 3. Activation z-scores of canonical pathways and upstream regulators of PHPT1 expression targets. Ingenuity Pathway Analyses (Quiagen) calculates a z-score of activation for known upstream regulators or canonical pathways based on uploaded significantly influenced proteins. Shown are the activation scores which are significant (2<z-score>-2) in at least one group(heterozygous induced (PHPT1 Het) and PHPT1 overexpression induced (PHPT1 OE)) with activation (orange) and Inhibition (blue) highlighted.

determine regulators, canonical pathways, and diseases related to the proteins identified as significantly changed. Finally, the attributes identified were directly compared to each other using a comparison analysis to determine trends between all three expression levels, overexpression, wild-type, and heterozygous. Using this method, we identified potential mechanisms and regulators of phosphohistidine regulation for further investigation.

The top pathways, diseases, and regulators identified are displayed in table 3. These are accompanied by the calculated z-scores for each, which signify the level of activation/inhibition that is predicted to occur. A z-score of greater 2 or less than -2 is indicative of significant activation of inhibition, respectively. Pathways are listed by largest change between heterozygous and overexpression z-score. The largest of these changes in the canonical pathways is the PPARα/RXRα activation. This pathway is predicted to be significantly inhibited in the heterozygous model and not in the overexpression group. This pathway is involved in lipid homeostasis and specifically in regulating β-oxidation of lipids for exportation [119]. A decrease in this pathway would result in greater susceptibility to steatosis. In addition, PHPT1 downregulation was predicted to activate multiple signaling pathways, all of which are related to

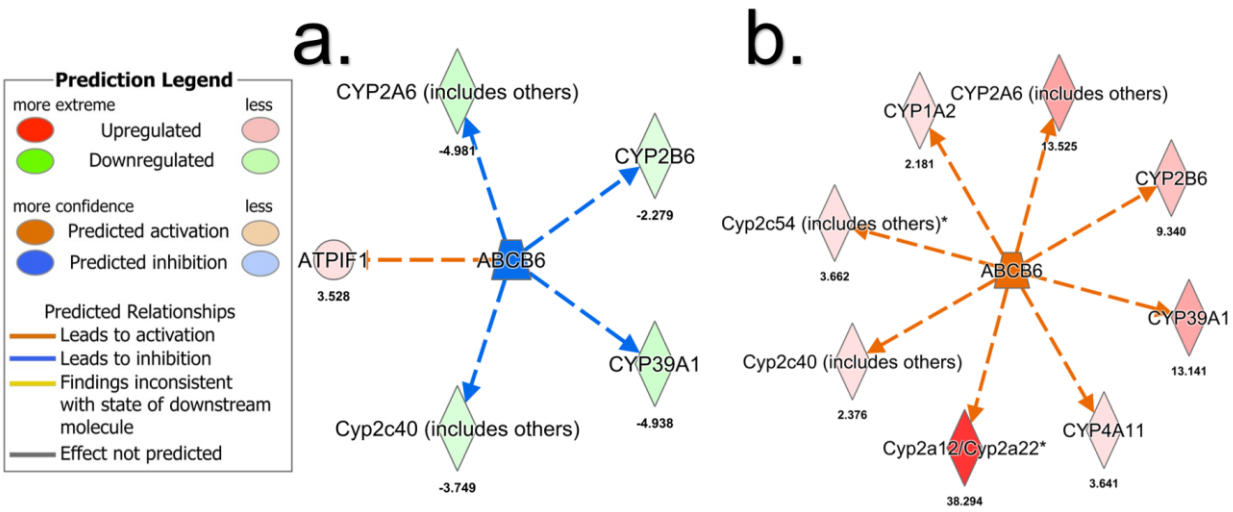

Figure 13. ABCB6 regulation network. The networks show the uploaded significantly changed proteins on the outer nodes and the predicted activation of the inner node, ABCB6. This protein was shown to be significantly a.) inhibited (z-score= -2.21) in the heterozygous model and significantly b.) activated (z-score= 2.20) in the PHPT1 overexpression model following ethanol exposure .

G-protein mediated signaling. This activation may be related to the regulation of G-protein activation by phosphohistidine. Also, NRF2-mediated oxidative stress response is active in both the over expression and heterozygous conditions. This pathway would be expected to be activated following ethanol exposure [120].

The top upstream regulator identified is ABCB6 and is predicted to be activated in the overexpression and wild-type group but inhibited in the PHPT1 heterozygous model (Table 3). This molecule is an ATPase binding cassette that plays a crucial role in heme synthesis and porphyrin transport [121]. Protein expression changes identified can be seen in the outer nodes of Figure 13a and b, which was used to determine predicted activation/inhibition of ABCB6. In both treatment types, the predominate enzymes involved in this prediction are cytochrome P450s that were downregulated in the heterozygous model and upregulated in the overexpression model. Cytochrome P450 regulation, in addition to steroid metabolism, are additional functions of ABCB6 [122]. The heterozygous model is predicted to activate MYC which is a well characterized oncogene involved in cell cycle regulation and angiogenesis (Table 3) [104]. MYC activation can lead to dysregulation of the cell cycle and often results in cell death via apoptosis [123]. PHPT1 overexpression is predicted to activate NR1I3 and ethanol as well. Both regulators are expected to be activated following ethanol response, as NR1I3 is a nuclear receptor involved in xenobiotic regulation [124]. In addition, NR1I3 is involved in RXRβ and alcohol dehydrogenase 3 regulation [124]. These regulators are not predicted to be activated in the heterozygous model.

Conclusion

No change in PHPT1 expression levels between the control and ethanol groups in the Ad-GFP and Ad-PHPT1 samples was unexpectedly observed. This observation, however, could be due to the limitation of sensitivity whilst analyzing expression levels with such a high dynamic range between them. In a side-by-side western blot analysis, the high intensity of PHPT1 in the Ad-PHPT1 samples, over-saturate the blot, making the wild-type PHPT1 levels difficult for

accurate detection. This same limitation in sensitivity was observed in the mass spectrometry samples in which PHPT1 intensity levels are upwards of 100-fold higher than the Ad-GFP samples. This dynamic range makes accurate quantification of PHPT1 in either sample difficult. Efforts to use a method with a much higher dynamic range were taken, however, were also either unsuccessful or not able to be completed. A PHPT1 ELISA kit was attempted but did not perform up to company standards based on its own internal controls and standards. The availability of additional PHPT1 ELISA kits is scarce due to the limitation of study that has been performed on this protein. In addition, absolute quantification could be accomplished using targeted mass spectrometry via either a triple-quadrupole instrument using single/multiple reaction monitoring or using the Q-Exactive parallel reaction monitoring (PRM) feature. Contrary, the heterozygous samples showed only 50% less in PHPT1 expression than the wild-type. This expression difference made the dynamic range for quantification much more attainable via western blot where total protein quantities could be increased to adjust for low protein concentrations. This adjustment allowed us to observe the expected significant decrease between treatments as shown in Figure 10f. With PHPT1 expression already low compared to many other natural liver proteins, PHPT1 expression was still difficult to quantify accurately using unfractionated total lysate samples with LC-MS/MS analysis using a 2-hour gradient in-line with an Orbitrap mass spectrometer. Utilizing a targeted method for PHPT1 quantification on a triple quad or using the PRM feature on the Q Exactive could have allowed for more accurate PHPT1 expression assessment [125, 126].

Nonetheless, PHPT1 expression ratios between models were consistent throughout treatments. This result provided us three consistent expression profiles for characterizing the role of PHPT1 during chronic ethanol exposure. Additional challenges included, disease prognosis where consistency among ALT, AST, and histology scoring was not obtained. These challenges were not without attempted solutions either. The ALT and AST scores were originally performed according to the NIAAA chronic plus binge model guidelines. The assay kits used

were the ones recommended by the guidelines [77], however, their success rate, even with their own standards, were low. Accordingly, we used a core facility with a high specificity instrument to obtain measurement the second time. Unfortunately, inconsistencies were observed for these samples as well due to the limitations in whole blood quantities obtained from the animals. However, these tests did provide us insight on changes in circulating TAG levels. This change is significant given the proteomic information found relating heavily to lipid homeostasis. Furthermore, professional steatosis scoring was only performed on the overexpression groups. This variation was due to that service no longer being available by the time the heterozygous treatment was performed. Therefore, scoring and histology assessment of these samples had to be performed in house. Although, not official, the assessments of histological markers of steatosis development were able to be identified based on numerous publications documenting hepatic steatosis injuries.

Even with the multiple challenges pertaining to disease phenotyping, we were able to conclude confidently that PHPT1 overexpression led to a milder disease progression than the wild-type, and heterozygous expression levels made the organism more susceptible to steatosis onset even without ethanol treatment. This result makes understanding the mechanisms behind the role of PHPT1 during chronic ethanol exposure even more vital. Using global proteomic data to determine significantly differentiated proteins between disease states allows us to determine possible pathways being influenced by PHPT1 expression. Making sense out of the colossal amount of data provided by mass spectrometry data is immensely easier to do using a software program such as IPA. This analysis gives investigators specific pathways and mechanisms to focus on to determined precisely what PHPT1 functions is influencing.

Our IPA data revealed multiple potential mechanisms of PHPT1 response to ethanol. Canonical pathways of significance include the PPARα/RXRα inhibition following ethanol treatment in the heterozygous model. The mechanism of this type of inhibition is unknown but the phenotype coincides with our other disease phenotype data. Inhibition of the PPARα/RXRα

would lead to a decrease in fatty acid β-oxidation resulting in lipid accumulation [32]. This mechanism is known to occur during chronic ethanol exposure [127], however, this is occurring in the heterozygous model independent of ethanol exposure (Figure 12). Significant inhibition of this pathway was only seen in the model with decreased PHPT1 expression. In addition, the heterozygous model showed activation of multiple pathways dependent on G-protein activation. PHPT1 has been shown to play a regulatory role in G-protein activation through the β-subunit phosphohistidine phosphorylation [37]. G-protein activation is involved in many cellular pathways and it is interesting that only these three would be influenced by a decrease in PHPT1 expression. Dysregulation of these specific pathways is known to be involved in abnormal cell cycle regulation (Rac [128] and CXCR4 [129]) and inflammation (Integrin [130]). Overactivation of these pathways is only seen in the heterozygous model. This overactivation again, coincides with inflammation and abnormalities seen in both our control and ethanol-treated heterozygous groups (Figure 12). These results are further supported by the predicted activation of MYC in the heterozygous model. MYC is a well characterized oncogene involved in cell cycle regulation, that often leads to cell death if dysregulated [123]. Hepatocyte cell death would induce an immune cell response and, if not impeded, would result in an inflammatory response [131].

The only mechanism that is predicted to be significantly activated during overexpression and inhibited in the heterozygous model is ABCB6 (Table 3). This result is interesting because ABCB6 functions as an ATP-binding cassette and has no known affiliations with phosphohistidine or ALD, however, it is known to be involved in other liver diseases [120]. ABCB6 inhibition has been known to negatively affect human health in a variety of diseases [132]. Other ATP-binding cassettes have also been shown to be involved in ROS removal and protection [122]. These studies would support the predicted results that ABCB6 inhibition is creating a more susceptible phenotype and activation would assist in a protective role against chronic ethanol exposure. Contrary to this finding, however, ABCB6 overexpression has also been seen consistently in hepatocellular carcinomas and is believed to be a result of disease

progression from steatosis to carcinoma [132]. In addition, ABCB6 has not been directly associated with chronic ethanol exposure or ethanol-induced hepatic steatosis previously. This association would make this mechanism a novel and impactful one to further investigate based on its predicted functions in chronic ethanol exposure response through phosphohistidine signaling.

These studies have provided a newfound insight on the significance of phosphohistidine signaling and PHPT1 in the onset of a universally contracted disease. Phosphohistidine modifications are potentially influencing previously known and unique mechanisms involved in the development of ALD. Our study has provided clear evidence that increased PHPT1 expression levels correlate with a milder response to chronic ethanol exposure, and decreased expression correlates with a higher susceptibility to steatosis and inflammation. In addition, we have identified numerous potential pathways through stringent statistical filtering and bioinformatic analysis that could be leading to this correlation. It is evident that there is much more to know about the role of phosphohistidine signaling in alcohol-induced liver injury and potentially other mechanisms of disease pathogenesis.

Chapter 5 – Conclusions and Future Directions

Conclusions

Overview

The initial development of ALD from a healthy liver to the onset of sometimes irreversible hepatoseatosis is poorly understood. There are many proposed mechanisms involved, including dysregulation of CYP2E1 [90] in the ethanol metabolism pathway, as well as increase in inflammatory [17] mechanisms through the JAK/STAT pathway, and loss of lipid homeostasis via PPAR (α and γ) [127]. However, more detail is needed about this mechanism to understand how these different pathways are affected by ethanol. This information is vital because early detection and treatment of ALD is critical in preventing development of more serious forms, such as cirrhosis, hepatitis, and eventually liver failure. Currently, hepatosteatosis is virtually asymptomatic and can only be diagnosed following a liver biopsy [11]. This obstacle leads to most cases of ALD being diagnosed either post-mortem or beyond the point of recovery. A deeper investigation into the mechanistic details of disease onset is necessary to better detect the early development of this disease.

Initial studies that were performed identified a potential novel player in ethanol metabolism. PHPT1 was identified as a target of ethanol-induced oxidation in an acute exposure model and identified to be downregulated in the chronic mouse model. Furthermore, the significance of PHPT1 phosphatase activity was poorly understood but it shared an overlapping target with ethanol metabolism, ATP-citrate lyase (ACL) [35]. PHPT1 is known to regulate ACL function [45] and ACL is a key regulator of the acetyl-CoA pool that is often dysregulated by increased ethanol metabolism [133]. There are believed to be many additional

targets of phosphohistidine phosphorylation that have yet to discovered as well [56]. This theory makes PHPT1 a probable novel regulator in the onset of ethanol-induced hepatosteatosis.

To investigate the significance of PHPT1, we initially focused on the oxidation modification induced by acute ethanol treatment. Our studies showed that although PHPT1 oxidation increased by 2-fold, there was no change in PHPT1 expression following acute exposure. This result led us to characterize the location and extent of oxidation on PHPT1 and to determine the modification's impact on phosphatase function. These studies were carried out using human recombinant PHPT1, and by developing a mass spectrometry-based phosphohistidine phosphatase assay. This investigation led us to discover that although PHPT1 was being selectively oxidized at Met95, which is a vital residue in substrate binding, it is not influencing PHPT1 phosphatase activity. Next, we further investigated the role PHPT1 expression was playing during chronic ethanol exposure models.

To understand the role of PHPT1 in ethanol induced hepatosteatosis, we used a mouse model to provide more biologically relevant information than cell cultures or recombinant proteins. This mouse model was treated for 10-days with the Lieber DeCarli diet composed of 5% ethanol mixed in with mouse chow in a liquid diet form. The control mice were also given a liquid diet, but it was supplemented with dextrose instead of ethanol to maintain caloric consistency between the two groups. Protocols were followed according to the NIAAA 10-day chronic ethanol plus binge model [77]. C57BL/6J mice were provided only the liquid diet for consumption over the course of 10 days. The level of consumption from each mouse was recorded and tracked daily. At the end of the 10-day period, the mice were given a gavage of 5g/kg (ethanol/body weight) 9 hours prior to sacrificing. Control mice were administered maltose dextrin (9 g/kg in water) instead of ethanol. Mouse livers were removed and used for determining the extent of ethanol induced liver damage using histology, steatosis scoring, and proteomics. Blood ethanol concentration (BEC) and clinical chemistry measuring AST, ALT, and

TAG levels were also assessed based on the blood samples. This method was used for all the chronic ethanol studies with varying strains of mice.

The initial study, which used the same wild-type male mice for the control and ethanol treated group, was performed to create a baseline and determine the significance of PHPT1 in wild-type mice. The BEC levels for the ethanol-treated mice were significantly higher than the control. The clinical chemistry performed showed a greater increase in AST, ALT, and TAG levels in the ethanol treated mice as well. Histology steatosis scoring reflected moderate to severe steatosis in ethanol treated mice samples, in comparison with mild to moderate in the control samples. Furthermore, mass spectrometry-based proteomics showed an increase in both EPHX1 and CYP2E1, as well as other indicators of ethanol induced hepatosteaosis in the ethanol-treated groups [24]. This proteomic analysis also identified PHPT1 expression as being significantly decreased in the treated samples by 2-fold. These results provided validation for the model in that it created a diseased state organism that differed from the control. It also allowed us to identify PHPT1 expression as significantly influenced following ethanol-induced hepatosteosis, making it a potential player in the disease onset. To further investigate this, we developed a PHPT1 liver-specific overexpression model and a PHPT1 knockout model.

PHPT1 overexpression was accomplished using an adenoviral-based vector coded with PHPT1 and an albumin promoter. This experiment was done in comparison to the same construct but with an eGFP sequence for amplification instead of PHPT1. This virus was injected intravenously with an albumin promoter for targeted expression in the liver. C57BL/J6 mice were sacrificed 5-days following injection to verify expression change. EGFP expression was verified using microscopy, ELISA, and mass spectrometry-based proteomics. PHPT1 levels were verified using western blot and proteomics as well. Expression levels were compared between tissue types (liver and spleen) to determine organ specificity, and between constructs (eGFP and PHPT1). EGFP expression was only identified in the Ad-eGFP animal's liver through

proteomic analyses and ELISA. Microscopy showed no expression of eGFP in the PHPT1 livers or in other tissues such as the spleen. PHPT1 expression was shown to be increased 3-fold in liver tissue compared to the Ad-GFP livers by western blot, and expression was increased 18-fold as determined by proteomic analysis. PHPT1 expression in either cohort's spleen tissue remained the same.

The knockout PHPT1 model was requested from the UC Davis KOMP repository. This mouse was genetically altered using Cre recombination to create a non-conditional knockout lacZ gene in a C57BL/6J mouse. These mice showed heterozygous expression of PHPT1 and the lacZ recombinant gene. Mice were bred over many generations, and they were genotyped using PCR and phenotyped using western blot, to confirm expression profiles. Genotypes were confirmed by PCR using a PHPT1 (WT) primer and a lacZ (KO) primer. Following multiple Het-Het cross (N>20) and genotyping of each viable offspring (N=128), we identified no homozygous knockouts. Using a chi-square test, we determined with a 99% confidence that this inheritance pattern did not follow that of Mendelian genetics. We then validated protein expression using western blot analysis of multiple tissue types to determine PHPT1 expression. We found that PHPT1 expression was decreased by an average of approximately 50% in each tissue analyzed from the heterozygous mice, as compared to the wild-type.

Following validation of the expression profiles, liver samples from each PHPT1 expression model were used for mass-spectrometry based phenotypic characterization. These models were then compared to wild-type mice of the same age and origin. Expression changes between each model and the complementary control model were then compared to determine any consistencies between all three models (Wild-type, PHPT1 overexpression, and PHPT1 heterozygous). This investigation found a significant p-value of overlap with both the over expression mouse model changes, and the heterozygous model changes, with upstream regulators involved in hormone-regulated transcriptional activation and with a cell cycle

regulatory molecule. Although, p-value of overlap was significant for both expression models, the proteins identified in each model that overlapped with the upstream regulator shared very few similarities. This result suggests different mechanism being influenced by PHPT1 overexpression as compared to the knockout.

Furthermore, each expression model showed significant p-values of overlap with unique canonical pathways. The targets predicted to be influenced by PHPT1 overexpression were glycogen, and S-methyl-5'-thioadenosine degradation. These are both involved in preparation of cell replication [134] and inflammatory pathways [135]. Overexpression also shows overlap with α-tocopherol degradation, which signifies an increase in β-oxidation and excess antioxidant production [108]. Alternatively, we see overlap in the heterozygous model with two pathways signaling immune response-mediated cell death and the type 1 diabetes signaling pathway. The identified pathways suggest that the PHPT1 overexpression cells are better suited for an external stress, whereas the heterozygous cells seem to be undergoing a stress response already, presumably induced by a decrease in PHPT1 expression.

Ethanol Studies

Following the development and characterization of the PHPT1 expression models, we determined how PHPT1 expression is influencing the onset of ethanol-induced hepatic steatosis. This investigation was carried out using the 10-day chronic plus binge ethanol consumption model [77]. In each case, mice were pair-fed with a control which consumed a dextrose supplemented diet without ethanol at a similar rate to that of the ethanol fed mouse. These mice were immediately sacrificed 9 hours after the gavage given on the 10^{th} day, and the livers were removed for analysis. To determine the influence of PHPT1 on ethanol-induced liver damage, each cohort underwent a variety of tests to determine the disease progression and the changes in proteomic expression levels. We also, validated PHPT1 expression differences between the models following the ethanol treatment using western blot, and proteomic analysis.

First, treatment validation was performed by testing the BEC. In addition, clinical chemistry of the mouse blood for circulating AST, ALT, and TAG levels was conducted to determine the initial changes in liver function following ethanol and control treatments. We did expect to see some increase in the control mice due to the high caloric intake, but the largest increase should be in the ethanol fed mice. Next, disease progression was determined using H&E staining and scoring for steatosis. Pair-fed mouse livers were selected for paraffin-embedding and formalin-fixed for H&E staining. Slides were then analyzed for steatosis scoring to determine the extent of ethanol-induced liver damage. Images of slides were taken as well, to be scored and analyzed for steatosis markers, such as lipid droplet formation, hepatocyte ballooning, and inflammation. Disease onset and treatment validation was also performed by quantifying known proteomic markers. Furthermore, PHPT1 expression was validated using western blot and LFQ intensity values from all samples. These data confirmed a consistent difference in PHPT1 expression levels, regardless of treatment type, between models. Additional expression validation was performed on the Ad-GFP samples using an ELISA, which provided absolute quantification. ELISA data reiterated that time or treatment type did not influence the expression of eGFP in the Ad-GFP samples.

Last, we performed mass spectrometry-based phenotypic characterization on all treated samples from all the PHPT1 expression models. Significant differentially expressed proteins were identified based on their LFQ intensity values and calculated using stringent statistical filtering. Fold-changes of identified significantly changed proteins were then uploaded to IPA for core analysis, to determine predicted regulators and canonical pathways influenced by PHPT1 expression. These results were compared between models, to determine differences in PHPT1 expression influence. Our results revealed that the PHPT1 heterozygous expression model is predicted to inhibit PPARα/RXRα pathway, while activating integrin, CXCR, and RAC signaling pathways. PPARα/RXRα inhibition would result in a decrease in fatty acid β-oxidation, which

leads directly to increased lipid accumulation. In addition, activation of the integrin pathway relates to cell signaling of many forms including adhesion, activation, or inflammation [130]. Whereas, Rac pathway activation leads to cytoskeletal rearrangement or cell cycle progression [128], and CXCR activation is known to relate with immune response [129] and has been associated with MYC-induced cancer progression [136]. This coincides with the predicted activation of MYC in the heterozygous model, as well. MYC is a known oncogene [104] involved in regulating cell survival pathways [123].

Alternatively, PHPT1 overexpression is predicted to activate the upstream regulator NR1I3 and ABCB6. NR1I3 activation would increase the RXRβ pathway, increase production of alcohol dehydrogenase, and is a protective protein during xenobiotic response [137]. Both NR1I3 and ABCB6 are regulators of cytochrome P450s, which are essential in ethanol exposure response [15, 121, 122, 124, 137]. The heterozygous PHPT1 model was predicted to inhibit ABCB6 activation, thus decreasing the xenobiotic response. These prediction models along with our disease phenotype data demonstrate that PHPT1 overexpression is playing a protective role against ethanol-induced liver injury, and the PHPT1 heterozygous model is more susceptible to liver damage.

Future directions

The completion of this study has brought about significant advances in understanding the contribution of a poorly characterized protein in a novel role. In addition, this study has provided new ways to investigate the enzymatic activity of PHPT1 and discovered, for the first time to the best of our knowledge, that a PHPT1 complete knockout results in early embryonic lethality. We have displayed a strong correlation with PHPT1 expression levels and susceptibility to fatty liver disease develop that has never been published before. Finally, we have suggested multiple novel pathways and mechanisms that phosphohistidine signaling is influencing in mammalian cells. Although the accomplishments of this study are significant,

there is much more to be done in order to fully understand the role of PHPT1 and phosphohistidine signaling in the onset of ALD.

Additional Mouse models

Ideally, more animal studies would have been utilized to fully understand how and why PHPT1 expression was influencing ethanol-induced liver injury. Our overexpression and heterozygous mouse showed the extreme conditions of PHPT1 expression, but many more questions are left to be answered following the investigation of these two models. Unfortunately, a complete animal wide knockout was not possible due to the embryonic lethality of the allele. However, it is possible to create a liver-specific siRNA-mediated knockout using an adenoviral based vector. In addition, an investigation using the liver-specific overexpression vector on the heterozygous model would show if a phenotypic rescue was possible. Furthermore, creation of an enzymatically inactive PHPT1 overexpression model would aid in determining if PHPT1 phosphatase activity was influencing disease progression or if this was being done through an alternative mechanism. The PHPT1 H52A mutant could be used in the viral construct just as in the Ad-PHPT1 overexpression. In addition, creating a PHPT1 rescue model using the Ad-PHPT1 virus to rescue the heterozygous would assist further in linking PHPT1 expression to ethanol-induced liver injury development. The means and materials to create these models and characterize their phenotype before and after ethanol treatment is available [138], and they would provide much greater insight into how phosphohistidine signaling is involved in injury onset.

Lipidomic analysis

Given the significant overlap in PHPT1 expression and numerous lipid homeostasis pathways, an in depth lipidomic analysis of tissues with varying PHPT1 expression and ethanol treatment would provide critical insight into the mechanisms of phosphohistidine signaling. It is already well known that lipid oxidation and metabolism are affected by chronic ethanol exposure [17]. This effect occurs via a combination of ethanol-induced insults including that of ROS [11]

and endoplasmic reticulum stress [13]. Oxidative stress combined with ethanol's inhibition of AMPK activation, leads to an increase in fatty acid and lipid production in hepatocytes, mediated by SREBP1-C [13]. Concurrently, ethanol causes a decrease in fatty acid β-oxidation via PPARα inhibition through oxidative stress [28]. This inhibition results in an increase in cellular fatty acids and creates the hepatocyte ballooning effect and lipid droplet formation commonly seen in liver histology [28]. This response is well characterized during chronic ethanol exposure; however, our data suggests that PHPT1 is influencing this response.

Our PHPT1 expression characterization data suggests phosphohistidine signaling is involved in key transcriptional regulatory pathways such a 17β-estradiol signaling, MYC activation, and other hormonal signaling pathways (See Chapter 3: results). Based on the ethanol studies (See Chapter 4: results), this seems to create a phenotype that is either better prepared for ethanol stress, in the case of PHPT1 overexpression, or more susceptible to development of steatosis, in our heterozygous model. This susceptibility was further shown by predicted inhibition of pathways, such as the PPARα/RXRα in the heterozygous models, and change in expression levels of key fatty acid metabolism enzymes, such as FABP4 and FABP5 in both models [139]. This overlap in PHPT1 expression levels with fatty acid metabolism enzymes and pathways suggests phosphohistidine signaling influences lipid homeostasis, following ethanol exposure. This trend was further validated by the steatosis scoring and histological staining performed on treated tissues, which showed a significantly lower development of steatosis for the tissues that were overexpressing PHPT1 than those at wild-type levels. In addition, histology showed tissues with the heterozygous genotype had greater steatosis development and lipid droplet formation induced by an increased calorie diet alone in the control groups. Tissues from mice treated with ethanol showed similar severity in damage between the heterozygous and wild-type. To further understand how PHPT1 is influencing the creation and regulation of these lipids, a lipidomic analysis of these tissues would be necessary.

Shotgun lipidomics is similar in technique to shotgun proteomics, in that it analyzes many forms of the biological molecule at one time [140]. This method would allow us to take a snapshot of the types of lipids being expressed in our various models of PHPT1 expression and disease state. This method is beneficial in that it would give us an idea as to which lipids are being influenced and would provide direction to further investigate specific lipid families [141]. However, the limitations of this method coincide with its robustness. The highly complex lipid molecules are often very abundant and usually lead to high degrees of overlap in parent ion mass between multiple lipid types [142]. This makes it far more difficult to quantify a specific conformation when no isolation or fractionation has occurred prior to analysis. The implementation of shotgun lipidomics would be the first step in analysis, and it will determine which lipid classes should be isolated for further investigation in each sample.

Following identification of lipid targets, ideally, we would be able to isolate and determine expression changes in these targets between cohorts. Quantification would be accomplished using parallel reaction monitoring (PRM) on the Q-Exactive hybrid Orbitrap instrument [126]. This instrument allows us to specify a parent ion mass and the product ions created from it by fragmentation to monitor intensity levels and quantify lipid classes specifically. PRM allows us to specify multiple parent ion targets (lipid classes) for quantification from the same sample simultaneously [126]. Targeted lipidomics via PRM will provide reliable and reproducible quantification of the lipids present in each sample to determine how their synthesis is influenced in each cohort, and it will provide additional insight into the mechanism of phosphohistidine signaling influencing lipid homeostasis.

Mechanistic Validation

The use of mass spectrometry to determine protein expression changes between treatment groups is currently a widely excepted method among many scientific fields [76, 143-147]. Instrumentation has advanced significantly over the past 20 years and provides highly reliable and reproducible results, which can be further solidified by technical or biological

replicates (See Chapter 1: Mass spectrometry-based proteomics). Regular instrumental maintenance and internal controls and standards contributes significantly to generating high resolution and high mass accuracy data. Samples should also be analyzed concurrently with multiple replicates, quality controls, and blanks included before, during, and after the sequence to maximize reproducibility. In addition, database search parameters should be set with high stringencies and low mass tolerance variabilities, as well as low false discovery rates to further insure high-resolution data is being correctly matched with the peptides and proteins they originate from [76]. Furthermore, stringent unbiased statistical analysis following identification decreases the false discovery rate, and accuracy is increased further by only accepting proteins identified in a majority of the biological replicates from a single cohort. All of these steps are taken in the previously described experimental methods (Chapter 3: Methods; Chapter 4: Methods) to ensure high quality accurate data, reflecting a snapshot of the proteomes under investigation. Thus, making western blot, or other validations of mass spectrometry-identified protein expressions, complementary but not a necessity.

However, further validation of the predicted influenced pathways identified through IPA is necessary to further understand the mechanisms being influenced by phosphohistidine signaling, during chronic ethanol exposure. Many of the identified pathways or upstream regulators are either regulated independently of protein expression, or instrumentation is not able to identify them due their expression levels or the sample's complexity. Regulation of this type includes post translation modifications, conformational alterations, or ligand binding. All mechanisms of regulation and specific protein expression can be verified using methods such as western blot, phosphoproteomics, immunoprecipitation, and many other methods specific to the regulatory element. Specifically, to verify the deactivation of the PPARα/RXRα pathway, predicted to be inhibited in the heterozygous ethanol treated mice, a western blot could be used to determine changes in PPARα expression levels as well as changes in one of the many downstream targets of PPARα, such as FABP1 [148]. In addition, activation of PPARα/RXRα

requires the formation of a heterodimer [137]. PPARα and RXRα co-localization can be determined using immunohistochemistry via antibodies against each protein. Furthermore, fatty acid β-oxidation is the downstream effect of PPARα/RXRα activation [149]. The levels of β-oxidation can be measured to validate inhibition or activation using one of many fatty acid β-oxidation assays available. Validation of all the predicted upstream regulators and pathways is necessary to better understand the mechanisms of PHPT1 regulation.

Targeted search for phosphohistidine phosphatase proteins

It is apparent from our findings that PHPT1 and phosphohistidine signaling play a much larger role in ethanol response in the liver than previously believed. It is very likely that this novel role is mediated through previously unidentified targets of phosphohistidine regulation. The next step in further understanding this mechanism is determining what proteins are directly targeted by phosphohistidine and influenced by PHPT1 expression and activity. However, identifying these targets in not an easy feat. The challenges of isolating and identifying phosphohistidine modified proteins are still difficult to overcome, even with modern scientific techniques. One improvement to the challenge, is the development of a pan-phosphohistidine antibody, specific for N-1 or N-3 phosphohistidine modification[60]. Development of this antibody was only made possible using a phosphohistidine analogs with higher stability than the modification [150, 151]. The developed antibody claims to bind only to proteins with the specified phosphohistidine modification (N-1 or N-3) [152]. This antibody has been tested in our lab with some success. Therefore, if the targets are accurate, western blot analysis using this antibody shows a great deal of phosphohistidine targets that have yet to be characterized. There is also a potential for this antibody to be used in an immunoprecipitation experiment, to isolate only those proteins that contain phosphohistidine modification. Proteins can then be characterized using mass spectrometry-based proteomics to determine their identity. Furthermore, an additional co-immunoprecipitation experiment can be performed using PHTP1 as the target and the identified phosphohistidine-containing proteins as the potential ligands.

This experiment could help determine if any of these targets of phosphohistidine are also targets of PHPT1. Confirmation of this type can be achieved for specific proteins using the mass spectrometry-based phosphohistidine phosphatase assay, previously described in this text (Appendix A: Scientific Reports). Furthermore, mass spectrometry methods have been developed to identify phosphohistidine-modified proteins based on neutral losses during CID [153]. Using this method, two novel sites of phosphohistidine modification including aldehyde-alcohol dehydrogenase were determined. This discovery potentially creates another link between PHPT1 expression and chronic ethanol exposure.

Identifying novel targets of phosphohistidine and PHPT1 would be beneficial in not only further understanding the role of phosphohistidine during ethanol exposure, but these targets could also lead to a better understanding of the role of PHPT1 in normal cellular functions [60]. PHPT1 has been identified in numerous diseases, including cancers, but often the pathways and mechanisms associated with its expression differ depending on the cell type [46, 66, 67, 112, 154]. These studies lead us to believe phosphohistidine signaling and PHTP1 regulation of this modification is playing a diverse role in cellular functions. A better understanding of this role would be accomplished by determining a more comprehensive list of phosphohistidine and PHPT1 targets.

Human tissue analyses

The question of translational relevance is always considered when using any model. In our case, the mouse model was the closest organism we could use for ethanol studies and still be able to create the PHPT1 overexpression and heterozygous genotypes in a relatively short time frame. However, human samples are always the end goal. Although altering the expression levels and disease state of a human sample would not be possible, there are currently human liver samples available which have known patient backgrounds and have developed varying states of ALD. These tissues are available by request from the Ibrahim El-Hefni liver biorepository and California Pacific Medical Center. Liver samples were taken from patients who

had a range of ALDs varying from mild steatosis up to severe late stage hepatitis. A majority of the samples, however, are from patients in the later stages and from individuals with backgrounds of existing liver disease, or familial history, making them less likely to fit the requirements for our study. This outcome is most likely due to the initial asymptomatic progression of the disease, making early onset very difficult to detect unless an existing liver disease is already present [11].

Nonetheless, human tissues could provide additional insight into the role of PHPT1 in progression of human ALD. It would not be difficult to screen the expression levels of PHPT1 in various disease states, and normal levels of PHPT1 expression in human liver tissue is already available. The human tissue aspect of this investigation would be the final step in validating any mechanism identified in the mouse model in human liver tissues. Therefore, although these tissues are currently available, it would make most sense to obtain them following all previously described experiments to make the most out of the sample provided. Human tissues could immediately be screened for other targets of PHPT1 and phosphohistidine identified, and for phosphohistidine modifications using the same methods described previously (Chapter 5: targeted search for phosphohistidine phosphatase proteins). Human tissue analyses would provide high confidence in terms of overall relevance of PHPT1 and phosphohistidine signaling in ALD pathogenesis, and these samples would provide a novel avenue of study on the role of phosphohistidine in mammalian cellular processes.

References

[1] Yoon, Y. H., Yi, H. Y., Liver cirrhosis and viral Hepatitis C infection mortality among Hispanic subgroups in the United States, 1999-2003: A multiple cause analysis. *Alcoholism-Clinical and Experimental Research* 2006, *30*, 168a-168a.
[2] Szabo, G., Mandrekar, P., Focus On: Alcohol and the Liver. *Alcohol Research & Health* 2010, *33*, 87-96.
[3] Hanson, M., Preventing alcohol abuse: Alcohol, culture, and control - Hanson,DJ. *J Soc Serv Res* 1996, *21*, 79-80.
[4] Lim, S. S., Vos, T., Flaxman, A. D., AlMazroa, M. A., Memish, Z. A., A comparative risk assessment of burden of disease and injury attributable to 67 risk factors and risk factor clusters in 21 regions, 1990-2010: a systematic analysis for the Global Burden of Disease Study 2010 (vol 380, pg 2224, 2012). *Lancet* 2013, *381*, 628-628.
[5] World Health Organization., *Global status report on alcohol and health 2014*, World Health Organization, Geneva 2014.
[6] Forouzanfar, M. H., Afshin, A., Alexander, L. T., Anderson, H. R*., et al.*, Global, regional, and national comparative risk assessment of 79 behavioural, environmental and occupational, and metabolic risks or clusters of risks, 1990-2015: a systematic analysis for the Global Burden of Disease Study 2015. *Lancet* 2016, *388*, 1659-1724.
[7] Schuckit, M. A., Alcohol-use disorders. *Lancet* 2009, *373*, 492-501.
[8] Crabb, D. W., Pathogenesis of alcoholic liver disease: newer mechanisms of injury. *Keio J Med* 1999, *48*, 184-188.
[9] MacSween, R. N., Scott, A. R., Hepatic cirrhosis: a clinico-pathological review of 520 cases. *J Clin Pathol* 1973, *26*, 936-942.
[10] Galambos, J. T., Natural history of alcoholic hepatitis. 3. Histological changes. *Gastroenterology* 1972, *63*, 1026-1035.
[11] O'Shea, R. S., Dasarathy, S., McCullough, A. J., Alcoholic Liver Disease. *Am J Gastroenterol* 2010, *105*, 14-32.
[12] Caballeria, J., Is there a role for pentoxifylline in the treatment of alcoholic hepatitis? *Gastroenterol. Hepatol.* 2016, *39*, 560-565.
[13] Gao, B., Bataller, R., Alcoholic Liver Disease: Pathogenesis and New Therapeutic Targets. *Gastroenterology* 2011, *141*, 1572-1585.
[14] Norberg, A., Jones, A. W., Hahn, R. G., Gabrielsson, J. L., Role of variability in explaining ethanol pharmacokinetics - Research and forensic applications. *Clin Pharmacokinet* 2003, *42*, 1-31.
[15] Cederbaum, A. I., Alcohol Metabolism. *Clin Liver Dis* 2012, *16*, 667-+.
[16] Lieber, C. S., Alcohol: Its metabolism and interaction with nutrients. *Annu Rev Nutr* 2000, *20*, 395-+.
[17] Lieber, C. S., Alcoholic fatty liver: its pathogenesis and mechanism of progression to inflammation and fibrosis. *Alcohol* 2004, *34*, 9-19.
[18] Cederbaum, A. I., Cytochrome P450 2E1-dependent oxidant stress and upregulation of anti-oxidant defense in liver cells. *J Gastroen Hepatol* 2006, *21*, S22-S25.
[19] Wheeler, M. D., Kono, H., Yin, M., Nakagami, M*., et al.*, The role of Kupffer cell oxidant production in early ethanol-induced liver disease. *Free Radical Bio Med* 2001, *31*, 1544-1549.

[20] Fernandezcheca, J. C., Ookhtens, M., Kaplowitz, N., Effects of Chronic Ethanol Feeding on Rat Hepatocytic Glutathione - Relationship of Cytosolic Glutathione to Efflux and Mitochondrial Sequestration. *J Clin Invest* 1989, *83*, 1247-1252.
[21] Fernandezcheca, J. C., Garciaruiz, C., Ookhtens, M., Kaplowitz, N., Impaired Uptake of Glutathione by Hepatic Mitochondria from Chronic Ethanol-Fed Rats - Tracer Kinetic-Studies Invitro and Invivo and Susceptibility to Oxidant Stress. *J Clin Invest* 1991, *87*, 397-405.
[22] Hirano, T., Kaplowitz, N., Tsukamoto, H., Kamimura, S., Fernandezcheca, J. C., Hepatic Mitochondrial Glutathione Depletion and Progression of Experimental Alcoholic Liver-Disease in Rats. *Hepatology* 1992, *16*, 1423-1427.
[23] Wheeler, M. D., Nakagami, M., Bradford, B. U., Uesugi, T.*, et al.*, Overexpression of manganese superoxide dismutase prevents alcohol-induced liver injury in the rat. *Journal of Biological Chemistry* 2001, *276*, 36664-36672.
[24] Gong, P. F., Cederbaum, A. I., Nieto, N., Heme oxygenase-1 protects HEPG2 cells against cytochrome P450 2E1-dependent toxicity. *Free Radical Bio Med* 2004, *36*, 307-318.
[25] Malhi, H., Kaufman, R. J., Endoplasmic reticulum stress in liver disease. *J Hepatol* 2011, *54*, 795-809.
[26] Ji, C., Deng, Q. G., Kaplowitz, N., Role of TNF-alpha in ethanol-induced hyperhomocysteinemia and murine alcoholic liver injury. *Hepatology* 2004, *40*, 442-451.
[27] Petrasek, J., Iracheta-Vellve, A., Csak, T., Satishchandran, A.*, et al.*, STING-IRF3 pathway links endoplasmic reticulum stress with hepatocyte apoptosis in early alcoholic liver disease. *Proceedings of the National Academy of Sciences of the United States of America* 2013, *110*, 16544-16549.
[28] Crabb, D. W., Liangpunsakul, S., Alcohol and lipid metabolism. *J Gastroen Hepatol* 2006, *21*, S56-S60.
[29] Ji, C., Kaplowitz, N., Betaine decreases hyperhomocysteinemia, endoplasmic reticulum stress, and liver injury in alcohol-fed mice. *Gastroenterology* 2003, *124*, 1488-1499.
[30] Endo, M., Masaki, T., Seike, M., Yoshimatsu, H., TNF-alpha induces hepatic steatosis in mice by enhancing gene expression of sterol regulatory element blinding protein-1c (SREBP-1c). *Exp Biol Med* 2007, *232*, 614-621.
[31] Kang, L., Sebastian, B. M., Pritchard, M. T., Pratt, B. T.*, et al.*, Chronic ethanol-induced insulin resistance is associated with macrophage infiltration into adipose tissue and altered expression of adipocytokines. *Alcoholism-Clinical and Experimental Research* 2007, *31*, 1581-1588.
[32] Fischer, M., You, M., Matsumoto, M., Crabb, D. W., Peroxisome proliferator-activated receptor alpha (PPAR alpha) agonist treatment reverses PPAR alpha dysfunction and abnormalities in hepatic lipid metabolism in ethanol-fed mice. *Journal of Biological Chemistry* 2003, *278*, 27997-28004.
[33] Molina, P. E., Alcohol - intoxicating roadblocks and bottlenecks in hepatic protein and lipid metabolism. *American Journal of Physiology-Endocrinology and Metabolism* 2008, *295*, E1-E2.
[34] Zhou, G. C., Myers, R., Li, Y., Chen, Y. L.*, et al.*, Role of AMP-activated protein kinase in mechanism of metformin action. *J Clin Invest* 2001, *108*, 1167-1174.
[35] Klumpp, S., Bechmann, G., Maurer, A., Selke, D., Krieglstein, J., ATP-citrate lyase as a substrate of protein histidine phosphatase in vertebrates. *Biochemical and biophysical research communications* 2003, *306*, 110-115.
[36] Boyer, P. D., Deluca, M., Ebner, K. E., Hultquist, D. E., Peter, J. B., Identification of phosphohistidine in digests from a probable intermediate of oxidative phosphorylation. *The Journal of biological chemistry* 1962, *237*, PC3306-PC3308.
[37] Maurer, A., Wieland, T., Meissl, F., Niroomand, F.*, et al.*, The beta-subunit of G proteins is a substrate of protein histidine phosphatase. *Biochemical and biophysical research communications* 2005, *334*, 1115-1120.

[38] Fujitaki, J. M., Fung, G., Oh, E. Y., Smith, R. A., Characterization of Chemical and Enzymatic Acid-Labile Phosphorylation of Histone H-4 Using P-31 Nuclear Magnetic-Resonance. *Biochemistry* 1981, *20*, 3658-3664.
[39] Srivastava, S., Zhdanova, O., Di, L., Li, Z.*, et al.*, Protein histidine phosphatase 1 negatively regulates CD4 T cells by inhibiting the K(+) channel KCa3.1. *Proceedings of the National Academy of Sciences of the United States of America* 2008, *105*, 14442-14446.
[40] Wagner, P. D., Vu, N. D., Phosphorylation of ATP-citrate lyase by nucleoside diphosphate kinase. *The Journal of biological chemistry* 1995, *270*, 21758-21764.
[41] Ek, P., Pettersson, G., Ek, B., Gong, F.*, et al.*, Identification and characterization of a mammalian 14-kDa phosphohistidine phosphatase. *European journal of biochemistry / FEBS* 2002, *269*, 5016-5023.
[42] Panda, S., Srivastava, S., Li, Z., Vaeth, M.*, et al.*, Identification of PGAM5 as a Mammalian Protein Histidine Phosphatase that Plays a Central Role to Negatively Regulate CD4(+) T Cells. *Molecular Cell* 2016, *63*, 457-469.
[43] Attwood, P. V., Ludwig, K., Bergander, K., Besant, P. G.*, et al.*, Chemical phosphorylation of histidine-containing peptides based on the sequence of histone H4 and their dephosphorylation by protein histidine phosphatase. *Bba-Proteins Proteom* 2010, *1804*, 199-205.
[44] Ek, P., Ek, B., Zetterqvist, O., Phosphohistidine phosphatase 1 (PHPT1) also dephosphorylates phospholysine of chemically phosphorylated histone H1 and polylysine. *Upsala journal of medical sciences* 2015, *120*, 20-27.
[45] Krieglstein, J., Lehmann, M., Maeurer, A., Gudermann, T.*, et al.*, Reduced viability of neuronal cells after overexpression of protein histidine phosphatase. *Neurochemistry international* 2008, *53*, 132-136.
[46] Kamath, V., Kyathanahalli, C. N., Jayaram, B., Syed, I.*, et al.*, Regulation of glucose- and mitochondrial fuel-induced insulin secretion by a cytosolic protein histidine phosphatase in pancreatic beta-cells. *American Journal of Physiology-Endocrinology and Metabolism* 2010, *299*, E276-E286.
[47] Cuello, F., Schulze, R. A., Heemeyer, F., Meyer, H. E.*, et al.*, Activation of heterotrimeric G proteins by a high energy phosphate transfer via nucleoside diphosphate kinase (NDPK) B and G beta subunits - Complex formation of NDPK B with G beta gamma dimers and phosphorylation of His-266 in G beta. *Journal of Biological Chemistry* 2003, *278*, 7220-7226.
[48] Beckman-Sundh, U., Ek, B., Zetterqvist, O., Ek, P., A screening method for phosphohistidine phosphatase 1 activity. *Upsala journal of medical sciences* 2011, *116*, 161-168.
[49] Yanicostas, C., Vincent, A., Lepesant, J. A., Transcriptional and Posttranscriptional Regulation Contributes to the Sex-Regulated Expression of 2 Sequence-Related Genes at the Janus Locus of Drosophila-Melanogaster. *Mol Cell Biol* 1989, *9*, 2526-2535.
[50] Yao, D. B., Peng, S. L., Dai, C. L., The role of hepatocyte nuclear factor 4alpha in metastatic tumor formation of hepatocellular carcinoma and its close relationship with the mesenchymal-epithelial transition markers. *Bmc Cancer* 2013, *13*.
[51] Xu, A., Hao, J., Zhang, Z., Tian, T.*, et al.*, 14-kDa phosphohistidine phosphatase and its role in human lung cancer cell migration and invasion. *Lung cancer* 2010, *67*, 48-56.
[52] Han, S. X., Wang, L. J., Zhao, J., Zhang, Y.*, et al.*, 14-kDa Phosphohistidine phosphatase plays an important role in hepatocellular carcinoma cell proliferation. *Oncology letters* 2012, *4*, 658-664.
[53] Sharma, S., Ray, S., Mukherjee, S., Moiyadi, A.*, et al.*, Multipronged quantitative proteomic analyses indicate modulation of various signal transduction pathways in human meningiomas. *Proteomics* 2015, *15*, 394-407.
[54] Matthews, H. R., Pesis, K., Kim, Y. K., Protein Histidine Phosphatase-Activity of Protein Phosphatase-1, Phosphatase-2a and Phosphatase-2c and Inhibition by Okadaic Acid. *Faseb Journal* 1995, *9*, A1347-A1347.
[55] Hunter, T., Sefton, B. M., Transforming Gene-Product of Rous-Sarcoma Virus Phosphorylates Tyrosine. *P Natl Acad Sci-Biol* 1980, *77*, 1311-1315.

[56] Attwood, P. V., Piggott, M. J., Zu, X. L., Besant, P. G., Focus on phosphohistidine. *Amino acids* 2007, *32*, 145-156.
[57] Busam, R. D., Thorsell, A. G., Flores, A., Hammarstrom, M.*, et al.*, First structure of a eukaryotic phosphohistidine phosphatase. *The Journal of biological chemistry* 2006, *281*, 33830-33834.
[58] Schaller, G. E., Histidine kinases and the role of two-component systems in plants. *Advances in Botanical Research Incorporating Advances in Plant Pathology, Vol 32: Plant Protein Kinases* 2000, *32*, 109-148.
[59] Attwood, P. V., Histidine kinases from bacteria to humans. *Biochemical Society transactions* 2013, *41*, 1023-1028.
[60] Piggott, M. J., Attwood, P. V., Post-translational modifications: Panning for phosphohistidine. *Nature chemical biology* 2013, *9*, 411-412.
[61] Tan, E. L., Besant, P. G., Zu, X. L., Turck, C. W.*, et al.*, Histone H4 histidine kinase displays the expression pattern of a liver oncodevelopmental marker. *Carcinogenesis* 2004, *25*, 2083-2088.
[62] Gong, W., Li, Y., Cui, G., Hu, J.*, et al.*, Solution structure and catalytic mechanism of human protein histidine phosphatase 1. *The Biochemical journal* 2009, *418*, 337-344.
[63] Ma, R., Kanders, E., Sundh, U. B., Geng, M.*, et al.*, Mutational study of human phosphohistidine phosphatase: effect on enzymatic activity. *Biochemical and biophysical research communications* 2005, *337*, 887-891.
[64] Gauci, S., Helbig, A. O., Slijper, M., Krijgsveld, J.*, et al.*, Lys-N and Trypsin Cover Complementary Parts of the Phosphoproteome in a Refined SCX-Based Approach. *Analytical Chemistry* 2009, *81*, 4493-4501.
[65] Martin, D. R., Dutta, P., Mahajan, S., Varma, S., Stevens, S. M., Jr., Structural and activity characterization of human PHPT1 after oxidative modification. *Sci Rep* 2016, *6*, 23658.
[66] Xu, A. J., Xia, X. H., Du, S. T., Gu, J. C., Clinical significance of PHPT1 protein expression in lung cancer. *Chinese Medical Journal* 2010, *123*, 3247-3251.
[67] Xu, A., Li, X., Wu, S., Lv, T.*, et al.*, Knockdown of 14-kDa phosphohistidine phosphatase expression suppresses lung cancer cell growth in vivo possibly through inhibition of NF-kappa B signaling pathway. *Neoplasma* 2016, *63*, 540-547.
[68] Bolotin, E., Liao, H. L., Ta, T. C., Yang, C. H.*, et al.*, Integrated Approach for the Identification of Human Hepatocyte Nuclear Factor 4 alpha Target Genes Using Protein Binding Microarrays. *Hepatology* 2010, *51*, 642-653.
[69] Wisely, G. B., Miller, A. B., Davis, R. G., Thornquest, A. D.*, et al.*, Hepatocyte nuclear factor 4 is a transcription factor that constitutively binds fatty acids. *Structure* 2002, *10*, 1225-1234.
[70] Iwazaki, N., Kobayashi, K., Morimoto, K., Hirano, M.*, et al.*, Involvement of hepatocyte nuclear factor 4alpha in transcriptional regulation of the human pregnane X receptor gene in the human liver. *Drug Metab Pharmacok* 2008, *23*, 59-66.
[71] Martinez-Jimenez, C. P., Kyrmizi, I., Cardot, P., Gonzalez, F. J., Talianidis, I., Hepatocyte Nuclear Factor 4 alpha Coordinates a Transcription Factor Network Regulating Hepatic Fatty Acid Metabolism. *Mol Cell Biol* 2010, *30*, 565-577.
[72] Wieland, T., Hippe, H. J., Ludwig, K., Zhou, X. B.*, et al.*, in: Simon, M. I., Crane, B. R., Crane, A. (Eds.), *Methods in Enzymology, Vol 471: Two-Component Signaling Systems, Part C*, Elsevier Academic Press Inc, San Diego 2010, pp. 379-402.
[73] Postel, E. H., Berberich, S. J., Flint, S. J., Ferrone, C. A., Human c-myc transcription factor puf identified as nm23-h2 nucleoside diphosphate kinase, a candidate suppressor of tumor-metastasis. *Science* 1993, *261*, 478-480.
[74] Ma, S. G., Zhu, M. S., Recent advances in applications of liquid chromatography-tandem mass spectrometry to the ana lysis of reactive drug metabolites. *Chem-Biol Interact* 2009, *179*, 25-37.

[75] Wisniewski, J. R., Zougman, A., Nagaraj, N., Mann, M., Universal sample preparation method for proteome analysis. *Nat Methods* 2009, *6*, 359-U360.
[76] Cox, J., Hein, M. Y., Luber, C. A., Paron, I.*, et al.*, Accurate Proteome-wide Label-free Quantification by Delayed Normalization and Maximal Peptide Ratio Extraction, Termed MaxLFQ. *Molecular & Cellular Proteomics* 2014, *13*, 2513-2526.
[77] Bertola, A., Mathews, S., Ki, S. H., Wang, H., Gao, B., Mouse model of chronic and binge ethanol feeding (the NIAAA model). *Nat Protoc* 2013, *8*, 627-637.
[78] Mayfield, J., Arends, M. A., Harris, R. A., Blednov, Y. A., in: Bell, R. L., Rahman, S. (Eds.), *Animal Models for Medications Screening to Treat Addiction*, Elsevier Academic Press Inc, San Diego 2016, pp. 293-355.
[79] Levine, R. L., Berlett, B. S., Moskovitz, J., Mosoni, L., Stadtman, E. R., Methionine residues may protect proteins from critical oxidative damage. *Mechanisms of Ageing and Development* 1999, *107*, 323-332.
[80] Reddy, V. Y., Desrochers, P. E., Pizzo, S. V., Gonias, S. L.*, et al.*, Oxidative Dissociation of Human Alpha(2)-Macroglobulin Tetramers into Dysfunctional Dimers. *Journal of Biological Chemistry* 1994, *269*, 4683-4691.
[81] Kanayama, A., Inoue, J., Sugita-Konishi, Y., Shimizu, M., Miyamoto, Y., Oxidation of I kappa B alpha at methionine 45 is one cause of taurine chloramine-induced inhibition of NF-kappa B activation. *Journal of Biological Chemistry* 2002, *277*, 24049-24056.
[82] Bartlett, R. K., Urbauer, R. J. B., Anbanandam, A., Smallwood, H. S.*, et al.*, Oxidation of Met(144) and Met(145) in calmodulin blocks calmodulin dependent activation of the plasma membrane Ca-ATPase. *Biochemistry* 2003, *42*, 3231-3238.
[83] Tuma, D., Casey, C., Dangerous byproducts of alcohol breakdown - Focus on adducts. *Alcohol Research & Health* 2003, *27*, 285-290.
[84] Deleve, L. D., Kaplowitz, N., Glutathione Metabolism and Its Role in Hepatotoxicity. *Pharmacol Therapeut* 1991, *52*, 287-305.
[85] Shepard, B. D., Tuma, P. L., Alcohol-induced protein hyperacetylation: mechanisms and consequences. *World journal of gastroenterology : WJG* 2009, *15*, 1219-1230.
[86] Chang, L. F., Karin, M., Mammalian MAP kinase signalling cascades. *Nature* 2001, *410*, 37-40.
[87] Matthews, H. R., Protein-Kinases and Phosphatases That Act on Histidine, Lysine, or Arginine Residues in Eukaryotic Proteins - a Possible Regulator of the Mitogen-Activated Protein-Kinase Cascade. *Pharmacol Therapeut* 1995, *67*, 323-350.
[88] Aksnes, H., Hole, K., Arnesen, T., in: Jeon, K. W. (Ed.), *International Review of Cell and Molecular Biology, Vol 316*, Elsevier Academic Press Inc, San Diego 2015, pp. 267-305.
[89] Fernandezcheca, J. C., Hirano, T., Tsukamoto, H., Kaplowitz, N., Mitochondrial Glutathione Depletion in Alcoholic Liver-Disease. *Alcohol* 1993, *10*, 469-475.
[90] Cederbaum, A. I., CYP2E1 - Biochemical and toxicological aspects and role in alcohol-induced liver injury. *Mt Sinai J Med* 2006, *73*, 657-672.
[91] Lieber, C. S., CYP2E1: from ASH to NASH. *Hepatol Res* 2004, *28*, 1-11.
[92] Dai, Y., Rashbastep, J., Cederbaum, A. I., Stable expression of human cytochrome-p4502e1 in hepg2 cells - characterization of catalytic activities and production of reactive oxygen intermediates. *Biochemistry* 1993, *32*, 6928-6937.
[93] Yin, D., Kuczera, K., Squier, T. C., The sensitivity of carboxyl-terminal methionines in calmodulin isoforms to oxidation by H2O2 modulates the ability to activate the plasma membrane Ca-ATPase. *Chemical Research in Toxicology* 2000, *13*, 103-110.
[94] Bell-Temin, H., Zhang, P., You, M., Liu, B., Stevens, S. M., Novel Insights into Ethanol-Induced Microglia Response Using Silac-Based Proteomics. *Alcoholism-Clinical and Experimental Research* 2013, *37*, 127a-127a.

[95] Schumacher, B., van der Pluijm, I., Moorhouse, M. J., Kosteas, T.*, et al.*, Delayed and accelerated aging share common longevity assurance mechanisms. *Plos Genet* 2008, *4*, e1000161.
[96] Wei, Y. F., Matthews, H. R., Identification of phosphohistidine in proteins and purification of protein-histidine kinases. *Methods in enzymology* 1991, *200*, 388-414.
[97] Peter, J. B., Hultquist, D. E., Deluca, M., Boyer, P. D., Kreil, G., Bound Phosphohistidine as an Intermediate in a Phosphorylation Reaction of Oxidative Phosphorylation Catalyzed by Mitochondrial Extracts. *Journal of Biological Chemistry* 1963, *238*, 1182-&.
[98] Wilson, C. G., Schupp, M., Burkhardt, B. R., Wu, J. M.*, et al.*, Liver-Specific Overexpression of Pancreatic-Derived Factor (PANDER) Induces Fasting Hyperglycemia in Mice. *Endocrinology* 2010, *151*, 5174-5184.
[99] Ramus, C., Hovasse, A., Marcellin, M., Hesse, A. M.*, et al.*, Benchmarking quantitative label-free LC-MS data processing workflows using a complex spiked proteomic standard dataset. *J Proteomics* 2016, *132*, 51-62.
[100] Marijanovic, Z., Laubner, D., Moller, G., Gege, C.*, et al.*, Closing the gap: I dentification of human 3-ketosteroid reductase, the last unknown enzyme of mammalian cholesterol biosynthesis. *Mol Endocrinol* 2003, *17*, 1715-1725.
[101] Evan, G. I., Wyllie, A. H., Gilbert, C. S., Littlewood, T. D.*, et al.*, Induction of apoptosis in fibroblasts by c-myc protein. *Cell* 1992, *69*, 119-128.
[102] Marino, M., Galluzzo, P., Ascenzi, P., Estrogen signaling multiple pathways to impact gene transcription. *Curr. Genomics* 2006, *7*, 497-508.
[103] Shehu, A., Albarracin, C., Devi, Y. S., Luther, K.*, et al.*, The Stimulation of HSD17B7 Expression by Estradiol Provides a Powerful Feed-Forward Mechanism for Estradiol Biosynthesis in Breast Cancer Cells. *Mol Endocrinol* 2011, *25*, 754-766.
[104] Mukherjee, B., Morgenbesser, S. D., Depinho, R. A., Myc family oncoproteins function through a common pathway to transform normal-cells in culture - cross-interference by max and trans-acting dominant mutants. *Genes & Development* 1992, *6*, 1480-1492.
[105] Wu, D. F., Cederbaum, A. I., Opposite action of S-adenosyl methionine and its metabolites on CYP2E1-mediated toxicity in pyrazole-induced rat hepatocytes and HepG2 E47 cells. *Am J Physiol-Gastr L* 2006, *290*, G674-G684.
[106] Guillou, V., Plourde-Owobi, L., Parrou, J. L., Goma, G., Francois, J., Role of reserve carbohydrates in the growth dynamics of Saccharomyces cerevisiae. *FEMS Yeast Res.* 2004, *4*, 773-787.
[107] Mustacich, D. J., Bruno, R. S., Traber, M. G., Vitamin E. *Vitam Horm* 2007, *76*, 1-21.
[108] Mustacich, D. J., Leonard, S. W., Patel, N. K., Traber, M. G., alpha-tocopherol beta-oxidation localized to rat liver mitochondria. *Free Radical Bio Med* 2010, *48*, 73-81.
[109] Wang, L., Zheng, Y. S., Gao, X. X., Liu, Y. C., You, X. Q., Retinoid X receptor ligand regulates RXR alpha/Nur77-dependent apoptosis via modulating its nuclear export and mitochondrial targeting. *International Journal of Clinical and Experimental Pathology* 2017, *10*, 10770-+.
[110] Berggre, P. O., Signal-transduction in type 1 diabetes mellitus. *Horm. Res.* 2008, *70*, 1-2.
[111] Liadis, N., Murakami, K., Eweida, M., Elford, A. R.*, et al.*, Caspase-3-dependent beta-cell apoptosis in the initiation of autoimmune diabetes mellitus. *Mol Cell Biol* 2005, *25*, 3620-3629.
[112] Shen, H. L., Yang, P. Q., Liu, Q. J., Tian, Y., Nuclear expression and clinical significance of phosphohistidine phosphatase 1 in clear-cell renal cell carcinoma. *J. Int. Med. Res.* 2015, *43*, 747-757.
[113] Dicker, E., Cederbaum, A. I., Potter, B. J., Cultured Rat Hepatocytes as a Model for Alcohol Metabolism. *Hepatology* 1986, *6*, 1191-1191.
[114] Rhodes, J. S., Best, K., Belknap, J. K., Finn, D. A., Crabbe, J. C., Evaluation of a simple model of ethanol drinking to intoxication in C57BL/6J mice. *Physiology & Behavior* 2005, *84*, 53-63.

[115] Rath, M., Nguyen, T. G., Peris, J., McLaughlin, J. P.*, et al.*, Characterization of a gelatin-based drinking in the dark mouse model of ethanol dependence: Role of microglia. *Alcoholism-Clinical and Experimental Research* 2017, *41*, 34A-34A.
[116] Simms, J. A., Steensland, P., Medina, B., Abernathy, K. E.*, et al.*, Intermittent access to 20% ethanol induces high ethanol consumption in Long-Evans and Wistar rats. *Alcoholism-Clinical and Experimental Research* 2008, *32*, 1816-1823.
[117] Becker, H. C., Lopez, M. F., Increased ethanol drinking after repeated chronic ethanol exposure and withdrawal experience in C57BL/6 mice. *Alcoholism-Clinical and Experimental Research* 2004, *28*, 1829-1838.
[118] Conigrave, K. M., Davies, P., Haber, P., Whitfield, J. B., Traditional markers of excessive alcohol use. *Addiction* 2003, *98*, 31-43.
[119] Nan, Y. M., Kong, L. B., Ren, W. G., Wang, R. Q.*, et al.*, Activation of peroxisome proliferator activated receptor alpha ameliorates ethanol mediated liver fibrosis in mice. *Lipids Health Dis* 2013, *12*.
[120] Gong, P. F., Cederbaum, A. I., Nrf2 is increased by CYP2E1 in rodent liver and HepG2 cells and protects against oxidative stress caused by CYP2E1. *Hepatology* 2006, *43*, 144-153.
[121] Krishnamurthy, P. C., Du, G. Q., Fukuda, Y., Sun, D. X.*, et al.*, Identification of a mammalian mitochondrial porphyrin transporter. *Nature* 2006, *443*, 586-589.
[122] Boswell-Casteel, R. C., Fukuda, Y., Schuetz, J. D., ABCB6, an ABC Transporter Impacting Drug Response and Disease. *Aaps J.* 2018, *20*.
[123] Nilsson, J. A., Cleveland, J. L., Myc pathways provoking cell suicide and cancer. *Oncogene* 2003, *22*, 9007-9021.
[124] Wang, Y. M., Ong, S. S., Chai, S. C., Chen, T. S., Role of CAR and PXR in xenobiotic sensing and metabolism. *Expert Opinion on Drug Metabolism & Toxicology* 2012, *8*, 803-817.
[125] Ronsein, G. E., Pamir, N., von Haller, P. D., Kim, D. S.*, et al.*, Parallel reaction monitoring (PRM) and selected reaction monitoring (SRM) exhibit comparable linearity, dynamic range and precision for targeted quantitative HDL proteomics. *J Proteomics* 2015, *113*, 388-399.
[126] Rauniyar, N., Parallel Reaction Monitoring: A Targeted Experiment Performed Using High Resolution and High Mass Accuracy Mass Spectrometry. *Int J Mol Sci* 2015, *16*, 28566-28581.
[127] Galli, A., Pinaire, J., Fischer, M., Dorris, R., Crabb, D. W., The transcriptional and DNA binding activity of peroxisome proliferator-activated receptor alpha is inhibited by ethanol metabolism - A novel mechanism for the development of ethanol-induced fatty liver. *Journal of Biological Chemistry* 2001, *276*, 68-75.
[128] Arneson, L. N., Leibson, P. J., Signaling in Natural Immunity: Natural Killer Cells. *Neuroimmune* 2005, *5*, 151-166.
[129] Busillo, J. M., Benovic, J. L., Regulation of CXCR4 signaling. *Bba-Biomembranes* 2007, *1768*, 952-963.
[130] Harburger, D. S., Calderwood, D. A., Integrin signalling at a glance. *J Cell Sci* 2009, *122*, 159-163.
[131] Brenner, C., Galluzzi, L., Kepp, O., Kroemer, G., Decoding cell death signals in liver inflammation. *J Hepatol* 2013, *59*, 583-594.
[132] Polireddy, K., Chavan, H., Abdulkarim, B. A., Krishnamurthy, P., Functional significance of the ATP-binding cassette transporter B6 in hepatocellular carcinoma. *Mol Oncol* 2011, *5*, 410-425.
[133] Yin, H. Q., Kim, M., Kim, J. H., Kong, G.*, et al.*, Differential gene expression and lipid metabolism in fatty liver induced by acute ethanol treatment in mice. *Toxicol Appl Pharm* 2007, *223*, 225-233.
[134] Sekiya, S., Suzuki, A., Glycogen synthase kinase 3 beta-dependent Snail degradation directs hepatocyte proliferation in normal liver regeneration. *Proceedings of the National Academy of Sciences of the United States of America* 2011, *108*, 11175-11180.
[135] Hevia, H., Varela-Rey, M., Corrales, F. J., Berasain, C.*, et al.*, 5 '-methylthioadenosine modulates the inflammatory response to endotoxin in mice and in rat hepatocytes. *Hepatology* 2004, *39*, 1088-1098.

[136] Saha, A., Ahn, S., Blando, J., Su, F.*, et al.*, Proinflammatory CXCL12-CXCR4/CXCR7 Signaling Axis Drives Myc-Induced Prostate Cancer in Obese Mice. *Cancer Res* 2017, *77*, 5158-5168.
[137] Waxman, D. J., P450 gene induction by structurally diverse xenochemicals: Central role of nuclear receptors CAR, PXR, and PPAR. *Archives of biochemistry and biophysics* 1999, *369*, 11-23.
[138] Shan, G., RNA interference as a gene knockdown technique. *International Journal of Biochemistry & Cell Biology* 2010, *42*, 1243-1251.
[139] Tan, N. S., Shaw, N. S., Vinckenbosch, N., Liu, P.*, et al.*, Selective cooperation between fatty acid binding proteins and peroxisome proliferator-activated receptors in regulating transcription. *Mol Cell Biol* 2002, *22*, 5114-5127.
[140] Schwudke, D., Liebisch, G., Herzog, R., Schmitz, G., Shevchenko, A., Shotgun lipidomics by tandem mass spectrometry under data-dependent acquisition control. *Lipidomics and Bioactive Lipids* 2007, *433*, 175-+.
[141] Jung, H. R., Sylvanne, T., Koistinen, K. M., Tarasov, K.*, et al.*, High throughput quantitative molecular lipidomics. *Biochimica et biophysica acta* 2011, *1811*, 925-934.
[142] Li, M., Zhou, Z. G., Nie, H. G., Bai, Y., Liu, H. W., Recent advances of chromatography and mass spectrometry in lipidomics. *Analytical and bioanalytical chemistry* 2011, *399*, 243-249.
[143] Zhang, W., Progress in Mass Spectrometry Acquisition Approach for Quantitative Proteomics. *Chinese J Anal Chem* 2014, *42*, 1859-1868.
[144] Prakash, A., Peterman, S., Ahmad, S., Sarracino, D.*, et al.*, Hybrid Data Acquisition and Processing Strategies with Increased Throughput and Selectivity: pSMART Analysis for Global Qualitative and Quantitative Analysis. *Journal of Proteome Research* 2014, *13*, 5415-5430.
[145] Kleparnik, K., Recent advances in combination of capillary electrophoresis with mass spectrometry: Methodology and theory. *Electrophoresis* 2015, *36*, 159-178.
[146] Tyanova, S., Temu, T., Sinitcyn, P., Carlson, A.*, et al.*, The Perseus computational platform for comprehensive analysis of (prote)omics data. *Nat Methods* 2016, *13*, 731-740.
[147] Aebersold, R., Mann, M., Mass-spectrometric exploration of proteome structure and function. *Nature* 2016, *537*, 347-355.
[148] Guzman, C., Benet, M., Pisonero-Vaquero, S., Moya, M.*, et al.*, The human liver fatty acid binding protein (FABP1) gene is activated by FOXA1 and PPAR alpha; and repressed by C/EBP alpha: Implications in FABP1 down-regulation in nonalcoholic fatty liver disease. *Biochimica Et Biophysica Acta-Molecular and Cell Biology of Lipids* 2013, *1831*, 803-818.
[149] Green, S., PPAR: A mediator of peroxisome proliferator action. *Mutat. Res.-Fundam. Mol. Mech. Mutagen.* 1995, *333*, 101-109.
[150] Mukai, S., Flematti, G. R., Byrne, L. T., Besant, P. G.*, et al.*, Stable triazolylphosphonate analogues of phosphohistidine. *Amino acids* 2012, *43*, 857-874.
[151] Kee, J. M., Oslund, R. C., Couvillon, A. D., Muir, T. W., A Second-Generation Phosphohistidine Analog for Production of Phosphohistidine Antibodies. *Organic letters* 2015, *17*, 187-189.
[152] Kee, J. M., Oslund, R. C., Perlman, D. H., Muir, T. W., A pan-specific antibody for direct detection of protein histidine phosphorylation. *Nature chemical biology* 2013, *9*, 416-U428.
[153] Oslund, R. C., Kee, J. M., Couvillon, A. D., Bhatia, V. N.*, et al.*, A phosphohistidine proteomics strategy based on elucidation of a unique gas-phase phosphopeptide fragmentation mechanism. *Journal of the American Chemical Society* 2014, *136*, 12899-12911.
[154] Cai, X. J., Srivastava, S., Surindran, S., Li, Z., Skolnik, E. Y., Regulation of the epithelial Ca2+ channel TRPV5 by reversible histidine phosphorylation mediated by NDPK-B and PHPT1. *Mol Biol Cell* 2014, *25*, 1244-1250.

Appendix A – Nature: Scientific Reports

SCIENTIFIC REPORTS

OPEN

Structural and activity characterization of human PHPT1 after oxidative modification

Received: 07 July 2015
Accepted: 07 March 2016
Published: 01 April 2016

Daniel R. Martin, Priyanka Dutta, Shikha Mahajan, Sameer Varma & Stanley M. Stevens Jr.

Phosphohistidine phosphatase 1 (PHPT1), the only known phosphohistidine phosphatase in mammals, regulates phosphohistidine levels of several proteins including those involved in signaling, lipid metabolism, and potassium ion transport. While the high-resolution structure of human PHPT1 (hPHPT1) is available and residues important for substrate binding and catalytic activity have been reported, little is known about post-translational modifications that modulate hPHPT1 activity. Here we characterize the structural and functional impact of hPHPT1 oxidation upon exposure to a reactive oxygen species, hydrogen peroxide (H_2O_2). Specifically, liquid chromatography-tandem mass spectrometry was used to quantify site-specific oxidation of redox-sensitive residues of hPHPT1. Results from this study revealed that H_2O_2 exposure induces selective oxidation of hPHPT1 at Met95, a residue within the substrate binding region. Explicit solvent molecular dynamics simulations, however, predict only a minor effect of Met95 oxidation in the structure and dynamics of the apo-state of the hPHPT1 catalytic site, suggesting that if Met95 oxidation alters hPHPT1 activity, then it will do so by altering the stability of an intermediate state. Employing a novel mass spectrometry-based assay, we determined that H_2O_2–induced oxidation does not impact hPHPT1 function negatively; a result contrary to the common conception that protein oxidation is typically a loss-of-function modification.

Phosphorylation of serine, threonine and tyrosine residues is vital to various cellular processes including signal transduction and cell metabolism; however, the role of histidine phosphorylation, specifically in the context of mammalian cell signaling, is relatively unexplored. Over the past several decades, several protein targets of histidine phosphorylation in eukaryotic systems have been identified including ATP-citrate lyase[1], G protein (beta subunit)[2], histone H4[3], the potassium ion channel KCa3.1[4] as well as the phosphorylated enzyme intermediates involved in phosphoryl group transfers to metabolites[5–7]. The addition or removal of the histidine phosphoryl group in these proteins is mediated through the action of histidine kinases or phosphatases, respectively, where only a few eukaryotic enzymes have been identified to date. These enzymes include nucleoside diphosphate kinase[8] as well as phosphohistidine phosphatase 1 (PHPT1)[9].

PHPT1 was identified in porcine liver in 2002 as a 14 kDa protein that possesses phosphatase activity for phosphohistidine residues[9] and has also been shown to catalyze the dephosphorylation of phosphoramidate[10] as well as phospholysine[11]. Since its discovery, PHPT1 has been shown to be involved in regulating the levels of known mammalian phosphohistidine targets. For example, PHPT1 plays a negative regulatory role when removing the histidine phosphoryl group in the potassium ion channel, KCa3.1[4]. Additionally, PHPT1 overexpression in neuroblastoma and primary neurons decreases ATP-citrate lyase activity and cell viability[12]. PHPT1 was also demonstrated to participate in G-protein mediated cell signaling in islet β cells[13]. PHPT1 is part of the Janus family of proteins, and the only phosphohistidine phosphatase identified within this family in humans to date according to family domain classification available on the Universal Protein Resource (www.uniprot.org). Janus family proteins are best characterized in *Drosophila melanogaster* where they are involved in sex differentiation; however, their role as phosphohistidine phosphatases is still unclear[14].

The human PHPT1 (hPHPT1) structure is composed of six β-strands flanked by two α-helices[15]. The substrate-binding site is positioned between two loops, one between α1 and β4, and the other between β5 and α2[15]. This site is composed of multiple residues that have been shown to be important for substrate binding, including Glu51, Tyr52, His53, Tyr93, and Met95[15]. Additionally, the NH groups of Ala54, Ala96, and His53 and the OH group of Ser94 are involved in stabilizing phosphate binding to the active site of hPHPT1[16].

Department of Cell Biology, Microbiology and Molecular Biology, University of South Florida, Tampa, FL 33620, USA. Correspondence and requests for materials should be addressed to S.M.S. (email: smstevens@usf.edu)

While the residues important for hPHPT1 activity and substrate binding have been characterized, there have been no studies concerning the structural and functional outcomes of post-translational modification (PTM) or chemical modification to this protein. To the best of our knowledge, N-terminal protein acetylation is the only PTM identified on hPHPT1[17]. Here, we investigate the impact of oxidation, specifically through the known reactive oxygen species (ROS), hydrogen peroxide (H_2O_2), on hPHPT1 structure and related activity using mass spectrometry and computational methods. ROS are highly reactive molecules that induce functional alterations in the cell and their overproduction is linked to fundamental biological processes, such as aging as well as pathophysiological processes of disease[18]. Using mass spectrometry, H_2O_2-induced global oxidation of recombinant hPHPT1 as well as site-specific quantitation of protein oxidation was performed. Additionally, a mass spectrometry-based activity assay was developed to determine the functional impact of hPHPT1 oxidation and to provide additional specificity compared to results from a colorimetric activity assay that employed a non-specific phosphatase substrate. Moreover, computational studies using molecular dynamics simulations were carried out to investigate structural outcomes from selective methionine oxidation of hPHPT1. The results from this combined experimental and computational study provide new insight into the significance of hPHPT1 as a target of ROS and highlight the importance of elucidating the correlation of structural to functional diversity brought about by protein modifications.

Materials and Methods

hPHPT1 oxidation. Human recombinant PHPT1 (referred to as hPHPT1) was obtained from Sino Biological Inc. (catalog number: 12473-H07E) and stored at a concentration of 1 mg/ml in phosphate buffered saline (PBS). This stock solution was used to create a 20 μM solution diluted in PBS for subsequent oxidation characterization and activity analysis using mass spectrometry. From this solution, 46 μl were combined with either 46 μL of water or H_2O_2, at various concentrations, to create a 10 μM solution of hPHPT1 with H_2O_2. The solution was then incubated in a heat bath at 37 °C for two hours to allow oxidation to occur. Each sample was then processed for either the phosphohistidine phosphatase activity assay using mass spectrometry or para-nitrophenyl phosphate assay described below. Two μg of protein, taken directly from the same samples used for the phosphohistidine phosphatase activity assay, were used for oxidative site mapping by mass spectrometry.

Oxidation site mapping using mass spectrometry. The hPHPT1 samples for oxidation site mapping by mass spectrometry were first reduced and alkylated with DTT and iodoacetamide, respectively, followed by dilution in a digestion buffer containing 25 mM ammonium bicarbonate. Protein digestion with trypsin (Promega) was carried out overnight at 37 degrees C and then the samples were desalted using Hypersep C18 columns (Thermo Scientific) columns. Following centrifugation of the samples under vacuum until dryness, samples were resuspended in 0.1% formic acid in water for mass spectrometric analyses. Peptides generated from the trypsin digestion were separated on an Acclaim PepMap C18 (75 μm × 50 cm) UPLC column (Thermo) using an EASY-nLC 1000 with a gradient time of 60 min (2–40% acetonitrile in 0.1% formic acid). Mass spectrometric analysis was performed by a hybrid quadrupole-Orbitrap instrument (Q Exactive Plus, Thermo), using a top 10 data-dependent acquisition method with a dynamic exclusion time of 20 seconds. Full scan and MS/MS resolution was 70,000 and 17,500, respectively.

High-resolution mass spectrometric data were searched against the Uniprot human database using the MaxQuant (version 1.5.0.3, maxquant.org) search algorithm. Variable modifications included mono-oxidation of methionine, cysteine, and tyrosine, di-oxidation of methionine, tryptophan, and cysteine, tri-oxidation of cysteine, and carbamidomethylation of cysteine. MaxQuant search parameters included a first search peptide tolerance of 20 ppm and a main search peptide tolerance of 4.5 ppm. Global-scale automated modification quantitation was performed using the MaxQuant calculation of mod/base ratio for each oxidative modification and then normalized to the most oxidized amino acid residue. Identifications were accepted at a protein and peptide false discovery rate of less than 1% and overall localization probabilities of $\geq$95% for modified peptides. The MaxQuant viewer and Scaffold (version 4.4.3, Proteome Software) were used to visualize annotated MS/MS spectra to confirm modification-specific locations. Xcalibur Qual Browser (ThermoScientific; version 2.2) was then employed to further quantify residue-specific oxidation using high mass accuracy, extracted ion chromatogram-based (XIC) quantitation for residues exhibiting significant changes in MaxQuant mod/base ratio values. In this approach, area-under-the-curve (AUC) values were determined for both the oxidized and non-oxidized peptide ions based on the m/z values of the monoisotopic and A + 1 peak using a mass tolerance of 5 ppm and a precision of 5 decimal places for chromatogram reconstruction. Ratios of the oxidized: non-oxidized peptides were determined for each replicate and then averaged for each treatment. These average ratios were then used to determine fold changes relative to the amount of oxidation that occurred in the control groups. Statistical significance was established at $p < 0.05$ using the Student's t-test (two-tailed, homoscedastic) with at least three replicates for all experiments.

Molecular Dynamics. The MD simulations of hPHPT1 and its oxidized form were carried out under identical conditions. The initial coordinates of hPHPT1 were taken from the NMR structure of its apo-state (PDB ID: 2OZX)[16], and those of its oxidized form were constructed by substituting Met95 in the NMR structure by methionine sulfoxide. Both forms of hPHPT1 were simulated in cubic boxes containing 13,130 water molecules and discrete K^+ and Cl^- ions, with their specific numbers corresponding to ionic strengths of 100 mM. The ionization states of the titratable groups in hPHPT1 were assigned according to the NMR data, and the charge neutrality of the unit cells was set by choosing appropriate differences between the numbers of K^+ and Cl^- ions. Both forms of hPHPT1 were simulated under isobaric-isothermal boundary conditions. Pressure was maintained at 1 bar using extended ensemble approach[19] with a coupling constant of 1 ps and a compressibility of 4.5×10^{-5} bar^{-1}. Temperature was maintained at 310 K using the velocity rescale approach[20] with a coupling constant of

1 ps. Electrostatic interactions were computed using the particle mesh Ewald scheme[21] with a Fourier grid spacing of 0.15 nm, a sixth-order interpolation, and a direct space cutoff of 10 Å. Van der Waals interactions were computed explicitly for inter atomic distance up to 10 Å. The bonds in proteins were constrained using the P-LINCS algorithm[22], and the geometries of the water molecules were constrained using SETTLE[23]. These constraints permitted use of an integration time step of 2 fs. The protein and ions were described using OPLS-AA parameters[24], and the water molecules were described using TIP4P parameters[25]. We used GROMACS version 4.5.3 for all MD simulations[26].

Phosphohistidine synthesis. To synthesize the phosphohistidine-containing peptide that is a reported substrate of PHPT1, phosphoramidate (5.4 mg) was first combined with the peptide (4.6 mg), suc-AHPF-pNA, (MW 690.7 Da, BaChem) in 200 µL of H_2O at pH 9 with NaOH. This solution was then shaken for 5 hours at room temperature to allow the phosphorylation reaction to occur. Immediately following the reaction, liquid chromatography was performed on the phosphohistidine-containing peptide. This was achieved using a glass pipette filled with Dowex 3 anion exchange resin, stopped with 2 mm of cotton. The resin was washed three times with 200 µl of 25 mM Tris buffer pH 9 to equilibrate the column prior to sample loading. A pipette stopper was used to speed up the chromatography movement and make sure the wash had completely flowed through before any sample was introduced. The full volume of approximately 205 µl of the phosphohistidine sample was then loaded onto the column followed by sample saturation on the column through positive pressure induced by the pipette stopper. Sample was collected and stored at 4 °C prior to mass spectrometry analyses with longer storage times resulting in greater histidine phosphorylation. This procedure yielded 35–40% histidine phosphorylation as approximated by mass spectrometric intensities of the phosphorylated and non-phosphorylated peptide ions in the product mixture.

Mass spectrometric phosphohistidine phosphatase activity assay. The hPHPT1 samples treated with H_2O_2 treatments or H_2O and PBS as a control were added to a custom reaction buffer (5:95% v/v acetonitrile: H_2O and 20 mM ammonium bicarbonate, pH 8.5, referred to as RB) to reach a final concentration of 0.37 µM and the phosphohistidine peptide solution was added to reach a final concentration of 2.4 mM. The solution was then vortexed for 5 s and analyzed by direct infusion combined with ESI-MS, using a hybrid linear ion trap-Orbitrap (Orbitrap XL, ThermoFisher) mass spectrometer to determine mass spectrometric peak intensities of the phosphorylated and non-phosphorylated peptide for 30 min in RB. The instrument was tuned to the phosphorylated peptide peak at m/z 771.2. The following electrospray ionization (ESI) source settings allowed for optimal signal of the phosphohistidine-containing peptide: Source Voltage: 5.00 V, Sheath Gas Flow Rate: 8 (arb), Capillary Voltage: 46.00 V, Capillary Temp: 275 °C, Tube Lens Voltage: 135 V. Samples were infused directly using a flow rate of 3 µl/min. These optimized settings were used for all experiments utilizing the phosphohistidine peptide on this instrument in order to minimize API source-mediated phosphate loss from the phosphopeptide substrate[27]. Non-phosphorylated and phosphorylated peptide sequences were confirmed used collision-induced dissociation with an isolation width of 2.0, a normalized collision energy of 33, an activation Q of 0.25, and an activation time of 30 ms in the linear ion trap followed by high resolution detection of the fragment ions in the Orbitrap mass analyzer. Full scan MS and MS/MS spectra were acquired in centroid mode.

After a delay of approximately 1 min between the start of the reaction and the direct infusion of the sample, intensity measurement was performed on several peaks corresponding to the non-phosphorylated peptide including m/z 691, 713, and 729 ($[M+H]^+$, $[M+Na]^+$, and $[M+K]^+$, respectively) in comparison with m/z 771, 793, and 809 peaks representing the phosphorylated peptide ($[M_{phospho}+H]^+$, $[M_{phospho}+Na]^+$ and $[M_{phospho}+K]^+$, respectively) over the time course of 30 min. Full MS spectra were averaged over 5 min time intervals (0–5 min, 5–10 min, etc.) and the intensities of each peak relating to the phosphorylated and non-phosphorylated peptide were then used to calculate the ratio of total phosphorylated: total non-phosphorylated peptide (Intensities of all the phosphorylated peptide peaks/intensities of all non-phosphorylated peptide peaks). The negative fold change, which corresponds to the conversion of the phosphorylated peptide by hPHPT1, was calculated and compared to the average ratio of the non-treated phosphohistidine peptide over all time points to account for any phosphohistidine loss during injection.

Colorimetric phosphatase activity assay. The hPHPT1 samples were treated and prepared similarly to the previous assay (see Methods: h*PHPT1 oxidation*). However, aliquots of 10 µg of total hPHPT1 were used for each treatment. The reaction buffer was prepared according to Gong *et al.* using a total volume of 300 µl, per sample, containing 50 mM Tris/HCl and 5 mM DTT where the pH was increased to 8.0 with NaOH[16]. The concentration of para-nitrophenyl phosphate (*p*NPP; MP Bio) used was 5 mM and was added to the reaction buffer immediately before being plated. The final concentration of hPHPT1 in the solution volume (300 µl) was 2.1 µM (10 µg) for each sample. All samples were kept one ice until plated in a 96 well plate. The reaction buffer and hPHPT1 samples were added to the well in triplicates where 100 µl were plated per replicate. The plate was then immediately added to the plate reader (heated to 37 °C) to begin the reaction after the initial absorbance measurement. The absorbance was measured at 405 nm for the non-phosphorylated product, *p*-nitrophenolate, and this measurement was taken every 3 min over the course of 2 h. Concentrations were determined using the molar extinction coefficient[16] of 17.8 $mM^{-1}cm^{-1}$ and the light path length calculated based on the average radius of the wells (r = 4 mm) and quantity of reaction mixture (100 µl) in the well.

Enzyme kinetic analysis was performed for the non-oxidized (non-treated) hPHPT1 samples and the 500 µM H_2O_2-treated hPHPT1 samples. A substrate concentration range of 0.8 mM – 40 mM pNPP was used to obtain initial reaction velocities for Michaelis-Menten kinetics. Initial reaction velocities were calculated using the slope of the most linear portion of the curve created by plotting the amount of non-phosphorylated substrate generated over time. Initial reaction velocities and pNPP concentrations were then analyzed using Prism, Graph Pad

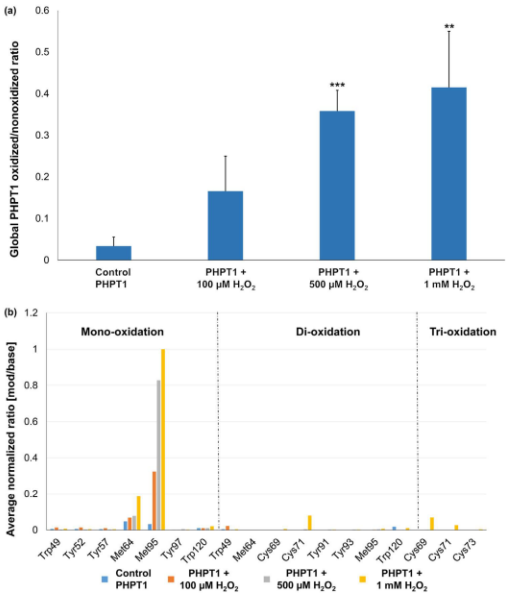

Figure 1. Global and amino acid-specific oxidation of hPHPT1. (**a**) Global hPHPT1 oxidized/non-oxidized ratios following treatment with H_2O_2 at various concentrations were determined using the sum of intensities for all oxidized peptides/sum of intensities for non-oxidized peptides based on identified hPHPT1-derived peptides from MaxQuant. Error bars represent standard deviation. **indicates $p < 0.01$, ***indicates $p < 0.001$ using Student's t-test comparison of treatment to control group (**b**) Control and H_2O_2-treated hPHPT1 were digested with trypsin and analyzed by LC-MS/MS. Mass spectrometric data were analyzed by MaxQuant and average mod/base values for oxidized peptides identified were normalized to the largest value (corresponding to mono-oxidation of Met95) and displayed for relative comparison of amino acid residues susceptible to oxidation (Trp, Tyr, Met, and Cys). Residues shown are present on hPHPT1-derived tryptic peptides from MaxQuant filtered at 1% FDR and >95% overall localization probability.

(version 6.07) by fitting to the Michaelis-Menten equation. Average K_m and V_{max} values for each non-oxidized and oxidized hPHPT1 were reported with a 95% confidence interval. The k_{cat} of each sample was then calculated using V_{max} values and the final concentration of hPHPT1 used in the assay.

Results

H_2O_2 induced oxidation of hPHPT1. The specific location and extent of protein oxidation induced by H_2O_2 was determined by LC- tandem mass spectrometry (MS/MS). Recombinant hPHPT1 was incubated for two hours in a heat bath at 37 °C with 0 μM, 100 μM, 500 μM, and 1 mM H_2O_2 (in triplicate). After LC-MS/MS analysis of trypsin-digested hPHPT1 from each treatment group, the mass spectrometric data were searched against the Uniprot human database with mono- and di-oxidation of Met, Cys, Tyr, and Trp as well as tri-oxidation of Cys set as variable modifications. hPHPT1 sequence coverage ranged from 95% to 99% and included all Met, Cys, Tyr, and Trp residues that were analyzed for oxidation quantitation. Using the MaxQuant intensity values for hPHPT1-derived peptides, the ratio of total oxidized peptide intensity/nonoxidized peptide intensity was calculated for each treatment group. As shown in Fig. 1a, a H_2O_2 concentration-dependent increase in hPHPT1 oxidation was observed. Furthermore, we used the MaxQuant value, mod/base, to assess the amount of residue-specific oxidation of Met, Cys, Tyr, and Trp residues. This analysis showed that Met95 was the most prominent site of H_2O_2 –induced oxidation, followed by Met64 (Fig. 1b). Additionally, di- and tri-oxidation of Cys71 was detected but only in the 1 mM H_2O_2 treatment group and at lower mod/base values than the methionine residues. Annotated MS/MS spectra (exported from Scaffold) for both Met64- and Met95-containing tryptic peptides as well as tri-oxidation of the Cys71-containing peptide are shown in Fig. 2. The MS/MS spectra allowed for confirmation of peptide sequence and oxidation site localization as well as peptide retention times used for manual extracted ion chromatogram (XIC)-based quantitation of oxidation with high mass accuracy.

Given the methionine residues of hPHPT1 were identified as a H_2O_2-induced oxidation target based on our unbiased screening approach using MaxQuant, XIC-based quantitation of oxidation at each of the two Met residues, Met64 and Met95, was performed with high mass accuracy in order to confirm and quantify oxidation with higher specificity. Representative XICs as well as the full scan mass spectrum averaged over the

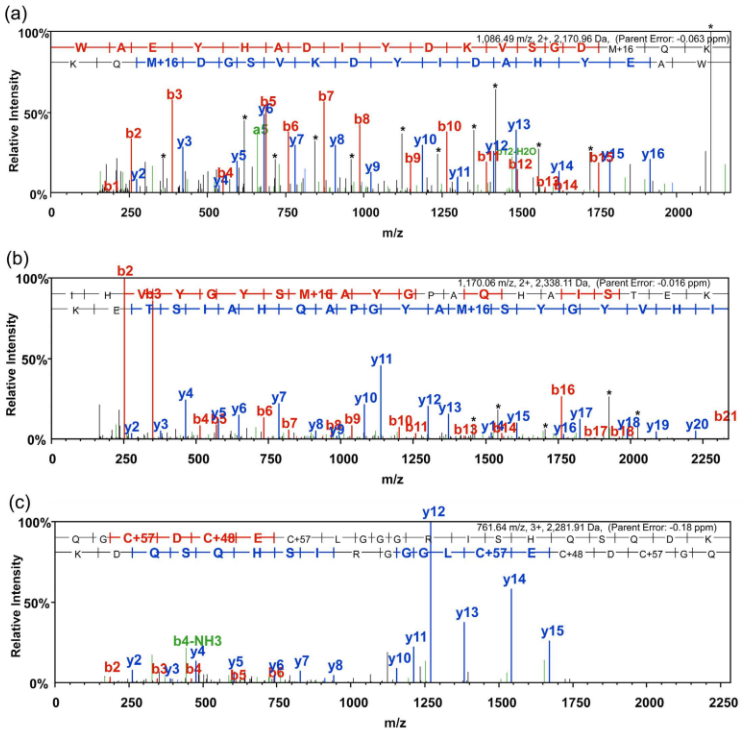

Figure 2. Representative MS/MS spectra of tryptic peptides derived from oxidized hPHPT1 used to identify the sequence and localize the oxidation site of (a) Met64 mono-oxidation, (b) Met95 mono-oxidation, (c) Cys71 tri-oxidation. Annotated MS/MS spectra were exported from Scaffold where b- and y-type ions represent location of amide bond cleavage from CID as shown in the sequence above the MS/MS spectrum. Peaks in black and marked with * of mono-oxidized methionine-containing peptides correspond to a neutral loss of 64 Da (-CH_4SO) from the fragment ions.

chromatographic peak width are shown for the Met95- and Met64-containing tryptic peptide in Fig. 3a,b, respectively. Area-under-the-curve (AUC) values from high mass accuracy-based XICs were then used to determine the relative abundance of oxidized peptides compared to non-oxidized peptides. The Met95-containing tryptic peptide showed a significant increase in oxidation between the control and all H_2O_2 treatments (Fig. 3c). An approximate 9-, 26-, and 41-fold increase in oxidation of Met95 was observed after 100 μM, 500 μM, and 1 mM H_2O_2 treatment, respectively. The Met64–containing tryptic peptide revealed lower levels of oxidation (up to 2-fold increase) and none significantly different from untreated hPHPT1 (Fig. 3c). The Met64-containing peptide was detected predominantly with one missed cleavage by trypsin; however, the peptide containing Met64 with no missed cleavage was also used for XIC-based quantitation. We note that the relatively higher oxidation of Met95 compared to that of Met64 is also consistent with the 3D structure of hPHPT1. As shown in Fig. 3d, while Met95 is exposed to solvent, Met64 is mostly buried and flanked by hydrophobic residues.

The significance of selective Met95 oxidation stems from the observation that it is located at hPHPT1's substrate-binding site and that it has been shown to be important to substrate binding[28]. It is, therefore, plausible that oxidation of Met95 could modulate substrate binding and/or phosphatase activity.

Effect of Met95 oxidation on the structure and dynamics of hPHPT1. All atom molecular dynamics (MD) simulations were employed to predict the response of Met95 oxidation on the structure and dynamics of hPHPT1. The study was restricted to hPHPT1's apo-state as currently there isn't sufficient experimental data to model the substrate-bound state. The basic strategy is to subject both oxidized and non-oxidized forms of hPHPT1 to MD simulations in explicit solvent and then systematically analyze the difference between them. Instead of generating one single MD trajectory, three separate 100 ns long MD trajectories were generated for each of the two forms – the motivation behind this was to enhance search in conformational space. We then

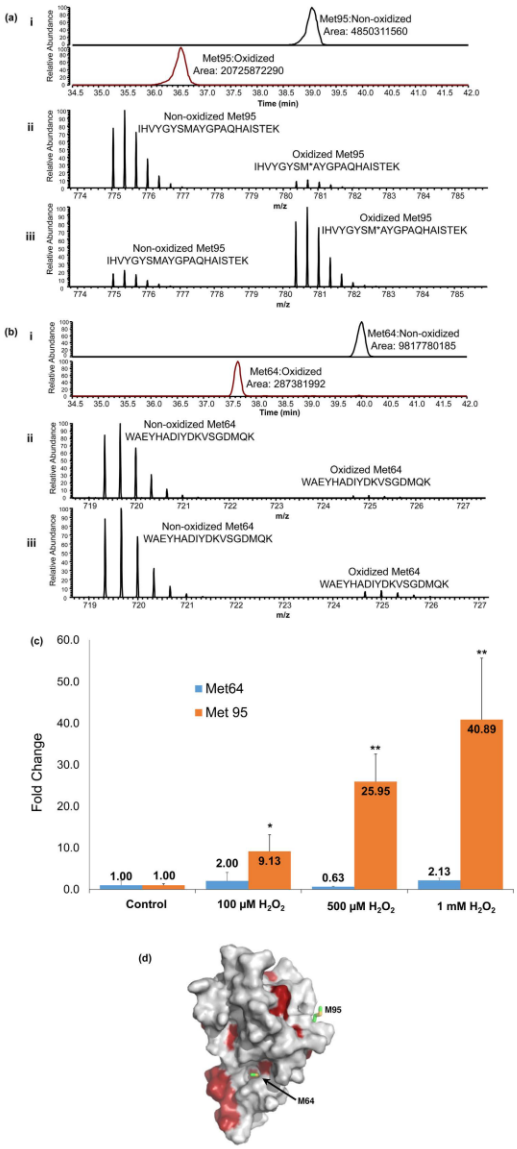

Figure 3. Quantitation of methionine oxidation in H_2O_2-treated hPHPT1. Representative accurate mass-based (< 5 ppm) extracted ion chromatograms (XIC) corresponding to 1 mM H_2O_2-treated samples were generated for the Met95- (**a**)(i) and Met64-containing (**b**)(i) tryptic peptides. Superimposed full scan mass spectrum reflecting the relative abundance of the non-oxidized peptide compared to the oxidized cognate peptide in control hPHPT1 (untreated) for the Met95- (**a**)(ii) and Met64-containing (**b**)(ii) peptides. Overlay (3D) was performed in the Qual Browser (Thermo) data viewer followed by spectrum normalization to the largest peak in the scan with multiple scans normalized all the same. Spectrum reflecting the same peptides following 1 mM H_2O_2 treatment for the Met95- (**a**)(iii) and Met64-containing (**b**)(iii) peptides. (**c**) Fold change increase in Met95 and Met64 oxidation following treatment with H_2O_2 at various concentrations. The average AUC across replicates was used to determine fold change of oxidation for that treatment. Error bars represent standard deviation. *Indicates $p < 0.05$; **Indicates $p < 0.01$ using the Student's t-test (**d**) NMR structure of hPHPT1 depicting the Met95 and Met64 residue location. Met64 is buried in a cavity that is partly hydrophobic (red indicates hydrophobic residues) while Met95 is surface-exposed.

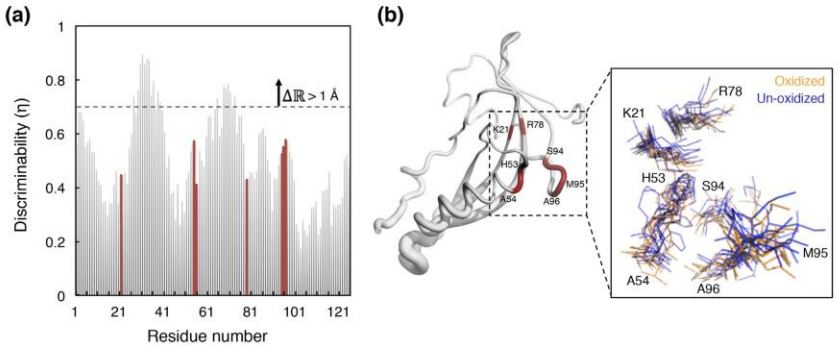

Figure 4. Effect of Met95 oxidation on the conformational density of hPHPT1. (**a**) The oxidation-induced conformational density shifts, $\Delta\mathbb{R}$, are shown individually for each of the 125 amino acids of hPHPT1, and indicated by a normalized quantity η (discriminability) that takes up values closer to unity for progressively larger shifts. The residues that have been implicated to contribute to the catalytic activity of hPHPT1 are highlighted in red. The dashed horizontal line denotes the η value beyond which the $\Delta\mathbb{R}$ is equivalent to a center-of-mass (CoM) deviation of 1 Å. (**b**) NMR structure of hPHPT1 depicting $\Delta\mathbb{R}$ in terms of the thickness of the backbone trace. The residues highlighted in red are the same residues highlighted in red in (**a**). The inset provides a perspective of the conformational densities of these selected residues through the use of twelve conformations selected randomly from the oxidized and non-oxidized forms.

combined the final 50 ns of the three trajectories of each form to obtain representative conformational ensembles for the two forms, $\mathbb{R}$ and $\mathbb{R}_o$.

These ensembles were then compared against each other to obtain the response of Met95 oxidation on the structure/dynamics of hPHPT1's apo state. Instead of comparing summary statistics of these ensembles against each other[29,30], we compared them directly against each other and obtained a quantitative estimate for the shift in conformational density, $\Delta\mathbb{R}$. A direct comparison is preferred over a comparison of summary statistics as it circumvents the issue concerning the selection of representative conformations from rugged potential energy surfaces. A further advantage of comparing ensembles directly is that the resulting quantification naturally embodies differences in conformational fluctuations.

Quantitative estimates were obtained for the oxidation-induced shifts in conformational density, $\Delta\mathbb{R}$, using a method we developed recently[31–33]. For a given pair of ensembles, this method returns a quantitative estimate of $\Delta\mathbb{R}$ that we refer to as discriminability, η. This quantity is normalized and bounded, that is, $\eta \in [0, 1)$, and it takes up a value closer to unity as the difference between the ensembles increases. We determined η separately for each of the 125 residues in the hPHPT1 between their representative ensembles in the oxidized and non-oxidized forms. Each ensemble was represented by 3001 conformations. These conformations were extracted at regular intervals of 50 ps from the combined 150 ns trajectory of each form. Note that all of the selected conformations are least square fitted on to the NMR structure. Structure fitting was necessary to remove the bias of η against whole molecule rotation and translation, as that was not the goal of this comparison.

Figure 4 shows the oxidation-induced shifts in the conformational density of hPHPT1. It was found that for most residues $\eta < 0.69$, which, in Euclidian space is equivalent to a center of mass (CoM) deviation smaller than 1 Å. The only contiguous sequence of residues whose $\eta > 0.69$ was that of loop L2 (residues 29–39), which is distant from the catalytic site. The relatively larger η values for the residues in this loop is still equivalent to centers of mass deviations <2 Å. The set of residues in the catalytic site, Lys21, His53, Ala54, Arg78, Ser94, Ala96, that are known experimentally to contribute to hPHPT1's activity[15,16], underwent only negligible (<0.8 Å) oxidation-induced changes in conformational density. The backbone amino groups of His53, Ala54, and Ala96 as well as the side chains of both His53 and Ser94 remain oriented toward the catalytic site and explored conformational spaces similar to those in the non-oxidized form. Residues Lys21 and Arg78 that have been implicated in substrate anchoring[15], and/or in stabilizing transition states[16], retain the conformational space they explore in the non-oxidized form. The structure/dynamics of Met95 also remains unaffected by its oxidation.

In all, these MD simulations predicted that Met95 oxidation induces only a minor change in the structure/dynamics of the apo-state of hPHPT1. Therefore, if Met95 oxidation affects hPHPT1 activity, then it would do so by altering the stability of the ligand-bound transition state.

Effect of H_2O_2 induced oxidation on hPHPT1 activity. To determine the effect of H_2O_2-induced oxidation on hPHPT1 activity, we utilized a novel mass spectrometry-based assay. In this assay, we measured the amount of a phosphohistidine-containing peptide substrate that remained after a specified time period of hPHPT1 treatment for both the non-oxidized and oxidized forms of the enzyme. Non-oxidized hPHPT1 should remove the phosphoryl group from phosphohistidine whereas oxidation, presumably through selective oxidation of Met95 that is within the substrate binding region, could induce changes in hPHPT1 phosphatase activity. The mass spectrometry assay allowed for detection and relative quantitation of both phosphorylated and

non-phosphorylated forms of the peptide substrate over a defined period of time in order to identify significant changes in hPHPT1 function that could occur due to oxidation.

The same hPHPT1 samples that were used for oxidation site mapping were assessed for phosphohistidine phosphatase activity using the phosphohistidine containing peptide, Succinyl-Ala-His-Pro-Phe-*p*-nitroanilide, which is a known substrate of PHPT1[9]. The peptide substrate that was not phosphorylated on histidine was used to establish the intrinsic spectral characteristics for this peptide (Fig. 5a, top spectrum). The phosphorylated peptide substrate that was not treated with hPHPT1 was used to determine the maximum amount of phosphorylated histidine present in the samples (Fig. 5a, bottom spectrum). The phosphorylated peptide substrate treated with only 1 mM H_2O_2 was used for confirming that the phosphohistidine was not dephosphorylated by H_2O_2 addition or that H_2O_2 introduced any chemical modifications in the peptide. MS/MS spectra of both the non-phosphorylated and phosphorylated substrate was obtained to confirm sequence and localization of the phosphorylation site (Fig. 5b). In addition to the neutral loss of HPO_3^- (M-80) corresponding to the fragmentation of the labile P-N bond of phosphohistidine, neutral losses of M-98 and M-116 were detected in the MS/MS spectra of the phosphohistidine-containing peptide substrate. The mechanism of gas-phase dissociation of phosphohistidine-containing peptides has been described previously[34], where the additional water losses arise from fragmentation of the phosphoryl group after gas-phase phosphate transfer from the phosphohistidine to a carboxyl group within the peptide sequence (most likely a phosphate transfer to the N-terminal succinyl group for the phosphopeptide substrate used in this study).

Initial substrate peptide phosphorylation levels were determined to be approximately 35–40% and showed no significant change in phosphorylation when subjected to 1 mM H_2O_2 treatment without hPHPT1 or PBS (Fig. 5c). Treatment with non-oxidized hPHPT1 decreased the phosphorylation level of the peptide by 100-fold after 10 min of reaction time (Fig. 5c). No protonated phosphopeptide was detectable after the 10-min time point; however, signal remained for the sodium and potassium adducts, permitting activity measurements at later time points. In addition to the correlation of selective Met95 oxidation that provides evidence of the reported higher order structure of hPHPT1 (Fig. 3), the mass spectrometry-based assay demonstrated robust activity of the recombinant hPHPT1 used in this study. Interestingly, however, hPHPT1 treated with H_2O_2 showed no systematic change in phosphatase activity compared to non-oxidized hPHPT1 (Fig. 5c). Heat-denatured hPHPT1 was also used as a negative control and demonstrated a marked decrease, but not total elimination of phosphatase activity, indicating a small amount of hPHPT1 refolds and was active after heat denaturation. The activity assay shows that oxidation of hPHPT1 does not affect its activity, at least with the peptide substrate used in this study.

In addition to the mass spectrometry-based assay, we also used the non-specific phosphatase substrate, para-nitrophenyl phosphate (*p*NPP), to measure product (p-nitrophenolate) generation associated with hPHPT1 activity through colorimetric detection[14]. Both hPHPT1 and 500 μM H_2O_2-treated hPHPT1 were used at five different substrate concentrations to determine Michaelis-Menten kinetics of hPHPT1 before and after ROS-induced oxidation. These experiments showed no significant change in the V_{max} and k_{cat} of hPHPT1; however, there was a 1.4-fold decrease in K_m following 500 μMH_2O_2 treatment (Supplemental Fig. 1).

Discussion

Identification and quantitation of protein modifications provide insight into protein functional outcomes in response to cellular stress or other stimuli. Additionally, characterizing modifications at site-specific levels establishes causality between structure and function. In this study, using high-performance liquid chromatography combined with high-resolution tandem mass spectrometry, we quantified oxidation of amino acid residues that are susceptible to oxidation (Met, Tyr, Trp, and Cys). The initial unbiased screening using MaxQuant demonstrated greater oxidation levels of the two methionine residues, Met64 and Met95, with significantly higher oxidation of Met95 observed with increased concentration of H_2O_2. Upon subsequent analysis using high mass accuracy XIC-based quantitation, we determined that the internally localized methionine residue, Met64, was not significantly oxidized following H_2O_2 treatment at concentrations up to 1 mM (maximum 2-fold increase). Met95, however, was oxidized in a concentration-dependent manner, with a site-specific oxidation increase of approximately 40-fold after the 2 hour treatment with 1 mM H_2O_2. This result is consistent with the 3D structure of hPHPT1 in that while Met95 is exposed to solvent, Met64 is buried in a partially hydrophobic cavity (Fig. 3d). In general, buried methionine residues are less susceptible to oxidation[35].

Interestingly, Met95 is also located in the substrate binding site of hPHPT1[16], indicating a distinct possibility that its oxidation could modulate hPHPT1 activity. In general, oxidative modifications, including those of methionine residues, have been shown to affect protein binding affinity and influence enzymatic activity negatively[36,37]. For example, methionine oxidation within calmodulin can negatively affect its ability to activate Ca-ATPase[38–40]. Methionine oxidation has also been shown to affect the function of other proteins such as actin[41] and IκBα[42]. In the context of PHPT1, a decrease in enzyme activity could prevent removal of phosphoryl groups of its phosphohistidine-containing protein substrates in the cell which include the beta subunit of G protein, ATP-citrate lyase, and the calcium activated potassium channel, KCa3.1. These phosphohistidine targets play vital roles in lipid metabolism and signaling pathways and it is tempting to speculate that alteration of PHPT1 activity, which includes changes due to ROS-induced modifications, could have an impact on these cellular processes.

In principle, Met95 oxidation can influence hPHPT1's catalytic activity by altering the structure/dynamics of its apo-state or its substrate-bound transition state. We carried out molecular dynamics simulations to predict the effect of Met95 oxidation on the structure/dynamics of hPHPT1's apo-state. Surprisingly, we found that the apo-state of the catalytic site was affected only marginally by the oxidation state of Met95. Additionally, since NMR studies have revealed no systematic effects of the binding of inorganic phosphate to the catalytic site[16], we predicted that Met95 oxidation might not affect the phosphate-loaded state of the catalytic site. Therefore, if Met95 oxidation influences hPHPT1 activity, then these studies predict that it would do so by altering the stability of a substrate-bound transition state.

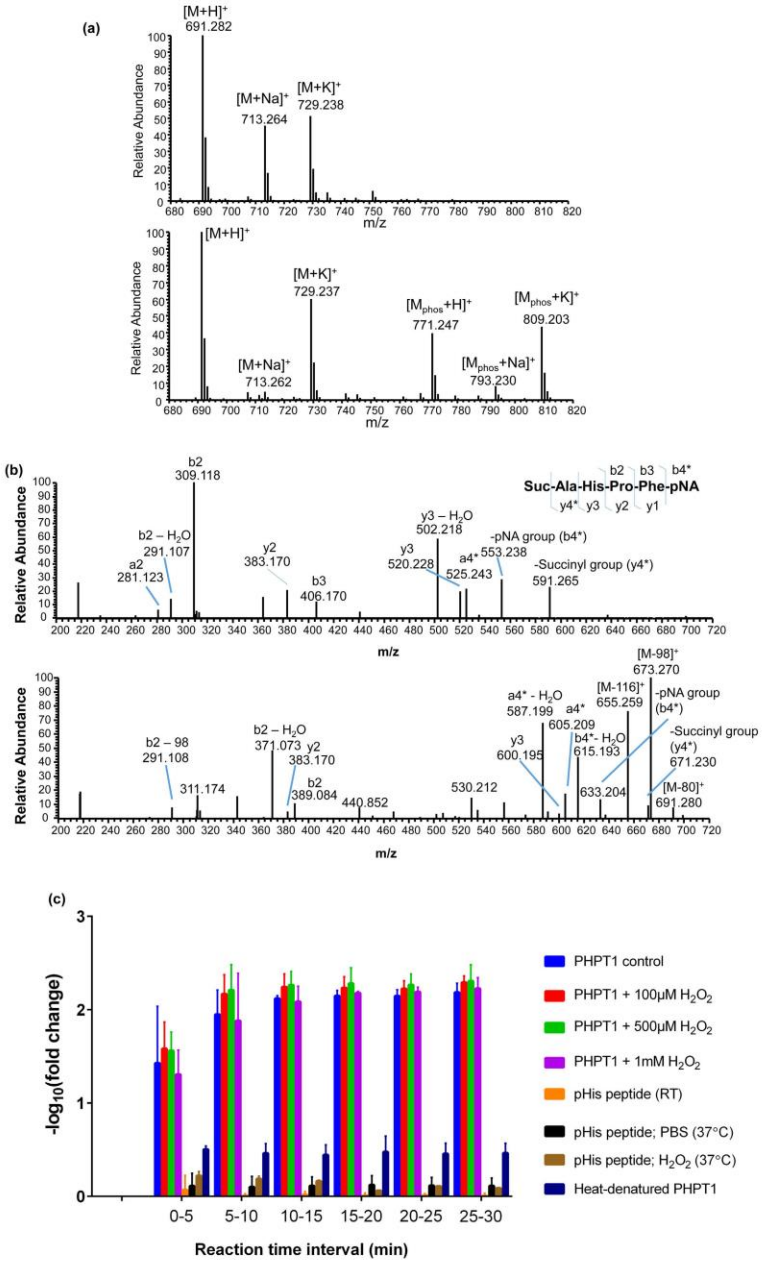

Figure 5. Effect of oxidation on hPHPT1 activity. (**a**) Full scan high-resolution mass spectrum (centroid mode) of the non-phosphorylated peptide (top spectrum), Suc-AHPF-pNA, at *m/z* 691. Signal corresponding to the phosphorylated peptide ion (*m/z* 771) was not detected. Full scan mass spectrum (centroid mode) of the histidine phosphorylated peptide is shown in the bottom spectrum, Suc-A(p)HPF-pNA, at *m/z* 771. Sodium and potassium adducts for both the non-phosphorylated (*m/z* 713 and 729, respectively) and phosphorylated peptide (*m/z* 793 and 809, respectively) are present as well. (**b**) Annotated high-resolution MS/MS spectrum (centroid) of the non-phosphorylated peptide (top spectrum) and phosphorylated peptide (bottom spectrum)

confirmed the sequence of the peptide substrate before and after chemical phosphorylation. b- and y-type fragment ions correspond to cleavage of the amide bond at specific locations on the peptide sequence as shown in the inset sequence (*indicates fragment ion corresponding to cleavage of amide bond linking succinyl or pNA to the N-terminus or C-terminus, respectively) (c) Mass spectrometry-based activity assay results showing the effect of H_2O_2 treatment on phosphohistidine-containing peptide substrate conversion to product by hPHPT1. The $-\log_{10}$(fold change) of the phosphorylated peptide was used to demonstrate the amount of the phosphorylated substrate converted to non-phosphorylated product by hPHPT1 relative to the amount of the untreated phosphorylated peptide over time. While the protonated phosphopeptide was not detectable after 10 min, the sodium and potassium adducts of the phosphopeptide allowed for activity measurement at later time points. The activity assay indicated potentially slower conversion of the sodium and potassium adducts. Error bars represent standard deviation from three technical replicates.

The impact of oxidative modification on hPHPT1 activity was assessed in two different ways. In one approach, we used a mass spectrometry-based activity assay in which a known phosphohistidine-containing peptide substrate of hPHPT1 was utilized. In the second approach, we used a colorimetric assay using the nonspecific substrate, p-nitro phenyl phosphate.

From an experimental standpoint, phosphohistidine has been recognized as an analytical challenge due to the acid labile nature of this modification[5]. We were able to generate a relatively high yield of the known hPHPT1 peptide substrate, Succinyl-Ala-His-Pro-Phe-*p*-nitroanilide (35–40% phosphorylated), that was also stable at 4 °C for months at a time (no significant loss as determined by mass spectrometry). Stability was achieved through solvent composition in which the buffer was at a high pH (pH 8.5–9) and low enough in salt components so as to not interfere with the mass spectrometric analysis. In addition, using a short peptide limited the possibility of alternatively phosphorylated residues and other potential side reactions from the phosphorylation reaction. To the best of our knowledge, this study represents the first time a mass spectrometry-based direct injection technique has been utilized to determine phosphohistidine phosphatase activity. This method is beneficial in that it provides specific detection through molecular weight and sequence information (through MS/MS) of a substrate and product rather than colorimetric or fluorometric assays[43], which could be nonspecific in detection depending on the matrix composition and complexity. Our reported method could potentially be replicated using other peptide or protein sequences and could also be multiplexed based on the mass resolving power of the mass spectrometer used.

Consistent with predictions from molecular simulations, we found no significant decrease in hPHPT1 activity following oxidation of hPHPT1, as demonstrated by the mass spectrometry-based activity assay. This result is contrary to the common conception that protein oxidation is typically a loss-of-function modification[36–42]. Furthermore, the colorimetric data demonstrated no significant differences in the k_{cat} or V_{max} of hPHPT1 following H_2O_2 treatment; however, the K_m value was slightly lower for oxidized hPHPT1. These data could suggest a small increase in substrate binding affinity when the hPHPT1 enzyme is oxidized, although the results are potentially less significant to our assessment of hPHPT1 activity based on the small change in kinetic parameters observed as well as significantly lower specificity of the substrate used in this assay compared to the mass spectrometry-based assay. Based on the results from both assays, we conclude that oxidation of hPHPT1 with concentrations up to 1 mM of H_2O_2 did not negatively impact the activity of hPHPT1.

Methionine oxidation has been shown in many cellular roles as a protein modification. Commonly, under conditions of oxidative stress, it is recognized as a ROS-induced modification that typically leads to loss of protein function. Methionine oxidation, however, is not exclusively limited to protein loss of function. For example, it has also been shown that glutamine synthetase in *E. coli* has 8 of its 16 methionine residues oxidized without a significant effect on its enzymatic activity[35]. The role of these multiple oxidation events is believed to be as an antioxidant function (i.e., a ROS "sponge") in order to protect against the oxidation of redox-sensitive residues of other more sensitive biological targets in ROS-abundant environments. hPHPT1 is unlikely to protect other protein targets in this context given hPHPT1 is a lower abundance protein depending on tissue type[15,43] and only has two methionine sites (one surface exposed) available for modification. It is plausible, though, that selective oxidation of Met95 protects proximal redox-sensitive residues within hPHPT1 that could affect activity, allowing for a functional enzyme even in the presence of high concentrations of ROS.

Although proteome diversity increases significantly through the addition of various post-translational and chemical modifications including oxidative stress-induced modifications such as methionine oxidation, the results from our study provide some evidence that proteome diversity through modifications does not necessarily correlate to functional diversity. Given our studies are limited to a single protein and modification type, it is clear that a significant amount of work is needed to address the functional impact of oxidation as well as other post-translational modifications on a broader scale.

Conclusion

We have successfully implemented a mass spectrometry-based approach to quantify site-specific oxidation of human PHPT1 (hPHPT1) following treatment with a known cellular ROS, H_2O_2. Furthermore, using mass spectrometry, we have shown that selective methionine oxidation at Met95 of hPHPT1 occurred but had no impact on phosphatase activity with the peptide substrate used in this study. Mass spectrometry-based structure and activity experiments were augmented by molecular dynamics simulations that showed methionine oxidation at Met95 had no significant structural impact on the catalytic site of hPHPT1. As our study is limited to small molecule and peptide substrates, other possible outcomes of hPHPT1 (or PHPT1 in other mammalian systems) oxidation need to be explored in a broader context including influence on protein-protein interactions as well as possible

changes in cell localization. Future studies aim to characterize PHPT1 structure and expression in various tissue types and conditions of oxidative stress in order to further understand regulation of PHPT1 and related functional consequences in the cell.

References

1. Klumpp, S., Bechmann, G., Maurer, A., Selke, D. & Krieglstein, J. ATP-citrate lyase as a substrate of protein histidine phosphatase in vertebrates. *Biochemical and biophysical research communications* **306,** 110–115 (2003).
2. Maurer, A. *et al.* The beta-subunit of G proteins is a substrate of protein histidine phosphatase. *Biochemical and biophysical research communications* **334,** 1115–1120 (2005).
3. Fujitaki, J. M., Fung, G., Oh, E. Y. & Smith, R. A. Characterization of Chemical and Enzymatic Acid-Labile Phosphorylation of Histone H-4 Using P-31 Nuclear Magnetic-Resonance. *Biochemistry* **20,** 3658–3664 (1981).
4. Srivastava, S. *et al.* Protein histidine phosphatase 1 negatively regulates CD4 T cells by inhibiting the K(+) channel KCa3.1. *Proceedings of the National Academy of Sciences of the United States of America* **105,** 14442–14446 (2008).
5. Boyer, P. D., Deluca, M., Ebner, K. E., Hultquist, D. E. & Peter, J. B. Identification of phosphohistidine in digests from a probable intermediate of oxidative phosphorylation. *The Journal of biological chemistry* **237,** PC3306–PC3308 (1962).
6. Peter, J. B., Hultquist, D. E., Deluca, M., Kreil, G. & Boyer, P. D. Bound phosphohistidine as an intermediate in a phosphorylation reaction of oxidative phosphorylation catalyzed by mitochondrial extracts. *The Journal of biological chemistry* **238,** 1182–1184 (1963).
7. Van Etten, R. L. & Hickey, M. E. Phosphohistidine as a stoichiometric intermediate in reactions catalyzed by isoenzymes of wheat germ acid phosphatase. *Archives of biochemistry and biophysics* **183,** 250–259 (1977).
8. Wagner, P. D. & Vu, N. D. Phosphorylation of ATP-citrate lyase by nucleoside diphosphate kinase. *The Journal of biological chemistry* **270,** 21758–21764 (1995).
9. Ek, P. *et al.* Identification and characterization of a mammalian 14-kDa phosphohistidine phosphatase. *European journal of biochemistry/FEBS* **269,** 5016–5023 (2002).
10. Attwood, P. V. *et al.* Chemical phosphorylation of histidine-containing peptides based on the sequence of histone H4 and their dephosphorylation by protein histidine phosphatase. *Bba-Proteins Proteom* **1804,** 199–205 (2010).
11. Ek, P., Ek, B. & Zetterqvist, O. Phosphohistidine phosphatase 1 (PHPT1) also dephosphorylates phospholysine of chemically phosphorylated histone H1 and polylysine. *Upsala journal of medical sciences* **120,** 20–27 (2015).
12. Krieglstein, J. *et al.* Reduced viability of neuronal cells after overexpression of protein histidine phosphatase. *Neurochemistry international* **53,** 132–136 (2008).
13. Kamath, V. *et al.* Regulation of glucose- and mitochondrial fuel-induced insulin secretion by a cytosolic protein histidine phosphatase in pancreatic beta-cells. *American Journal of Physiology-Endocrinology and Metabolism* **299,** E276–E286 (2010).
14. Yanicostas, C., Vincent, A. & Lepesant, J. A. Transcriptional and Posttranscriptional Regulation Contributes to the Sex-Regulated Expression of 2 Sequence-Related Genes at the Janus Locus of Drosophila-Melanogaster. *Mol Cell Biol* **9,** 2526–2535 (1989).
15. Busam, R. D. *et al.* First structure of a eukaryotic phosphohistidine phosphatase. *The Journal of biological chemistry* **281,** 33830–33834 (2006).
16. Gong, W. B. *et al.* Solution structure and catalytic mechanism of human protein histidine phosphatase 1. *Biochemical Journal* **418,** 337–344 (2009).
17. Gauci, S. *et al.* Lys-N and Trypsin Cover Complementary Parts of the Phosphoproteome in a Refined SCX-Based Approach. *Analytical Chemistry* **81,** 4493–4501 (2009).
18. Finkel, T. & Holbrook, N. J. Oxidants, oxidative stress and the biology of ageing. *Nature* **408,** 239–247 (2000).
19. Parrinello, M. & Rahman, A. Polymorphic transition in single crystals: a new molecular dynamics method. *Journal of Applied Physics* **52,** 7182–7190 (1981).
20. Bussi, G., Donadio, D. & Parrinello, M. Canonical sampling through velocity rescaling. *J Chem Phys* **126,** 014101–014107 (2007).
21. Darden, T., York, D. & Pedersen, L. Particle mesh Ewald: an Nlog(N) method for Ewald sums in large systems. *J Chem Phys* **98,** 10089–10092 (1993).
22. Hess, B. P-LINCS: A parallel linear constraint solver for molecular simulation. *Journal of Chemical Theory and Computation* **4,** 116–122 (2008).
23. Miyamoto, S. & Kollman, P. A. SETTLE: an analytical version of the SHAKE and RATTLE algorithm for rigid water models. *Journal of Computational Chemistry* 13, 952–962 (1992).
24. Kaminski, G. A., Friesner, R. A., Tirado-Rives, J. & Jorgensen, W. L. Evaluation and reparametrization of the OPLS-AA force field for proteins via comparison with accurate quantum chemical calculations on peptides. *Journal of Physical Chemistry B* **105,** 6474–6487 (2001).
25. Jorgensen, W. L., Chandrasekhar, J., Madura, J. D., Impey, R. W. & Klein, M. L. Comparison of simple potential functions for simulating liquid water. *J Chem Phys* **79,** 926–935 (1983).
26. Hess, B., Kutzner, C., van der Spoel, D. & Lindahl, E. GROMACS 4: Algorithms for highly efficient, load-balanced, and scalable molecular simulation. *Journal of Chemical Theory and Computation* **4,** 435–447 (2008).
27. Ross, A. R. S. Identification of histidine phosphorylations in proteins using mass spectrometry and affinity-based techniques. *Method Enzymol* **423,** 549–572 (2007).
28. Ma, R. *et al.* Mutational study of human phosphohistidine phosphatase: effect on enzymatic activity. *Biochemical and biophysical research communications* **337,** 887–891 (2005).
29. Varma, S., Chiu, S. W. & Jakobsson, E. The influence of amino acid protonation states on molecular dynamics simulations of the bacterial porin OmpF. *Biophys J* **90,** 112–123 (2006).
30. Varma, S. & Jakobsson, E. The cPLA2 C2alpha domain in solution: structure and dynamics of its Ca2+ -activated and cation-free states. *Biophys J* **92,** 966–976 (2007).
31. Leighty, R. E. & Varma, S. Quantifying Changes in Intrinsic Molecular Motion Using Support Vector Machines. *J Chem Theory Comput* **9,** 868–875 (2013).
32. Dutta, P., Botlani, M. & Varma, S. Water Dynamics at Protein-Protein Interfaces: Molecular Dynamics Study of Virus-Host Receptor Complexes. *J Phys Chem B* **118,** 14795–14807 (2014).
33. Varma, S., Botlani, M. & Leighty, R. E. Discerning intersecting fusion-activation pathways in the Nipah virus using machine learning. *Proteins* **82,** 3241–3254 (2014).
34. Oslund, R. C. *et al.* A phosphohistidine proteomics strategy based on elucidation of a unique gas-phase phosphopeptide fragmentation mechanism. *Journal of the American Chemical Society* **136,** 12899–12911 (2014).
35. Levine, R. L., Berlett, B. S., Moskovitz, J., Mosoni, L. & Stadtman, E. R. Methionine residues may protect proteins from critical oxidative damage. *Mechanisms of Ageing and Development* **107,** 323–332 (1999).
36. Johnson, D. & Travis, J. Oxidative Inactivation of Human Alpha-1-Proteinase Inhibitor - Further Evidence for Methionine at the Reactive Center. *Journal of Biological Chemistry* **254,** 4022–4026 (1979).
37. Reddy, V. Y. *et al.* Oxidative Dissociation of Human Alpha(2)-Macroglobulin Tetramers into Dysfunctional Dimers. *Journal of Biological Chemistry* **269,** 4683–4691 (1994).

38. Bartlett, R. K. *et al.* Oxidation of Met(144) and Met(145) in calmodulin blocks calmodulin dependent activation of the plasma membrane Ca-ATPase. *Biochemistry* **42,** 3231–3238 (2003).
39. Bigelow, D. J. & Squier, T. C. Thioredoxin-dependent redox regulation of cellular signaling and stress response through reversible oxidation of methionines. *Molecular Biosystems* **7,** 2101–2109 (2011).
40. Yin, D., Kuczera, K. & Squier, T. C. The sensitivity of carboxyl-terminal methionines in calmodulin isoforms to oxidation by H_2O_2 modulates the ability to activate the plasma membrane Ca-ATPase. *Chemical Research in Toxicology* **13,** 103–110 (2000).
41. Lee, B. C. *et al.* MsrB1 and MICALs Regulate Actin Assembly and Macrophage Function via Reversible Stereoselective Methionine Oxidation. *Molecular Cell* **51,** 397–404 (2013).
42. Kanayama, A., Inoue, J., Sugita-Konishi, Y., Shimizu, M. & Miyamoto, Y. Oxidation of I kappa B alpha at methionine 45 is one cause of taurine chloramine-induced inhibition of NF-kappa B activation. *Journal of Biological Chemistry* **277,** 24049–24056 (2002).
43. Zhang, X. Q., Sundh, U. B., Jansson, L., Zetterqvist, O. & Ek, P. Immunohistochemical localization of phosphohistidine phosphatase PHPT1 in mouse and human tissues. *Upsala journal of medical sciences* **114,** 65–72 (2009).

Acknowledgements

We thank the USF Center for Drug Discovery and Innovation for access to the high-resolution mass spectrometers used in this study. We acknowledge support from the High Performance Research Computing center of the University of South Florida. We also thank the National Institute on Alcohol Abuse and Alcoholism at the National Institutes of Health (grant AA021247) and the USF Foundation for financial support.

Author Contributions

Conceived and designed the molecular dynamics simulations and experiments: S.V. and S.M.S., respectively. Performed the mass spectrometry experiments and data analysis: D.R.M. Provided assistance in phosphohistidine synthesis and the PHPT1 activity assay development: S.M. Performed molecular dynamics simulations: P.D. and S.V. Wrote the paper: D.R.M., P.D., S.V. and S.M.S.

Additional Information

Supplementary information accompanies this paper at http://www.nature.com/srep

Competing financial interests: The authors declare no competing financial interests.

How to cite this article: Martin, D. R. *et al.* Structural and activity characterization of human PHPT1 after oxidative modification. *Sci. Rep.* **6,** 23658; doi: 10.1038/srep23658 (2016).

Appendix B – Nature: Scientific Reports, Supporting Information

Supplemental Information

Structural and activity characterization of human PHPT1 after oxidative modification

Daniel R. Martin, Priyanka Dutta, Shikha Mahajan, Sameer Varma and Stanley M. Stevens Jr.*

Department of Cell Biology, Microbiology and Molecular Biology, University of South Florida, Tampa, FL 33620

*corresponding author; Email: smstevens@usf.edu

Keywords:

Oxidative stress, phosphohistidine, PHPT1, mass spectrometry, molecular dynamics

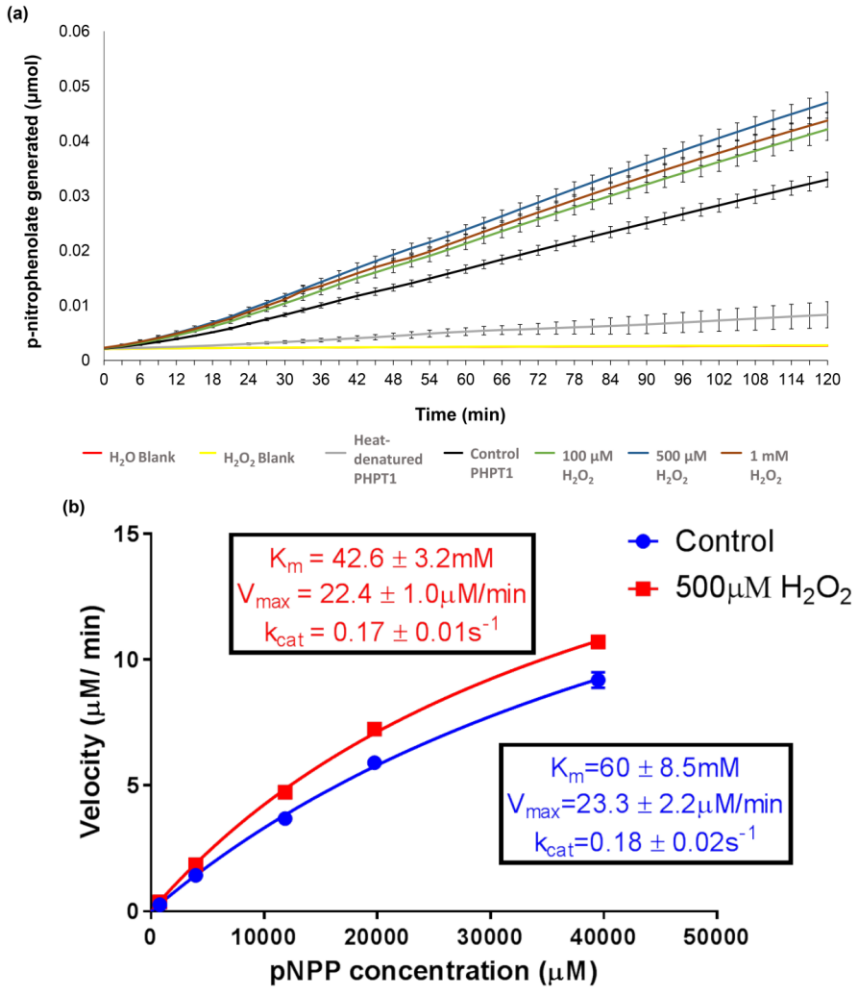

Supplemental Figure 1. Colorimetric phosphatase activity assay results using the p-nitrophenyl phosphate (*p*NPP) substrate for PHPT1 before and after H_2O_2 treatment. **(a)** Representative colorimetric assay reading over 2 h at 5 mM initial pNPP concentration where error bars represent standard deviation. Error bars represent standard deviation of plated and technical replicates (n=9). **(b)** Nonlinear regression using the Michaelis-Menten equation was performed for control and 500 µM H_2O_2-treated PHPT1 with a substrate concentration range from 0.8mM-40mM. K_m, V_{max}, and k_{cat} values are shown with error representing 95% confidence intervals.

Appendix C – Scientific Reports: Permissions

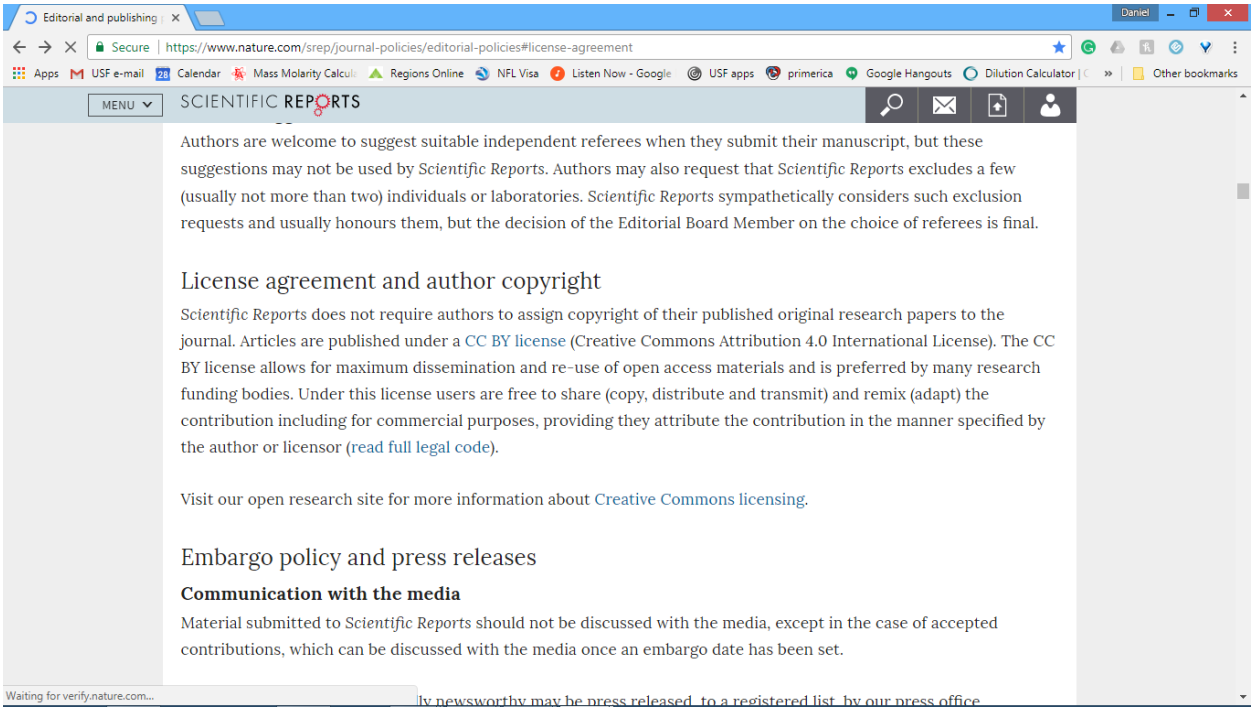
Editorial and publishing
Daniel
Secure
https://www.nature.com/srep/journal-policies/editorial-policies#license-agreement
Apps
USF e-mail
Calendar
Mass Molarity Calcul
Regions Online
NFL Visa
Listen Now - Google
USF apps
primerica
Google Hangouts
Dilution Calculator
Other bookmarks
MENU
SCIENTIFIC REPORTS
Authors are welcome to suggest suitable independent referees when they submit their manuscript, but these suggestions may not be used by *Scientific Reports*. Authors may also request that *Scientific Reports* excludes a few (usually not more than two) individuals or laboratories. *Scientific Reports* sympathetically considers such exclusion requests and usually honours them, but the decision of the Editorial Board Member on the choice of referees is final.
License agreement and author copyright
Scientific Reports does not require authors to assign copyright of their published original research papers to the journal. Articles are published under a CC BY license (Creative Commons Attribution 4.0 International License). The CC BY license allows for maximum dissemination and re-use of open access materials and is preferred by many research funding bodies. Under this license users are free to share (copy, distribute and transmit) and remix (adapt) the contribution including for commercial purposes, providing they attribute the contribution in the manner specified by the author or licensor (read full legal code).
Visit our open research site for more information about Creative Commons licensing.
Embargo policy and press releases
Communication with the media
Material submitted to *Scientific Reports* should not be discussed with the media, except in the case of accepted contributions, which can be discussed with the media once an embargo date has been set.
Waiting for verify.nature.com...